Measurement Of Several Rate Coefficients For The Helium - Neon Laser Plasma.

MEASUREMENT OF SEVERAL RATE COEFFICIENTS FOR THE He-Ne LASER PLASMA

by

Heinrich-Joachim Siebeneck

A Dissertation
Presented to the Graduate Committee
of Lehigh University
in Candidacy for the Degree of
Doctor of Philosophy
in
Electrical Engineering

Lehigh University
1974

CERTIFICATE OF APPROVAL

Approved and recommended for acceptance as a dissertation in partial fulfillment of the requirements for the degree of Doctor of Philosophy.

Nov. 20, 1974
(date)

Ernest E. Bergmann
Professor in Charge
E. Bergmann

Accepted 11/20/74
(date)

Special committee directing the doctoral work of Mr. Heinrich-Joachim Siebeneck

Nikolai Eberhardt
Chairman
N. Eberhardt

D. Leenov
D. Leenov

R. Folk
R. Folk

ACKNOWLEDGEMENT

The author expresses his gratitude to Professor Ernest E. Bergmann, who suggested this problem, for his guidance and assistance during all phases of this investigation. He also thanks the members of his committee, Professor Nikolai Eberhardt, Professor Robert T. Folk and Professor Daniel Leenov for their advice.

The author also would like to thank a fellow graduate student, Vikram Kumar, for his continued help.

The financial assistance provided by Lehigh University is also acknowledged.

TABLE OF CONTENTS

TABLE OF CONTENTS - (CONTINUED)

LIST OF TABLES

LIST OF FIGURES

LIST OF FIGURES - (CONTINUED)

LIST OF GRAPHS

ABSTRACT

Modulation of spontaneously omitted sidelight due to laser induced perturbations in a He-Ne laser plasma has been observed by several authors. The study of these modulations can be employed to obtain rate coefficients of the He-Ne plasma. The method was first described by Parks and Javan who studied the pressure variations of sidelight intensity changes in a Ne plasma perturbed by a 1.15μ laser radiation field. Their results yielded energy exchange rates between the $4s'(1/2)_1^0$ and $4s'(1/2)_0^0$ levels of the Ne due to atom-atom collisions. Similar studies were carried out by Lilly and Holmes for the $5s'(1/2)_1^0$ and $5s'(1/2)_0^0$ levels of Ne using a 6328Å laser radiation field. Khaikin studied the electronic excitation of Ne levels lying above the $5s'(1/2)_1^0$ upper laser level for a He-Ne plasma oscillating in the 6328Å or 3.39 μ transitions.

Since in a He-Ne plasma energy exchange between excited states can be caused simultaneously by electron-atom and atom-atom collisions, we investigated selected cases in which both energy transfer mechanisms occur. Unlike the authors mentioned previously, we studied current and pressure dependence of sidelight changes in the region of laser operation and fitted our experimental values to equations which contained both electronic and atomic parameters. In particular, we studied the de-excitation rates of the upper

and lower laser level, $5s'(1/2)^0_1$ and $3p'(1\ 1/2)_2$, in a laser operating in the 6328Å transition. Furthermore, we investigated the energy exchange between the $5s'(1/2)^0_1$ and $5s'(1/2)^0_0$ levels in Ne as well as between the $5s'(1/2)^0_1$ and $4d(3\ 1/2)^0_3$ levels. In the latter case the energy exchange occurs between two states of different azimuthal quantum numbers, and we found that energy exchange due to electron-atom collisions occurs, but is small compared to the exchange between atoms of the same azimuthal quantum number.

In some cases collisional coupling between atoms of different levels was too complicated to analyze. In those cases we made measurements for different pressures and extrapolated to zero pressures in order to obtain the pure electronic effect. This was true for the 4d', 5d', $6s'(1/2)^0_0$ and the $5s(1\ 1/2)^0_2$ levels.

I. INTRODUCTION

The basic mechanism of operation of the He-Ne laser has been extensively described in literature, and simple theories have been established. There are, however, many mechanisms in the plasma which are only described qualitatively and which are not included in those theories. For example, radiation from the 5s, 4s and 3s states to the ground state of Ne will be greatly self-absorbed, thus leading to an increased lifetime of these transitions, typically in the order of 10^{-6} sec. Thus, direct transition to the ground state is not an important de-excitation mechanism for the 5s and 4s levels. For the 3s state, it is the only means of radiative de-excitation. Under steady-state conditions, the density of atoms in the 3s states should therefore build up. As this process goes on, transitions terminating in the 3s state may also become self-absorbed. This eventually must lead to a bottleneck for laser transitions terminating on 3p levels, since 3p-3s transitions are necessary for maintaining inversion. This is one mechanism which can be used for the explanation of saturation phenomena.

A further complication is introduced by inelastic collisions between electrons and atoms. For example, if a substantial population of the 3s level is built up, mainly through collisions between electrons and atoms in the ground state, inelastic electron collisions with 3s atoms will in-

crease the population of the 3p levels. This effect adds to any enhancement of the 3p population arising from entrapment of 3p-3s radiation; in this way inelastic electron collisions add to the bottleneck and the saturation effect arising therefrom.

No one has yet tried to use these qualitative ideas for the construction of a quantitative theory describing more accurately the operation of a He-Ne laser. Part of the reason is that only very limited data about the excitation and de-excitation mechanisms exists, and much more data is needed. Also the problem is complicated, because of the complexity of the Ne spectrum.

In our work, we will focus our attention on non-radiative excitation and de-excitation mechanisms between excited states in a He-Ne plasma, especially on those which involve electron impact phenomena. One way to measure electron-atom collision cross-sections is to send a monoenergetic beam of electrons into a gas and measure the rate of some resulting reaction. For excitation, for example, the rate may be determined from the decrease of the electron current or from measurements of the absolute intensities of all the spectral lines coming from the excited atom. Another way to measure excitation and de-excitation rates is to employ spectroscopic techniques, and a laser plasma is a suitable object for using such techniques. In a laser it is possible to perturb se-

lectively, out of the whole set of atomic levels, the populations of only a very few levels. Other levels can only be perturbed if they are somehow connected, either through radiative, electronic or atomic processes, to one of the originally perturbed levels. The study of these perturbations will give us information about some of the excitation and de-excitation mechanisms in the gas plasma.

The latter method will be used in our experiment, and the theory will be described in the following Chapter (II). In Chapter III the experiment will be explained, and the results will be discussed in Chapter IV.

The notation for the atomic levels used throughout this work will be the Racah notation for j-ℓ coupling as used by C. Moore[1].

II. THEORY

II.1 Concept of Effective Collision Cross-Sections

Different effects may result from the encounter of an electron with a gas atom or molecule. They can be distinguished as elastic, inelastic, superelastic, or radiative. If no energy exchange takes place between the internal motion of the atom and the electron, the collision is called elastic. The only change occurring is in the translational energy which can increase or decrease for either electron or atom after such a collision.

In an inelastic collision some kinetic energy is lost by the electron in increasing internal motion in the atom. Distinction may be made between ionizing and non-ionizing collisions, depending on whether or not sufficient energy is transferred to cause ejection of one or more electrons from the atom. Non-ionizing inelastic collisions will involve excitation of distinct atomic states. It is this kind of collision we will mainly encounter in a He-Ne gas laser.

Superelastic collisions can occur only between an electron and an excited atom. They are such that an electron gains energy from the internal motion of the atom. This is, of course, only possible if the atom is in an excited state. Collisions of this type occur predominantly between electrons and metastable atoms.

Collisions may also occur in which electromagnetic radiation is emitted. They are essentially inelastic as far as the electron is concerned, but differ in that the whole or part of the additional energy is lost as radiation.

In order to understand the concept of effective cross section, we imagine the following experiment carried out in a real gas. A beam of electrons of homogeneous velocity is directed into a gas. The probability per unit distance W, that one electron interacts with a gas particle in a distance dz is

$$Wdz = n_o \sigma^e dz \qquad \text{(II.1)}$$

n_o is the density of the gas particles, and σ is called the effective cross section for this process. If n_e is the total-number of electrons, the number of electrons undergoing a collision in a distance dz is given by

$$dn = n_o \times n_e \times \sigma^e(v_e)dz \qquad \text{(II.2)}$$

The number of collisions per unit time is given by

$$\frac{dn}{dt} = n_o \times n_e \times \sigma^e(v_e)v_e \qquad \text{(II.3)}$$

In the case that the electrons have a certain velocity spectrum, equation (II.3) can be written, with $n_e = \int n v_e dv_e$

$$\frac{dn}{dt} = n_o \int n v_e v_e \sigma^e(v_e) dv_e \qquad (II.4)$$

Normally, however, nv_e and $\sigma^e(v_e)$ are not known, and one uses the approximation

$$\frac{dn}{dt} = n_o \times n_e \times \bar{v}_e \times \bar{\sigma}^e \qquad (II.5)$$

where $\bar{v}_e$ is the average electron velocity and $\bar{\sigma}^e$ is the average effective cross section for the collision process.

This is the classical derivation of the effective collision cross section, and no specifications are made what kind of collisions, elastic or inelastic, is described by the effective collision cross section $\bar{\sigma}^e$. Thus we can define effective cross sections for both processes, elastic collisions and inelastic collisions. For the total collision cross section we can write

$$\bar{\sigma}^e = \bar{\sigma}^e_o + \Sigma \bar{\sigma}^e_n \qquad (II.6)$$

$\bar{\sigma}^e_o$ is the collision cross section for the elastic collision, and $\bar{\sigma}^e_n$ is the collision cross section for inelastic collisions involving excitation of the nth state of the atom.

The same definition of an effective cross section $\bar{\sigma}^a$ can be made for atomic collisions. In analogue to equation (II.6) we can write

$$\bar{\sigma}^a = \bar{\sigma}_o^a + \Sigma\bar{\sigma}_n^a \qquad \text{(II.6a)}$$

In our experiment, the measured cross sections will be those of inelastic collisions. Our experiment will give information about the changes in the internal motions of the atoms caused by electronic and atomic impact.

The derivation above was made on the classical assumption that the colliding particles are rigid spheres. The actual gas particles are not rigid spheres with defined boundaries - the force between atom and electron will fall off continuously and not drop suddenly to zero. Classically, as long as a field exists between electron and atom for all distance, some deviation of the path of the colliding partners will occur, thus yielding an infinite collision cross section. However, taking into account quantum uncertainty effects, it turns out that a finite value of the total effective cross section is to be expected, provided the force between an atom and an electron falls off faster than r^{-3} for large separations, r.[2]

II.2 Modulation of the Upper and Lower Laser Levels

In the following discussion we will restrict ourselves to a He-Ne laser operating in the 6328Å line. For such a laser, population inversion has been produced between the $5s'(1/2)^0_1$ and the $3p'(1\ 1/2)_2$ levels of neon. The $5s'(1/2)^0_1$ level has been selectively excited through inelastic collision of Ne ground state atoms with metastable 2^1S_oHe atoms via the process

$$\text{Ne(ground state)} + \text{He}(2^1S_o) \rightarrow \text{Ne}(5s'(1/2)^0_1) + \text{He(ground state)} \qquad \text{(II.7)}$$

This process results in the desired population inversion. Figure (II.1) represents the energy level diagram for neon and shows processes involved in the 6328Å laser transition.

For the case of population inversion, we can write for the populations of the $5s'(1/2)^0_1$ - level and the $3p'(1\ 1/2)_2$ - level the following inequality

$$g_{(3p'(1\ 1/2)_2)} \cdot n(5\ '(1/2)^0_1) > g_{(5s'(1/2)^0_1)} \cdot n(3p'(1\ 1/2)_2) \qquad \text{(II.8)}$$

where $g_{(3p'(1\ 1/2)_2)}$ and $g_{(5s'(1/2)^0_1)}$ are the statistical

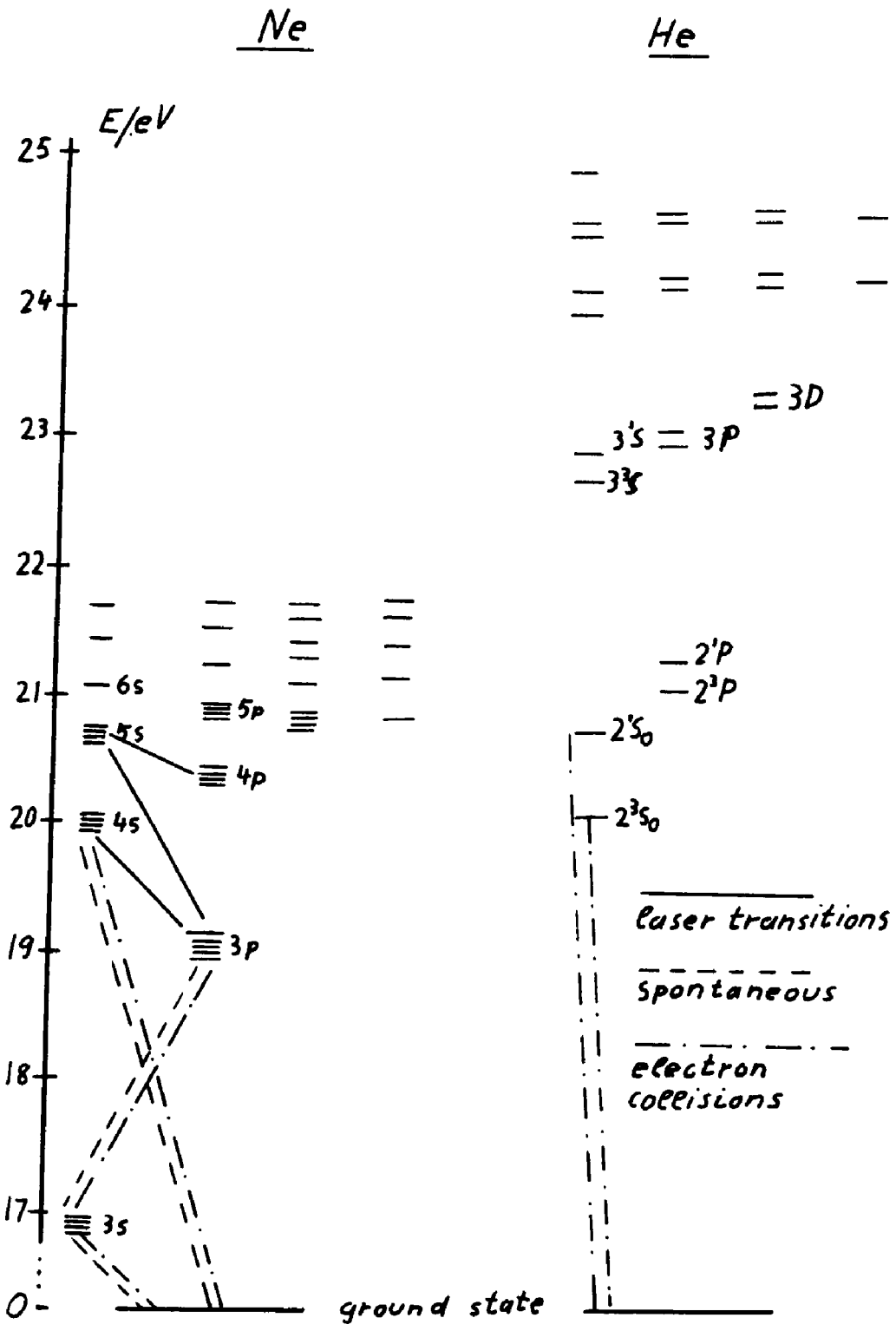

Figure II.1 - Simplified He and Ne Level Diagrams

weights of the corresponding levels.

An applied electromagnetic signal, which is in resonance with the $5s'(1/2)_1^0$ - $3p'(1\ 1/2)_2$ transition, will lead to an increase in the rate of transitions of the atoms between the $5s'(1/2)_1^0$ level and the $3p'(1\ 1/2)_2$ level through stimulated emission and adsorption. In the absence of the electromagnetic signal, the transition rate is mainly determined by the spontaneous transition probability $A(5s'(1/2)_1^0 - 3p'(1\ 1/2)_2)$. Therefore, in the presence of the electromagnetic signal, the population of the $5s'(1/2)_1^0$ level decreases, while at the same time the population of the $3p'(1\ 1/2)$ level increases. If the signal is removed, the upper $5s'(1/2)_1^0$ level is again heavily populated through the already described collisions of the ground state Ne atoms with the metastable $1S_0$He atoms. For the population changes $\Delta n(5s'(1/2)_1^0)$ and $\Delta n(3p'(1\ 1/2)_2)$, i.e., the difference of the populations in the presence and absence of the electromagnetic signal, we can write:

$$\Delta n(5s'(1/2)_1^0) = n_{5s'(1/2)_1^0}(\text{signal present}) - n_{5s'(1/2)_1^0}(\text{signal absent}) \qquad \text{(II.9)}$$

$$\Delta n(3p'(1\ 1/2)_2) = n_{3p'(1\ 1/2)_2}(\text{signal present}) - n_{3p(1\ 1/2)_2}(\text{signal absent}) \qquad \text{(II.10)}$$

We see also that the population changes carry opposite signs. If we now interrupt the electromagnetic signal periodically at a certain frequency, the populations of the two levels involved will be modulated at this frequency carrying opposite phase. The changes in the populations of any two levels are related to the changes in the intensities of spontaneously emitted light from these levels through[3]

$$\frac{\Delta n_1}{\Delta n_2} = \frac{\lambda_1}{\lambda_2} \frac{A_2}{A_1} \frac{\Delta I_1}{\Delta I_2} \qquad \text{(II.11)}$$

A_2/A_1 is the ratio of the Einstein coefficients for spontaneous emission from the levels (1) and (2), λ_1 and λ_2 are the wavelengths of the spontaneously emitted lines.

Thus, by measuring the changes in the intensities, we are able to observe changes in the populations of different levels in the Ne-He gas mixture.

II.3 De-excitation of the Upper and Lower Laser Levels

In this and the following paragraphs we will describe several cases where the measurement of the spontaneously emitted sidelight intensity changes can be employed to determine atomic and electronic parameters of excitation and de-excitation in the gas plasma.

If we are only interested in the de-excitation of the upper and lower laser levels through radiative and collisional processes, a simple analysis may be used to determine the de-excitation parameters for these two levels. The situation is shown in Figure (II.2) for a He-Ne laser operating in the 6328Å line. In the presence of the electromagnetic signal, the rate equations for the populations of the upper and lower levels under steady state conditions can be written:

$$\frac{dn_2}{dt} = R_2 - B(n_2-n_1) - \gamma_2 n_2 + \gamma_{12} n_1 = 0 \qquad \text{(II.12)}$$

$$\frac{dn_1}{dt} = R_1 + B(n_2-n_1) - \gamma_1 n_1 + \gamma_{21} n_2 = 0 \qquad \text{(II.13)}$$

n_1, n_2 are the populations of the upper and lower laser levels, respectively. B is the Einstein coefficient of stimulated emission. γ_i is the total de-excitation rate of the level i, containing radiative and collisional effects. γ_{ik} is the rate of excitation from level i to level k. R_i

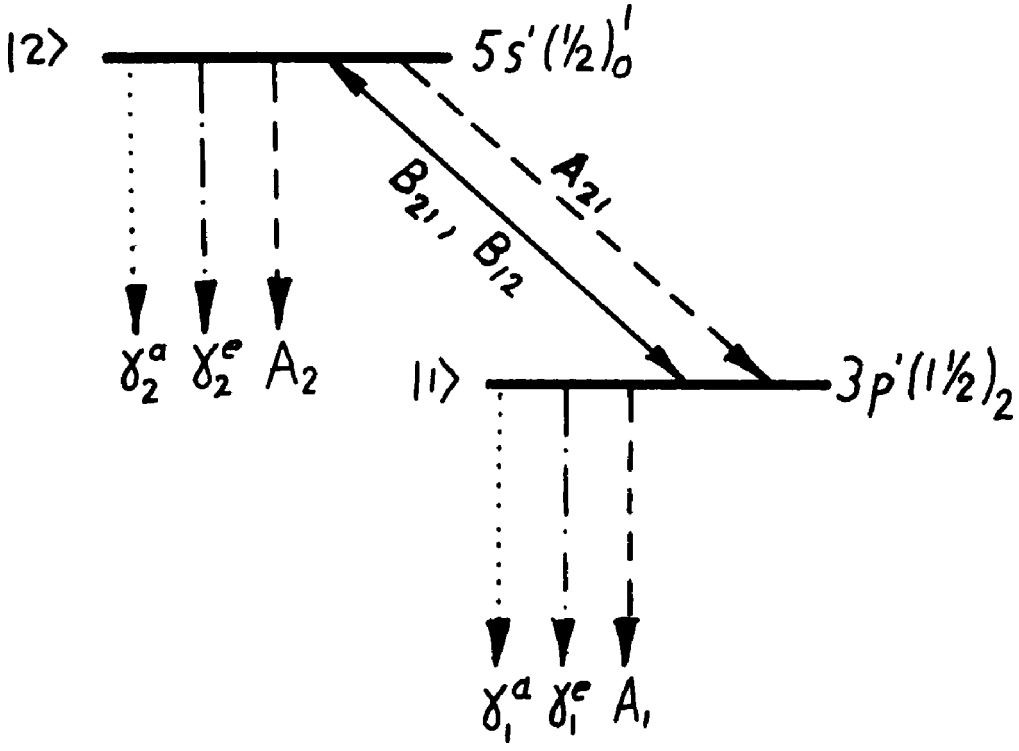

Figure II.2 - Excitation and De-excitation Parameters

is the pumping rate of level i due to all remaining processes, i.e., processes due to electron impact from the ground state, and, for the upper laser level, collisions of Ne ground state atoms with the ^1S_oHe metastables. Cascading transitions from higher levels into (1) and (2) are also included in R_i.

If we remove the electromagnetic signal, we can write a second set of rate equations for our steady state atomic system.

$$\frac{dn_2'}{dt} = R_2' - \gamma_2 n_2' + \gamma_{12} n_1' = 0 \qquad \text{(II.12a)}$$

$$\frac{dn_1'}{dt} = R_1' - \gamma_1 n_1' + \gamma_{21} n_2' = 0 \qquad \text{(II.13a)}$$

n_1', n_2' are the populations of the upper and lower laser levels in the absence of the electromagnetic field. The pumping rate R_i are functions of pressure and current. In order to eliminate their effects, we assume that they are basically unchanged by the presence of the laser radiation field. We can justify this assumption by pointing out that the R_i represent excitations from levels which are not directly involved in the lasing mechanism. We thus assume:

$$R_1 = R_1' \qquad \text{(II.14a)}$$

$$R_2 = R_2' \qquad \text{(II.14b)}$$

Subtracting now equation (II.12a) from equation (II.12) and equation (II.13a) from equation (II.13) and forming the ratio $\Delta n_1/\Delta n_2$, we obtain:

$$\frac{\Delta n_1}{\Delta n_2} = - \frac{\gamma_2 - \gamma_{21}}{\gamma_1 - \gamma_{12}} \qquad \text{(II.15)}$$

The transition rates on the right hand side of equation (II.15) contain radiative parts as well as effects due to atom-atom collisions and electron atom collisions. We can write more explicitly:

$$\gamma_2 = A_2 + \gamma_2^a + \gamma_2^e \qquad \text{(II.16)}$$

$$\gamma_1 = A_1 + \gamma_1^a + \gamma_1^e \qquad \text{(II.17)}$$

$$\gamma_{21} = A_{21} + \gamma_{21}^a + \gamma_{21}^e \qquad \text{(II.18)}$$

$$\gamma_{12} = \gamma_{12}^a + \gamma_{12}^e \qquad \text{(II.19)}$$

A_1, A_2 are the total radiative transition probabilities from level $|1\rangle$ and $|2\rangle$. A_{21} is the Einstein coefficient for spontaneous emission from level $|2\rangle$ to level $|1\rangle$, in our case for the transition $\lambda = 6328\text{Å}$ $(5s'(1/2)_1^0 \rightarrow 3p'(1\ 1/2)_2)$. The index a indicates that only atoms are involved in the excitation and de-excitation, while the index e signifies the participation of only electrons in the energy transfer

processes.

Since the upper and lower levels, $5s'(1/2)_1^0$ and $3p'(1\ 1/2)_2$, are 1.9625 ev apart, a thermal energy exchange between atoms of these two levels is very unlikely because the energy separation between them is much larger than $k \cdot T$. [$\approx$ .03 ev]. We thus neglect the atomic coupling parameters γ_{12}^a and γ_{21}^a, and equation (II.15) becomes:

$$\frac{\Delta n_1}{\Delta n_2} = - \frac{A_2+\gamma_2^a+\gamma_2^e-\gamma_{21}^e-A_{21}}{A_1+\gamma_1^a+\gamma_1^e-\gamma_{12}^e} \qquad \text{(II.20)}$$

Since γ^a is proportional to the density of the ground state atoms and thus to the pressure, and γ^e is proportional to the electron density and thus to the current (this is accurate for He-Ne lasers), the measurement of $\Delta n_1/\Delta n_2$ in dependence of pressure and current will give us information about the electronic and atomic parameters in equation (II.20).

The collisional de-excitation is mainly due to processes of the kind

$$Ne(3p'(1\ 1/2)_2) + Ne(0) \rightleftarrows Ne(3p) + Ne(0) \pm \Delta E \qquad \text{(II.21)}$$

for the lower laser level and

$$Ne(5s'(1/2)_1^0) + Ne(0) \rightleftarrows Ne(5s) + Ne(0) \pm \Delta E \qquad \text{(II.22)}$$

$$Ne(5s'(1/2)^0_1) + He(0) \rightleftarrows Ne(0) + He(2^1S_0) \pm \Delta E \quad \text{(II.22a)}$$

Ne(0) and He(0) represent Ne and He atoms in the ground state, and ΔE is the kinetic energy lost or gained by the atoms in the collision. We clearly see that, through collisional coupling the other 5s levels will be modulated. Transitions from these levels to the lower laser level will influence the modulation of the lower level. This effect is not included in our theory. However, the modulation of those levels is small, in the order of 1-3 percent, compared to 20-30 percent modulation of the $5s'(1/2)^0_1$ level and may therefore be neglected, at least in a first approximation.

II.4 Excitation and De-excitation of Levels other than the Laser Levels

Experimentally it is observed that the populations of a large number of levels not directly participating in the lasing mechanism, are modulated.[4] This shows that these levels are somehow connected to the laser levels, either through radiative or collisional processes. Lilly and Holmes[5] observed strong atomic collisional coupling between the $5s'(1/2)_1^0$ upper laser level and the adjacent $5s'(1/2)_0^0$ level. This can be expected since these two levels are less than 1kT apart. The process responsible for this energy exchange can be written

$$Ne(5s'(1/2)_0^0) + Ne(0) \rightleftarrows Ne(5s'(1/2)_1^0 + Ne(0) \pm \Delta E \qquad (II.23)$$

The study of the pressure dependence of this effect will yield the atomic collision rates involved in this process. We further observed a current dependence of the energy exchange between the two levels, suggesting that besides atom-atom collisions, atom electron collisions are also responsible for the energy transfer between the two levels.

$$Ne(5s'(1/2)_0^0) + e \rightleftarrows Ne(5s'(1/2)_1^0) + e \qquad (II.24)$$

The situation is, in a simplified version, shown in Figure (II.3).

The rate equation for level $|1\rangle$ $(5s'(1/2)^0_0)$ is given, in the presence of the laser radiation field, under steady state conditions:

$$\frac{dn_1}{dt} = R_1 - \gamma_1 n_1 + \gamma_{21} n_2 = 0 \qquad \text{(II.25)}$$

where the γ's have the same meaning as in the foregoing Chapter. A similar equation can be written down for the case of the absence of the laser radiation field.

$$\frac{dn_1'}{dt} = R_1' - \gamma_1 n_1' + \gamma_{21}' n_2' = 0 \qquad \text{(II.26)}$$

We assume again that the pumping rate of level $|1\rangle$, which accounts for the excitation of level $|1\rangle$ through all remaining mechanisms which are not directly connected with the lasing action, does not change in the presence of the laser radiation field. Hence we can set

$$R_1 = R_1' \qquad \text{(II.27)}$$

Subtracting equation (II.26) from equation (II.25), a simple expression for the population change ratios $\Delta n_1/\Delta n_2$ is obtained

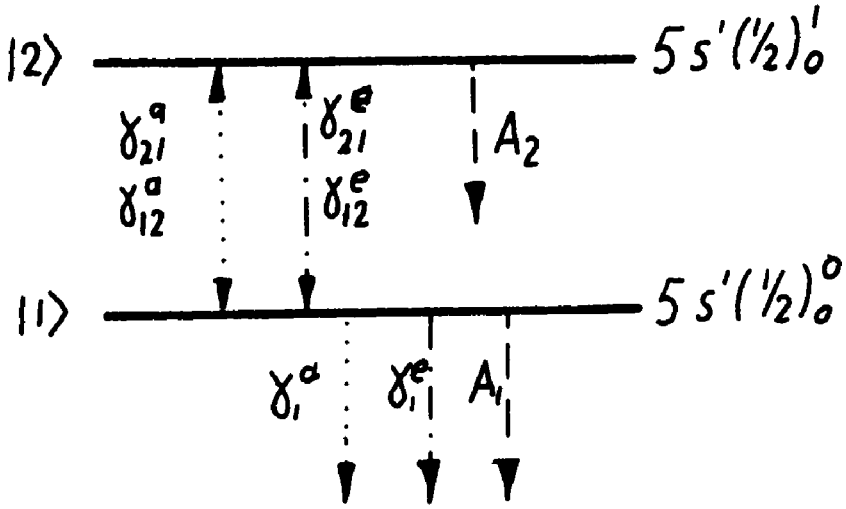

Figure II.3 - Coupling Parameters Between the $5s'(1/2)_1^0$ and the $5s'(1/2)_0^0$ Levels in Ne

$$\frac{\Delta n_1}{\Delta n_2} = \frac{\gamma_{21}}{\gamma_1} \qquad \text{(II.28)}$$

γ_{21} which describes the coupling between the $5s'(1/2)_1^0$ and the $5s'(1/2)_0^0$ levels, contains a pressure dependent part, γ_{21}^a, which is due to the atom-atom collisions, and a current dependent part, γ_{21}^e, which is due to electron-atom collisions. γ_1, the total de-excitation rate for level $|1\rangle$, is the sum of the radiative, atomic and electronic de-excitation rates. We write more explicitly for equation (II.28)

$$\frac{\Delta n_1}{\Delta n_2} = \frac{\gamma_{21}^a+\gamma_{21}^e}{A_1+\gamma_1^a+\gamma_1^e} \qquad \text{(II.29)}$$

Since the atomic parameters are proportional to the pressure unit the electronic parameters are proportional to the current, we expect in general for the intensity ratio of lines originating from the two levels:

$$\frac{\Delta I_1}{\Delta I_2} = \frac{a\cdot p + b\cdot i}{c + d\cdot p + e\cdot i} \qquad \text{(II.30)}$$

A more complicated case arises if we want to study collisional coupling between several levels. The following example may illustrate the situation (Figure II.4). If we are interested in the excitation of the $5s(1\ 1/2)_2^0$ level, for instance, we will have to consider energy transfer contributions from all other 5s levels. The rate equations for this system of atomic levels are:

$$\frac{dn_1}{dt} = R_1 - \gamma_1 n_1 + \gamma_{21} n_2 + \gamma_{31} n_3 + \gamma_{41} n_4 \qquad \text{(II.31)}$$

$$\frac{dn_2}{dt} = R_2 - \gamma_2 n_2 + \gamma_{12} n_1 + \gamma_{32} n_3 + \gamma_{42} n_4 \qquad \text{(II.32)}$$

$$\frac{dn_3}{dt} = R_3 - \gamma_3 n_3 + \gamma_{13} n_1 + \gamma_{23} n_2 + \gamma_{43} n_4 \qquad \text{(II.33)}$$

$$\frac{dn_4}{dt} = R_4 - \gamma_4 n_4 - B(n_4 - n_0) + \gamma_{14} n_1 + \gamma_{24} n_2 + \gamma_{34} n_3 \qquad \text{(II.34)}$$

$$\frac{dn_0}{dt} = R_0 - \gamma_0 n_0 + \gamma_{10} n_1 + \gamma_{20} n_2 + \gamma_{30} n_3 + \gamma_{40} n_4 + B(n_4 - n_0) \qquad \text{(II.35)}$$

These five equations lead to a quite complicated expression for the ratios $\Delta n_i / \Delta n_k$. It is almost impossible to analyze these expressions since products of excitation and de-excitation rates will occur, and no decision can be made about one factor if the other is not known.

A possible way to avoid these difficulties is to record the ratio $\Delta I_i / \Delta I_k$ as a function of the current for various pressures. We then can extrapolate our measured curves to zero pressure in order to obtain just the pure electronic effect. This method, however, will be inaccurate since we do not know exactly either to use linear, quadratic or other extrapolation. Since we are, however, working at very low pressures, a linear extrapolation may be justified in many

cases.

The above mentioned difficulty does not occur for the excitation of a group of levels which lie well above the upper laser level, so that atom-atom collisions can be excluded as a possible mechanism of energy transfer. This has been experimentally confirmed (See Chapter IV.7). The modulation of the populations of these levels are mainly caused by collisions of electrons with atoms of the $5s'(1/2)_1^0$ upper laser level and the $3p'(1\ 1/2)_2$ lower laser level. The levels excited through these almost pure electronic processes are the $nd(n\geq 4)$, $np(n\geq 5)$, $ns(n\geq 6)$ and $nf(n\geq 4)$ levels. Khaikin[6] has shown that the contribution of atoms excited by electrons from the lower laser level is very small. Thus we can write down the rate equation for this process which is illustrated in Figure (II.5)

$$\frac{dn_2}{dt} = R_2 - \gamma_2^e n_2 + \gamma_{12}^e n_1 = 0 \qquad \text{(II.36)}$$

This is the equation for the presence of the laser field. A second equation can be written down, for steady state, in the absence of the radiation field

$$\frac{dn_2'}{dt} = R_2' - \gamma_2 n_2' + \gamma_{12}^e n_1' = 0 \qquad \text{(II.37)}$$

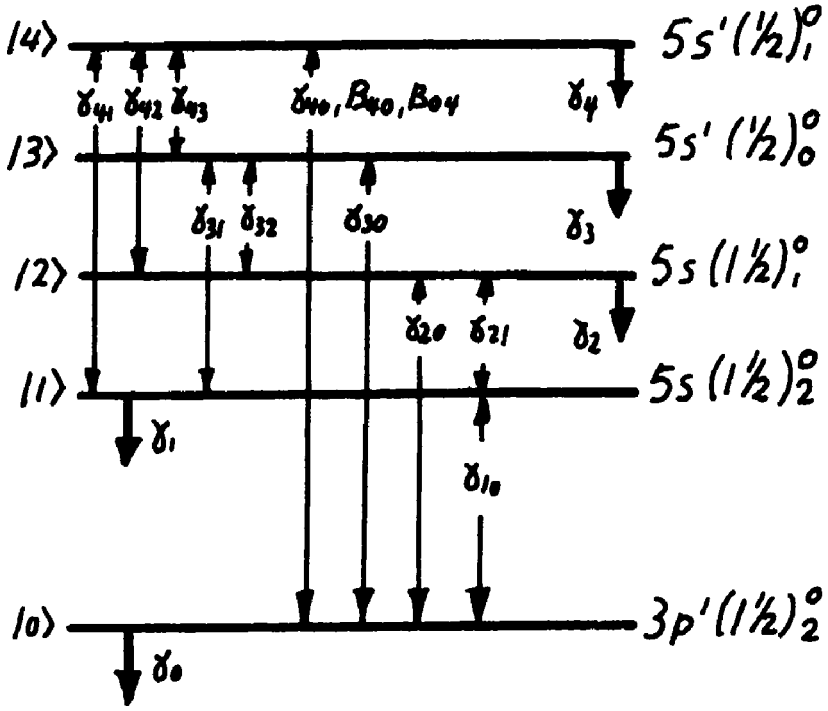

Figure II.4 - Coupling Parameters Between the 5s Levels in Ne

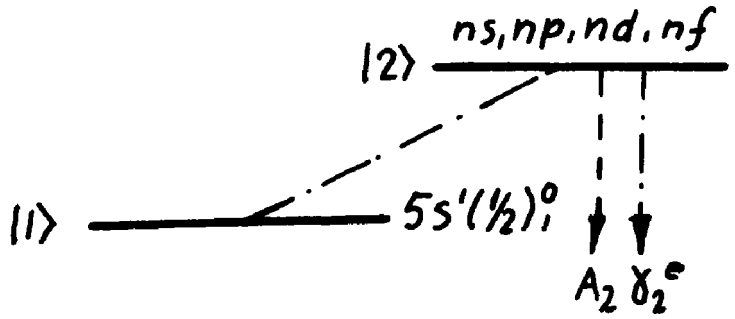

Figure II.5 - Excitation of Ne Levels above the $5s'(1/2)_1^0$ Level

From these two equations we obtain for the population change ratio

$$\frac{\Delta n_1}{\Delta n_2} = \frac{\gamma_{12}^e}{\gamma_2} \tag{II.38}$$

or more explicitly

$$\frac{\Delta n_1}{\Delta n_2} = \frac{\frac{\gamma_{12}^e}{A_2}}{1+\gamma_2^e/A_2} \tag{II.39}$$

Thus, for the intensity change ratio of two lines originating from level $|2\rangle$ and level $|1\rangle$ we expect the following dependence on the current:

$$\frac{\Delta I_2}{\Delta I_1} = \frac{a \cdot i}{1+b \cdot i} \times \text{const.} \tag{II.40}$$

III. THE EXPERIMENT

III.1 The Experimental Configuration

For our experiment we chose a He-Ne laser oscillating in the 6328Å line. It was also capable of oscillating in other lines in the visible. The experimental configuration is shown in Figure (III.1).

A Brewster angle laser tube, filled with a He-Ne gas mixture, is placed into a cavity consisting of two mirrors and a prism. The mirrors are dielectrically coated and have a reflectivity larger than 99% for 6328Å. Their curvatures are 2m and 3m, respectively. The prism is designed so that light enters and leaves at Brewster's angle, thus minimizing surface losses. It serves two purposes. First it helps suppress the competing infrared transitions, and second it enables us to select different laser transitions by reduction of dominance.[7]

The addition of a third electrode to the laser tube allows us to vary the current through only a small section of the gas discharge (between electrodes A and B), while the current through the long section (between electrodes B and C) is kept constant. Thus we can optimize, for a given pressure, the laser output power of the long section and assume the strongest interaction between the laser radiation field and the plasma in the small section between electrodes A and B. In our experiment we were able to vary the current in

the small section of the tube between 5mA and 70mA. The current range for the large section was between 5mA to 40mA, a range large enough to choose an optimum current for maximum laser output for all pressures considered in this experiment.

A ballast volume is attached to the laser tube, slowing down the process of contamination of the gas in the discharge tube. The tube is permanently connected to a vacuum system with an oil diffusion pump which is capable of pumping the system down to 10^{-5} Torr.

Both ends of the laser tube are enclosed by plexiglass cells, one of which if filled with methane gas. The cells help to reduce dust in the optical path, and the methane gas strongly absorbs radiation of the 3.39μ infrared laser transition in the He-Ne laser.[8]

In order to suppress superradiant infrared transitions in the laser tube, small permanent magnets are placed along the discharge tube. In resonators with small losses it is sufficient to broaden the gain profile of the infrared lines through Zeeman splitting by a few hundred MH_z.[9] The Doppler widths of the visible transitions which are around 1.6 GH_z, are hardly affected by the magnetic splitting, while the gain of the infrared transitions with Doppler widths of a few hundred MH_z is strongly reduced. Permanent magnets*

*Available from Edmund Scientific, No. P-40, 818.

of only a few hundred Oersted are sufficient to achieve the desired gain reduction.

The spontaneously emitted sidelight from the small discharge tube section is focused by means of a lens and, optionally, through a slit and a wratten filter #15 into a 1/4 meter Ash Jarrel monochromater, and detected by a photo-multiplier, type RCA IP 28. The signal is fed into a PAR lock-in amplifier, model HR-8. The laser beam is interrupted at a rate of 50 H_z by means of a chopping wheel which also provides the reference signal, by means of an electrostatic probe. The change ΔI of the sidelight intensity indicated by the lock-in amplifier, is recorded as a function of the discharge current on a XY-recorder.

In order to reduce the heat produced by very high currents in the small discharge section, a blower was used to cool down this section of the tube.

In the following paragraphs we will describe in more detail the procedure of setting up this experiment.

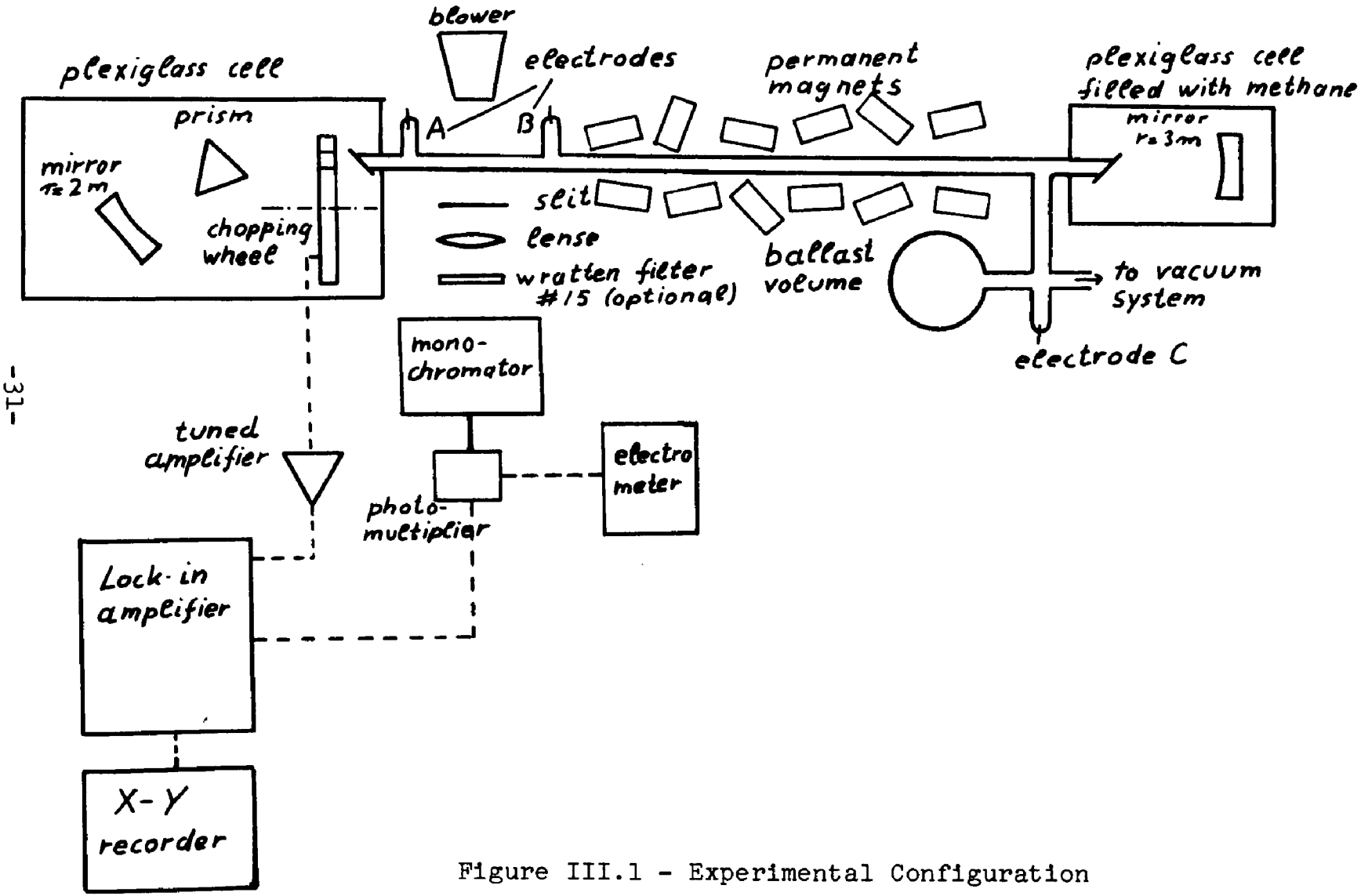

Figure III.1 - Experimental Configuration

III.2 Construction, Alignment and Operation of the Laser

Our experiment was set up on an I beam of 29 cm width and 350 cm length. As discharge tube we chose heavy wall pyrex tubing of 4.2 mm inner diameter. The tube was supported by seven kinematic mounts which were attached to magnetic bases, (Figure III.2).

In order to guarantee optimum straightness of the laser tube, we employed the following procedure of alignment, (Figure III.3). With the high transmission mirror removed, the 6328Å alignment laser beam was centered on the high reflectivity mirror parallel to the supporting surface plane. This adjustment was performed with the aid of the two plane mirrors, a and b. The high reflecting mirror then was adjusted that the reflected beam was directed back into the direction of the incident beam. Next, we inserted the high transmission mirror into the beam's path, thus forming a spherical Fabry Pérot resonator together with the high reflecting mirror. After a few minutes of adjusting the high transmission mirror, we were able to observe resonance in the cavity.

Next we positioned the kinematic supports one by one. A mirror was temporarily introduced to divert the beam to a distant screen. A 30 cm long test tube section of exactly the same cross sectional dimensions as the later employed discharge tube, was placed between support 1 and support 2.

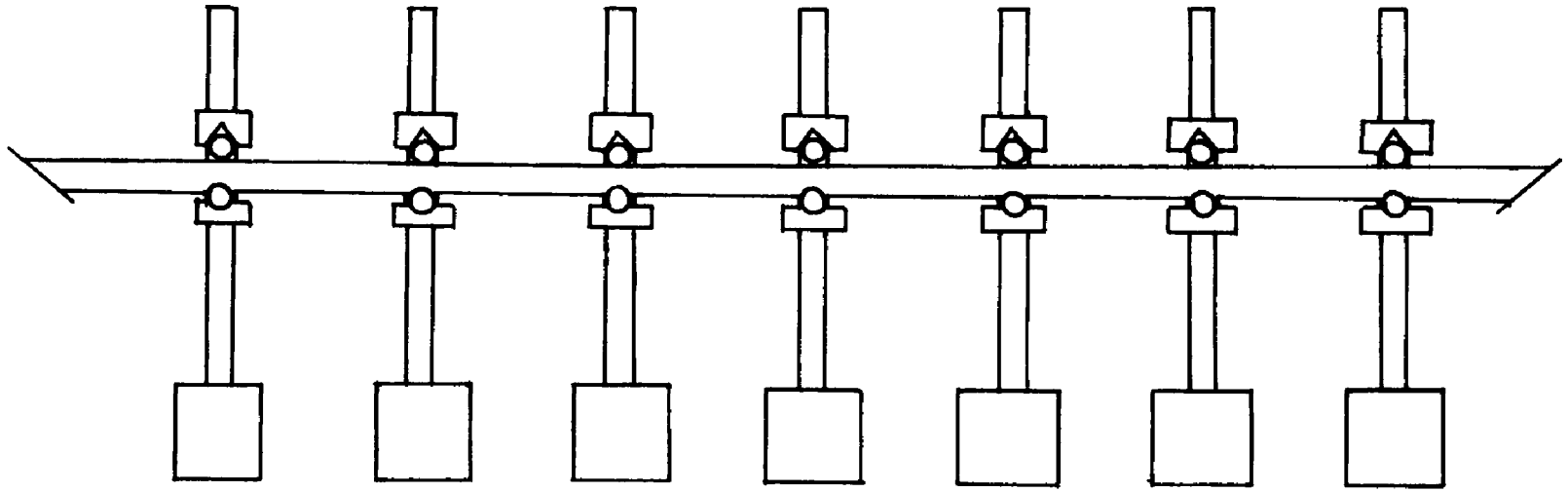

Figure III.2 - Laser Tube Supports

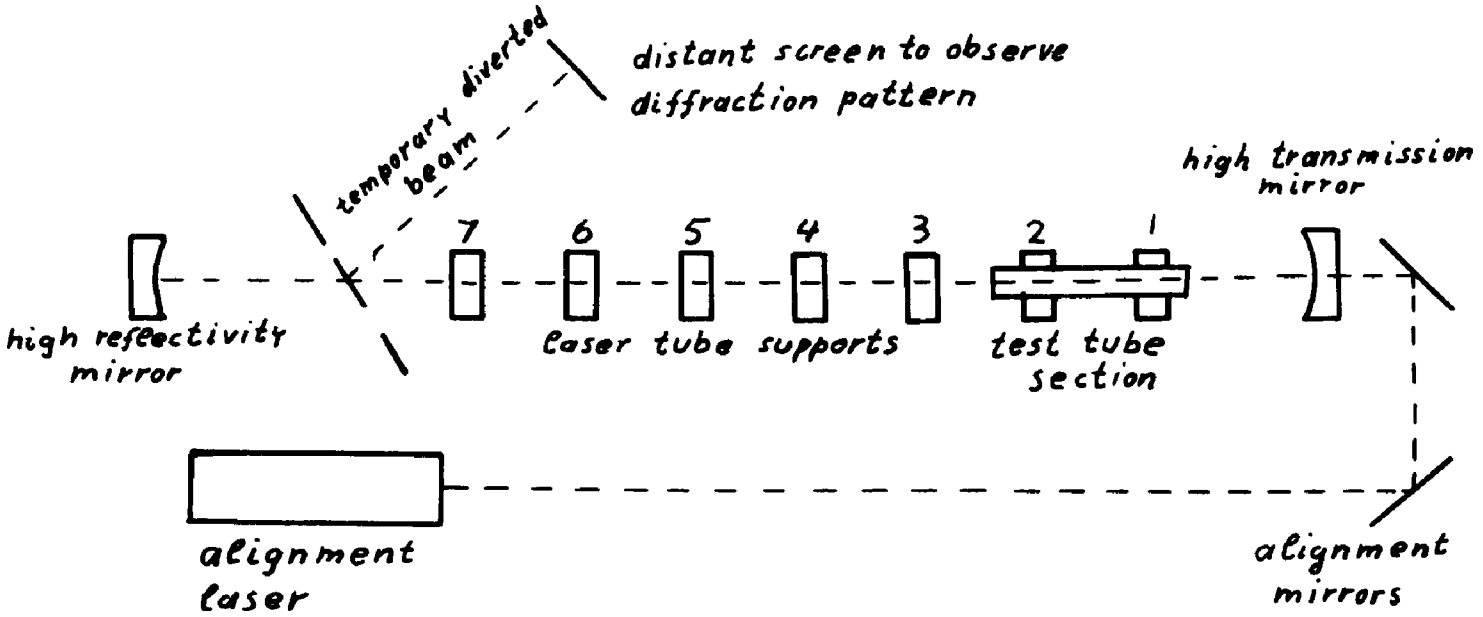

Figure III.3 - Laser Cavity Alignment Procedure

The two kinematic supports then were adjusted so that the transmitted beam through the tube section showed a totally symmetric circular diffraction pattern at the distant screen. This procedure then was repeated in sequence for the supports 2-3, 3-4, 4-5, 5-6 and 6-7.

The discharge tube then was placed on the kinematic supports and thoroughly tightened. Since tubing of the described kind is available normally in lengths of 110 cm, we had to join two pieces of tubing between support 5 and support 6.

At one end of the tube an assembly of a 9/18 pyrex ball joint and a commercial pyrex Ne sign electrode* of 15 mm outer diameter was attached, while on the other end an assembly of a 9/18 pyrex ball joint, a Ne sign electrode and an outlet arm to the vacuum system was attached. In order to add a third electrode, a small section of pyrex tubing of 15 mm outer diameter was placed between section a and b, and the third electrode then was connected at this place to the discharge tube. The arrangement is shown in Figure (III.4).

Next, stems of socket joints were cut at an angle of 56° which is approximately the Brewster angle for our quartz windows. The cut surface then was ground successively with

*Available from E.G.L. Company, Newark, New Jersey.

320, 400, 500 and 600 grit emergy paper, using dish detergent as a lubricant. Hereafter, the socket joints were attached to the ball joints, using DOW CORNING high vacuum grease. With the vacuum system pumping on the laser tube, the windows were glued to the ground surfaces of the socket joint with Torr Seal*. Figure (III.5) shows an assembly of a socket joint and a window.

After the Torr Seal had hardened, the alignment procedure was continued. The high transmission mirror and the window next to it were removed out of the ray path. A polaroid was introduced, and the window on the side of the high reflectivity mirror was adjusted for minimum reflection to the sides, i.e., at Brewster's angle. Here one of the advantages of using ball and socket joints is evident. It is not necessary to cut the socket joint at exactly Brewster's angle since the angle can be adjusted throughout the experiment. Since the alignment beam is refracted by the window glass, the high reflectivity mirror had to be readjusted to reflect the alignment beam back into itself. Hereafter the second window was attached to the tube, adjusted for minimum reflection to the sides, and the beam was readjusted again with the aid of the high reflectivity mirror. At the end, the high transmission mirror was placed back into the beam path and adjusted for resonance. Thus the preliminary optical alignment was completed (tube clamped straight, Brewster

*Available from Varian Associates, Palo Alto, California.

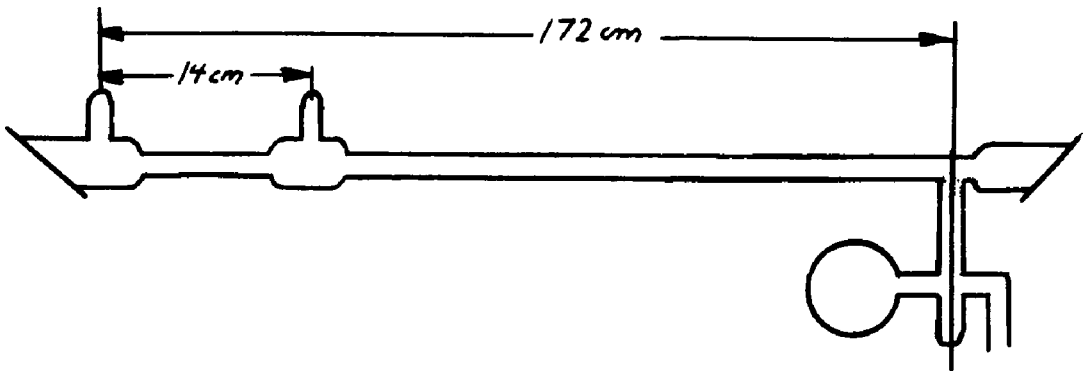

Figure III.4 - Discharge Tube

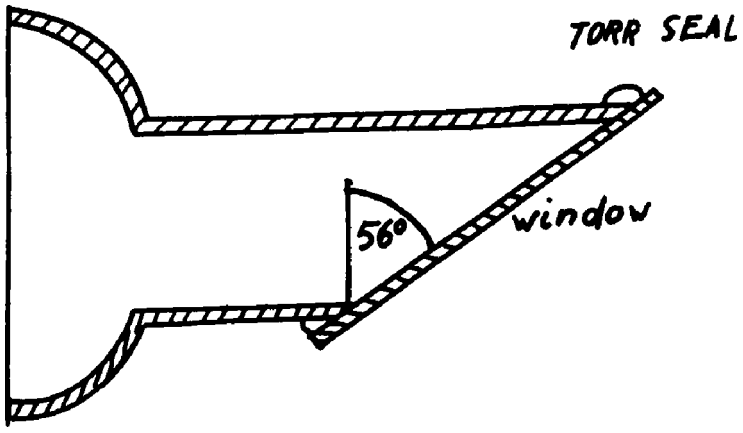

Figure III.5 - Socket Joint and Window Assembly

windows adjusted and laser mirrors aligned).

In the next step, the discharge tube had to be outgased. Contaminants exist on the glass walls, in the electrodes, in the grease between the ball and socket joints and at the stopcock separating the discharge tube from the vacuum system. The discharge tube was pumped down to approximately 3×10^{-5} torr and then filled with the He-Ne gas mixture to a pressure of approximately 1 torr. An ac-voltage of several thousand volts then was applied to two of the electrodes. After the tube had warmed up, the gas was pumped out slowly by periodically opening the stopcock to the vacuum system for a short moment. The tube was filled again, and the high ac voltage was applied between the third electrode and one of the remaining electrodes, and after the tube had warmed up, the gas was pumped out again. This whole procedure had to be repeated about 10 to 15 times. Throughout the outgasing procedure, a heat tape was wound around the ballast volume and the arm to the vacuum system in order to achieve outgasing of these parts, too.

After the described outgasing process, we found that the output power of the laser remained constant over a period of a week. This is a necessary requirement for the consistency of our measurements. Especially since currents up to 10mA were flowing through the small section of our laser tube, a thorough outgasing was essential for this experiment.

At this point we may remark that it is possible to use ball and socket joints with grease and still be able to achieve constant output power over a longer period of time. Ball and socket joints have basically two advantages. One was already mentioned earlier; we can easily adjust the windows at Brewster's angle. The second advantage is that we can remove the windows and use them again when we are required to change electrodes or do other changes to our system. The crucial point for using ball and socket joints is to outgas properly the discharge tube.

As for the outgasing procedure, we may note here that at low pressures over-zealous outgasing should be avoided. At high currents the electron bombardment can soften the glass walls opposite side of the electrodes.

After having established the basic operation of the laser in the 6328Å line, we wanted to introduce a prism into the cavity for two reasons. First we wanted to suppress the competing 1.15μ and 3.39μ infrared transitions, and secondly we wanted to have the option of selecting different visible laser transitions. This phenomena is called "Removal of Dominance" and was the first time described by A. L. Bloom[7]. In our experiment we used a special glass prism with very high dispersion. It was designed so that light enters and leaves at Brewster's angle, thus minimizing surface losses due to reflections. The alignment was accomplished in the following way: With both mirrors removed, the prism was ad-

justed for minimum deviation. The high reflecting mirror was put back and adjusted till the reference beam was back reflected into itself. Then the high transmission mirror was introduced again into the ray path and adjusted for resonance. The gas discharge then was initiated, and the output power of 6328Å laser line was optimized by alternately adjusting the two mirrors.

In order to achieve laser oscillation of some other visible lines (6401Å, 6293Å and 6118Å), we had to minimize the cavity losses because of the low gain of those lines. Therefore we replaced the high transmission mirror by a high reflectivity mirror, and after having chosen the right pressure, ($\simeq$ 1 Torr), we were able to separate the three wavelengths mentioned above.

A further reduction of the losses was accomplished by enclosing both ends of the laser tube by relatively airtight plexiglass boxes, thus cutting down on dust movement in the optical path. As already mentioned before, one of the boxes was filled with methane gas* which absorbs at the competing 3.39μ infrared laser transition.

Finally, small permanent ceramic magnets were placed along the discharge to tube to suppress superradiant infrared transitions in the laser tube (see Chapter III.1), and the blower was directed to the small discharge section in order

*See Chapter III.1.

to cool it.

We were now in a position to carry out our experimental investigation. The laser output was constant for a sufficiently long period of time (1 week), enabling us to make reproducible measurements. Also, we had made sure that laser oscillation occurred at only one transition at a time. In addition to the 6328Å line, the 6293Å, the 6401Å or the 6118Å lines could be made to lase. The post-alignment configuration is shown in Figure (III.6).

In the following paragraphs we will describe the vacuum system, the mechanical and electronical equipment necessary for the performance of our experiment.

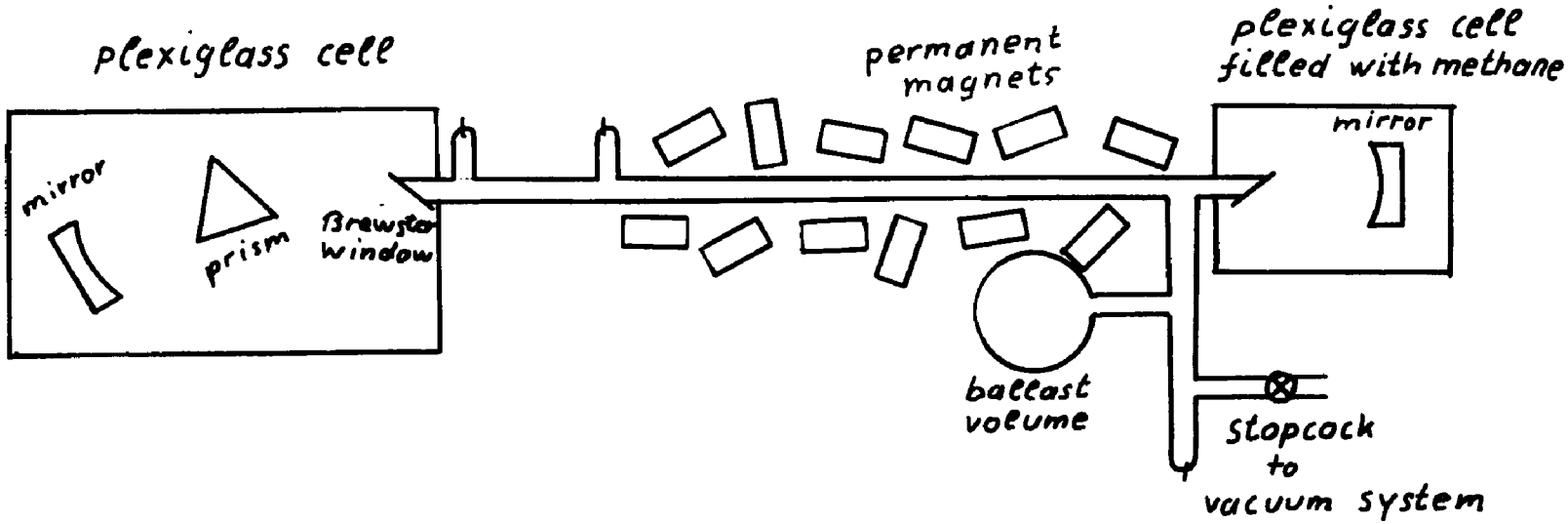

Figure III.6 - Post Alignment Configuration

III.3 The Vacuum System

An all glass vacuum system was employed in this experiment. It is shown schematically in Figure (III.7). A mechanical forepump of the type CENCO HVAC 14 was used to rough-pump the vacuum vessel. It was connected with a rubber hose to an oil trap, which again was connected via rubber hoses to the roughing line and to the oil diffusion pump. The oil trap was connected to the atmosphere through a stopcock which was opened after use of the vacuum system in order to prevent oil from the forepump to be sucked into the vacuum vessel. A cold trap was placed between the oil trap and the vacuum vessel to reduce contamination of the vacuum system with forepump oil. The vacuum vessel could be separated from the cold trap leading to the oil trap by means of a stopcock. As a vapor pump we employed a water cooled oil diffusion pump which could be separated from the oil trap by clamping the hose. A cold trap between the diffusion pump and the vacuum vessel prevented oil from the diffusion pump back steaming into the vacuum vessel. A 1 cm aperture vacuum stopcock separated the oil diffusion pump from the vacuum vessel. The cold traps used liquid nitrogen.

In order to measure the pressure, three different gauges were attached to the vacuum vessel. The thermcouple gauge measured pressures down to a few microns, the ion gauge could measure the lowest pressures we were able to obtain, about 10^{-5} mm Hg (Torr). The McLeod gauge, which

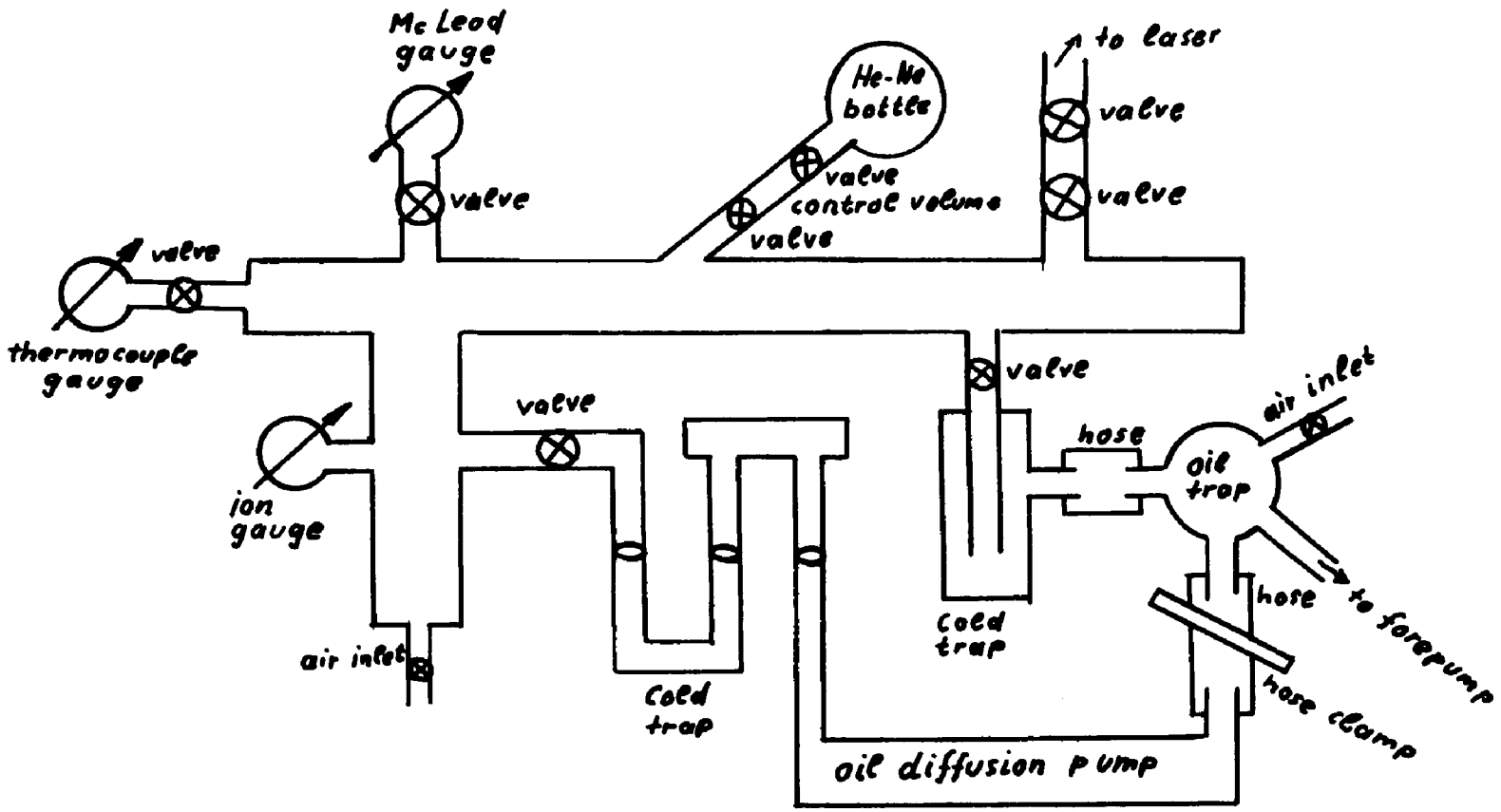

Figure III.7 - Vacuum System

could be separated from the vacuum vessel by means of a stopcock, was used to measure our filling pressures.

In order to fill the gas discharge tube, a pyrex bottle filled with a He-Ne mixture of 5:1 partial pressure ratio was attached to the vacuum vessel through two stopcocks. The small control volume between the two stopcocks controlled the amount of gas admitted to the vacuum vessel. In the following paragraphs we describe the procedure to attach a new gas bottle to the vacuum system.

The problem is to open the sealed bottle without contamination of the He-Ne gas mixture. A heavy piece of glass, which is later used to break the seal, is carefully pushed into the neck. A stopcock is then attached to the bottle neck, and this whole assembly is connected to the vacuum vessel. The neck is then evacuated to about 10^{-5} torr. At this pressure, the stopcock is closed and the assembly is broken off the vacuum vessel. The bottle seal is broken by tilting the bottle and letting the heavy glass piece fall on the seal. Hereafter, the assembly is again blown onto the vacuum system.

III.4 Calibration of Pressure Measurement

Since a pressure gauge which could directly be attached to the discharge tube, was not available, we had to resort to an indirect way of calibrating the pressure in the discharge tube. In Figure (III.8), v_1 is the volume of the

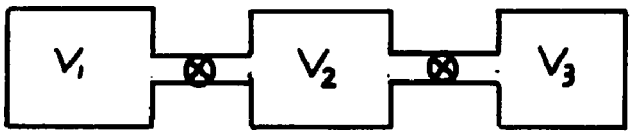

Figure (III.8) - Calibration of Pressure Measurement

gas discharge tube, v_2 is the control volume, and v_3 is the volume of the vacuum vessel. The volumes are separated by stopcocks S1 and S2.

Let us assume that volume v_1 is filled with the pressure p_0 and the two other volumes, v_2 and v_3, are evacuated, i.e., p_1, $p_2 << p_0$. If now stopcock 2 is closed and stopcock S1 is opened, we obtain the simple relationship, with p_{12} being the pressure in volume $v_1 + v_2$

$$\frac{p_0}{p_{12}} = \frac{v_1+v_2}{v_1} = \text{const} = \frac{p_0}{(1-\Delta)p_0} = \frac{1}{1-\Delta} \qquad \text{(III.1)}$$

where Δ, the percentage decrease of the pressure, is given by:

$$\Delta = \frac{v_2}{v_1+v_2} \cdot 100\% \qquad \text{(III.2)}$$

We now close stopcock 1 and evacuate the control volume v_2. Thereafter, stopcock 2 is closed and stopcock 1 is opened again. The pressure in v_1 was p_{12}, and the pressure in v_1 and v_2 is now p'_{12}. We can write

$$\frac{p_{12}}{p'_{12}} = \frac{v_1+v_2}{v_1} = \text{const} = p_{12}\,\frac{1}{p_{12}(1-\Delta)} \qquad \text{(III.3)}$$

Using equation (III.1), we can write

$$p'_{12} = p_{12}(1-\Delta) = p_0(1-\Delta)(1-\Delta) = p_0(1-\Delta)^2 \qquad \text{(III.4)}$$

If we repeat this procedure n times, we obtain for the nth pressure

$$p_{12}^{(n)} = p_0(1-\Delta)^n \qquad \text{(III.5)}$$

From this expression, we obtain for the percentage decrease of pressure per "squirt"

$$\Delta = 1 - e^{-\frac{1}{n}\,\ell n\,\frac{p_0}{p_{12}^{(n)}}} \qquad \text{(III.6)}$$

In order to obtain the calibration curve, we filled the discharge tube with a He-Ne gas mixture of 8 torr pres-

sure. Volumes v_2 and v_3 were evacuated, stopcock 2 was closed, stopcock 1 opened and closed again. Hereafter, stopcock 2as was opened, and the pressure in the vacuum vessel was measured with McLeod gauge. Then v_2 and v_3 were evacuated again, etc. The whole procedure was repeated 30 times, and the calibration curve is shown in Graph (III.1). The obtained value for Δ from this curve was

$$\Delta = 3.47\% \qquad \text{(III.7)}$$

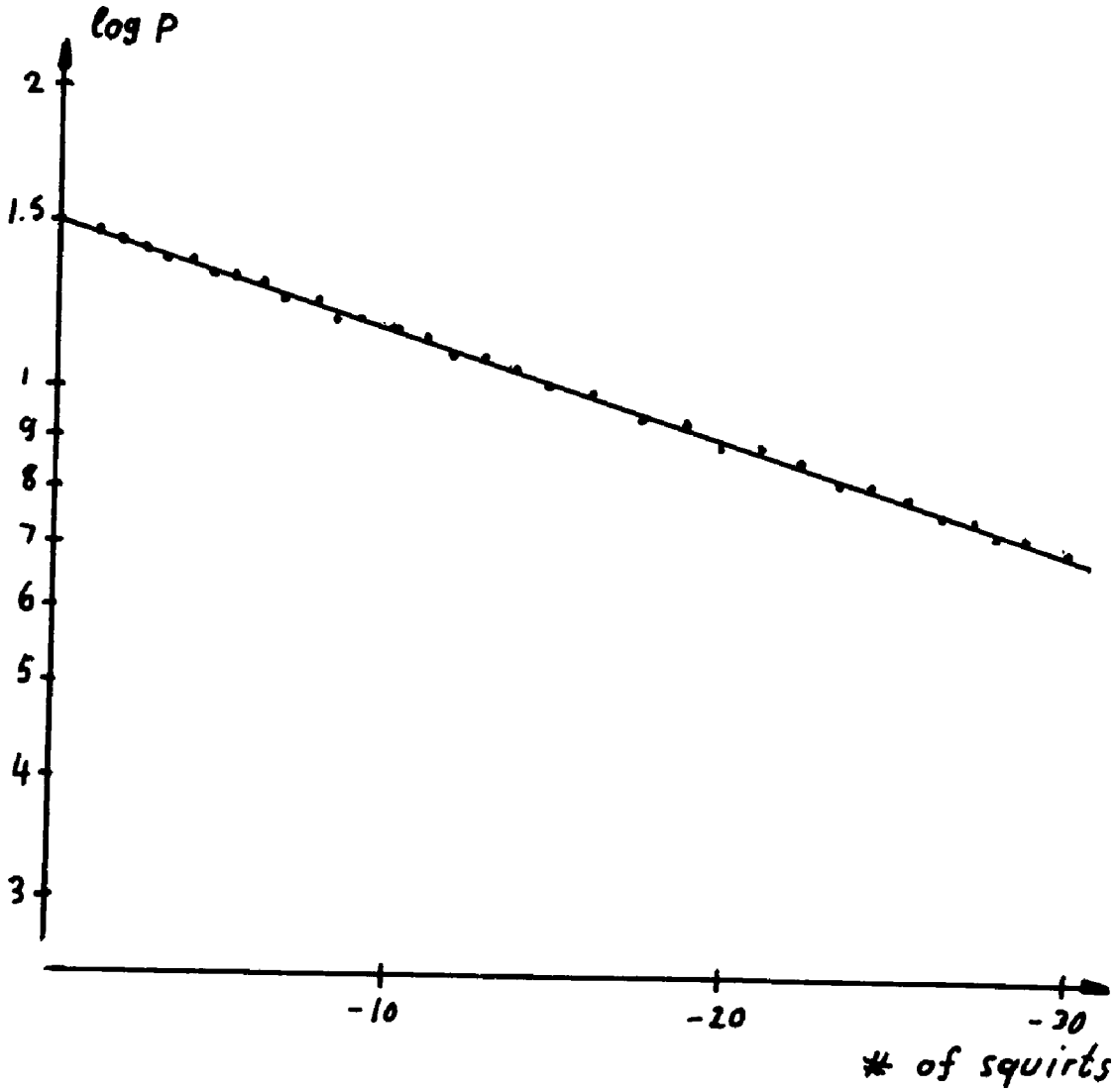

Graph III.1 - Pressure Calibration Curve

III.5 Mechanical Details

The basic mechanical equipment used in this experiment consisted of two laser mirror mounts and seven kinematic supports for the laser tube as well as two kinematic mirror mounts for the alignment mirrors. The alignment procedure requires the temporary use of two utility mirror mounts. The laser mirror mounts are shown in Figure (III.9) and Figure (III.9a).

On steel plate A two steel balls, B_1 and B_2 (not visible in figures) are exposed along its vertical axis. The steel balls are kept in position by a pivot shaped (P_1) and a V-groove shaped (V_1) bearing screwed to the mirror stand C. The plate can be moved around its vertical axis with the aid of micrometer head M_1 which bears against steel ball B_3 on plate A and is attached to the mirror stand C with a set screw. The holding force between the stand C and plate A is provided by small permanent ceramic magnets* m. In order to obtain movement in the horizontal plane, a second plate (D) is attached to plate A. Two steel balls, E_1 and E_2, are exposed on plate D along its horizontal axis. The steel balls are kept in position by a V-groove shaped (V_1) and a pivot shaped (P_2) bearing attached to plate A. The plate can be moved around its horizontal axis with the aid of a micrometer head which bears against a steel ball E_3 exposed

*Available from Edmund Scientific, No. P-40, 818.

on a cylindrical steel rod R extending from plate D. Again, the holding force is provided by small permanent magnets. On plate D, the aluminum mirror holder H is attached with screws. The two plates, A and D, as well as the stand C have a 1" diameter bore in the center, thus we did not have to move the mirror mount if we wanted to remove the mirror. We just removed plate D by overcoming the force of the magnets, and since the position of plate D is kinematically fixed, we could always maintain our alignment.

The design of the mirror holder H is quite simple and is shown in Figure (III.10). The mirror is pushed into the ring-shaped holder H. A protruding lip L prevents the mirror M from slipping through the holder. On the back, the mirror is kept in place by a plastic retaining ring G which is fastened by a set screw W.

The clamps for the laser tube are shown in Figure (III.11).

They consist of two separate pieces which ride on a 1/2" D post atop a magnetic base*. The lower piece has two steel balls while the upper piece has a groove in which retains a cylindrical brass rod. The laser tube is clamped between the steel balls and the brass rod so that exactly three points of contact exist. By loosening the set screws and by twisting slightly the lower half of the clamp, the

*Available from Ralmike's Tool-A-Rama, Springfield, New Jersey.

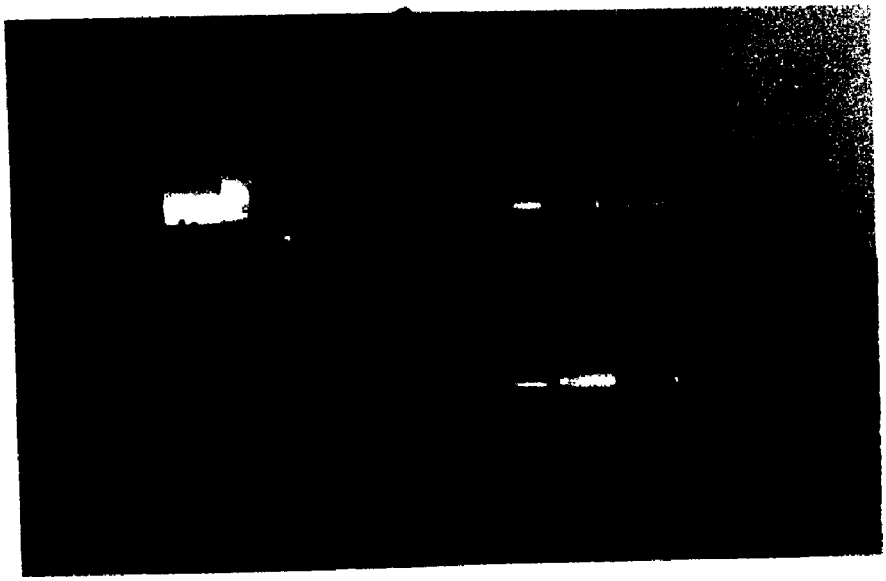

Figure III.9a - Laser Mirror Mount

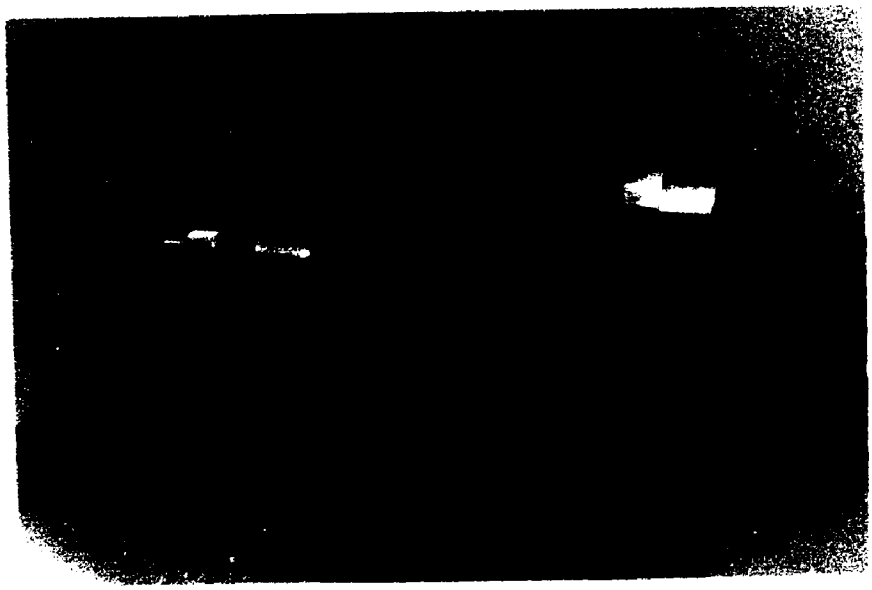

Figure III.9b - Laser Mirror Mount

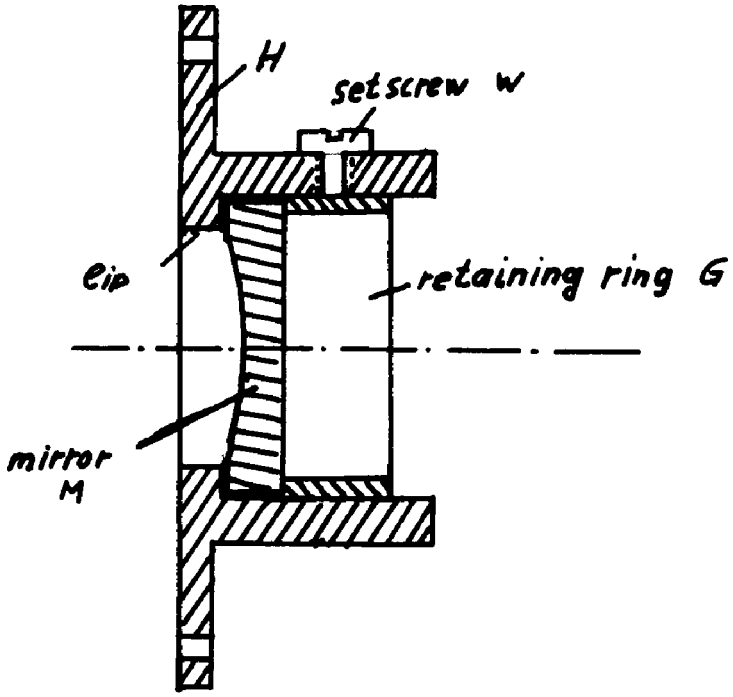

Figure III.10 - Laser Mirror Holder

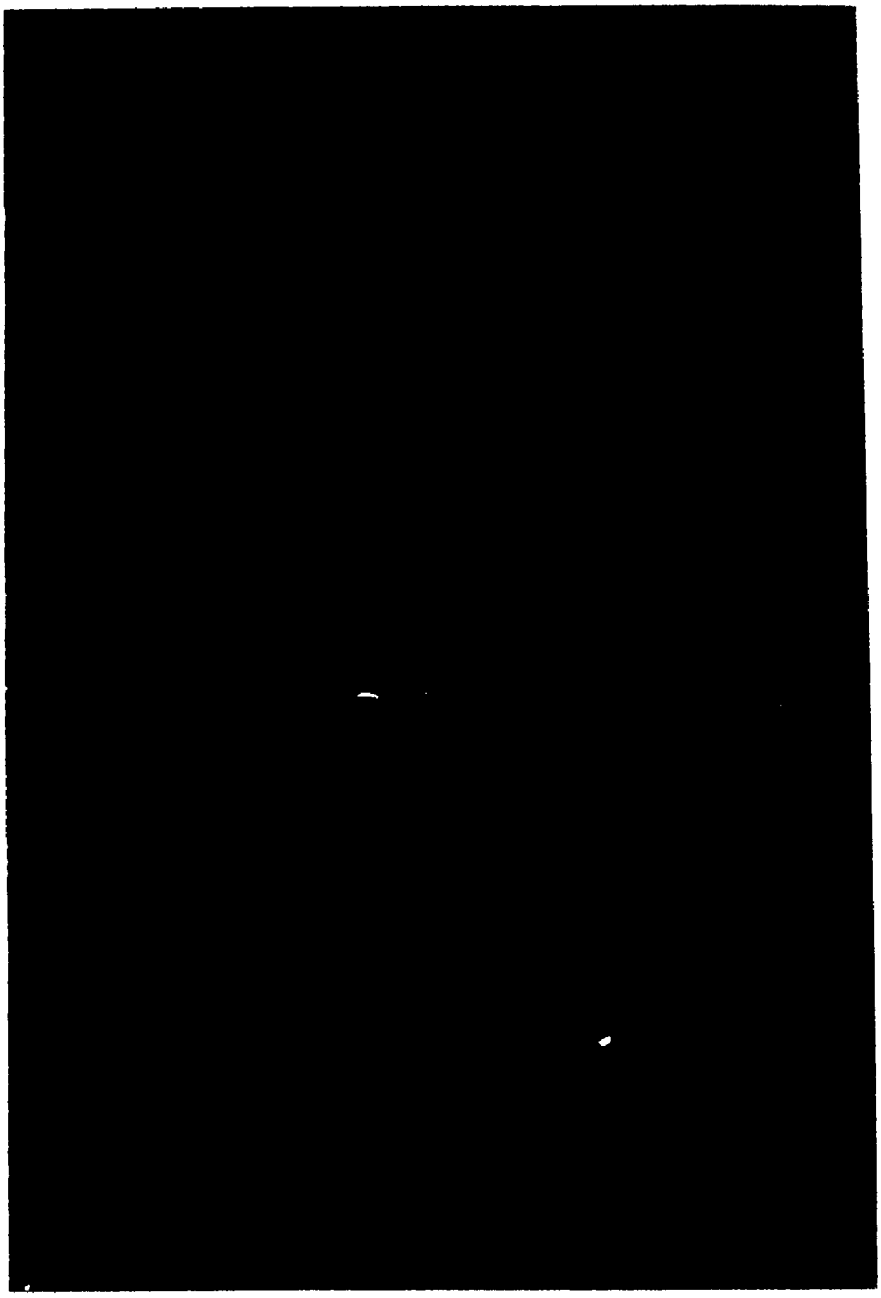

Figure III.11 - Laser Tube Clamp

position of the laser tube can be readjusted.

A picture of the kinematic mounts for the alignment mirror is shown in Figure (III.12).

The utility mirror mounts consist of two plexiglass plates, A and B. Plate A rides on a 1/2" D post P atop a magnetic base M and holds two micrometer heads C_1 and C_2. Three steel balls, S_1, S_2 and S_3, are exposed to plate B. Steel ball S_1 is gliding in a vertical V groove attached to plate A (not visible in figures), while S_2 and S_3 glide on 45° surfaces F_1 and F_2 glued to plate A and bear against the micrometer heads, C_1 and C_2. The holding force between the two plates is provided by a spring G and is directed in a way that the steel balls S_2 and S_3 are pressed against the 45° surfaces.

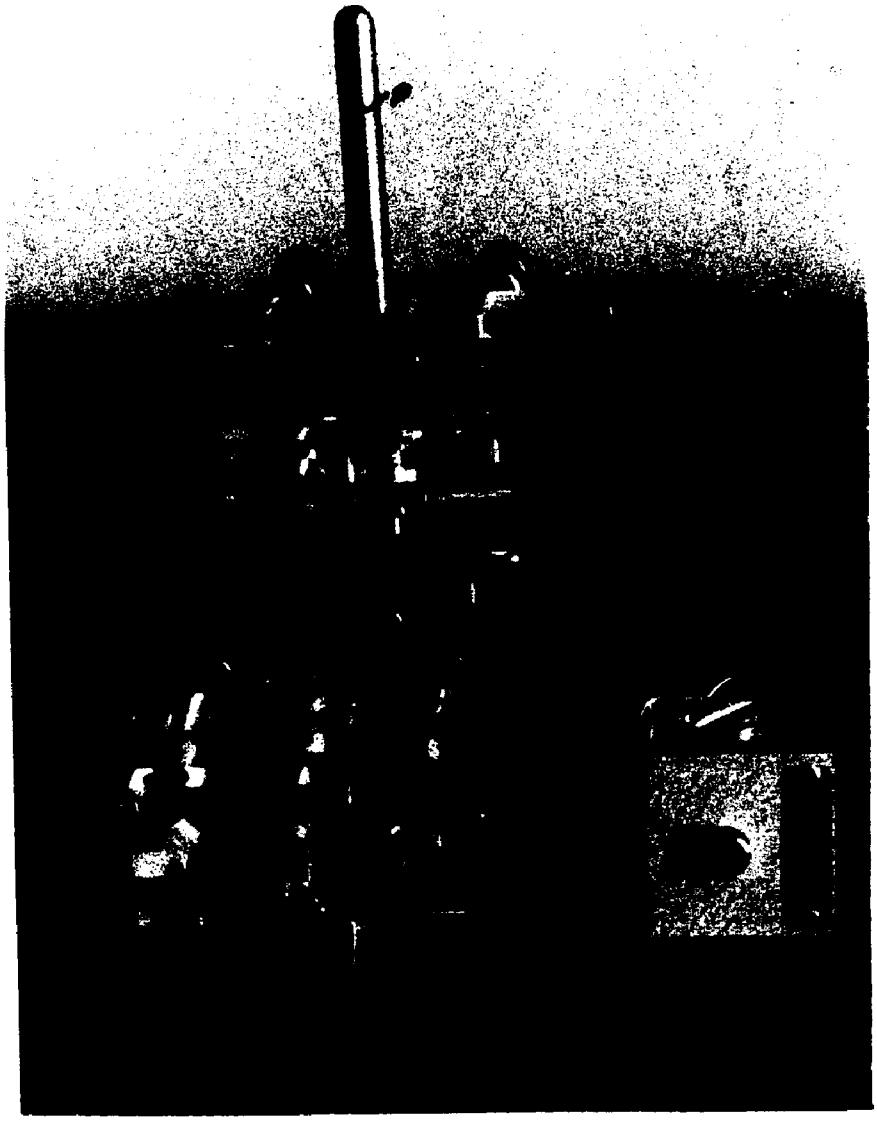

Figure III.12 - Alignment Mirror Mounts

III.6 Electronics

In order to maintain a dc-discharge through both sections of the laser tube and to vary the current independently in each section, we had to use two separate power supplies with two separate current regulators. Figure (III.13) shows a block diagram of the electrical circuit. The two high voltage power supplies were unregulated but filtered. The current regulation was provided by the two current regulators which allowed us to vary the current from 5-70 mA in the small section and from 5-40 mA in the large section of the discharge tube. The two resistors, R_1 and R_2, mounted close to the electrodes, were necessary to prevent plasma oscillations, since the gas discharge represents a negative resistance, and thus oscillations may occur due to stray capacitance.

Since only one HV power supply was available, we had to design a high voltage supply ourselves which would deliver around 9000V and a current of about 90 mA. The circuit is shown in Figure (III.14). The primary voltage of the HV transformer was controlled by two variacs. The AC voltage was rectified by a 1N3016 silicon diode* (PIV = 36000V) and filtered by a RC-combination. The output voltage was monitored by a micro ammeter in series with a 10MΩ resistor.

*Available from Semitronics Corporation, New York, New York.

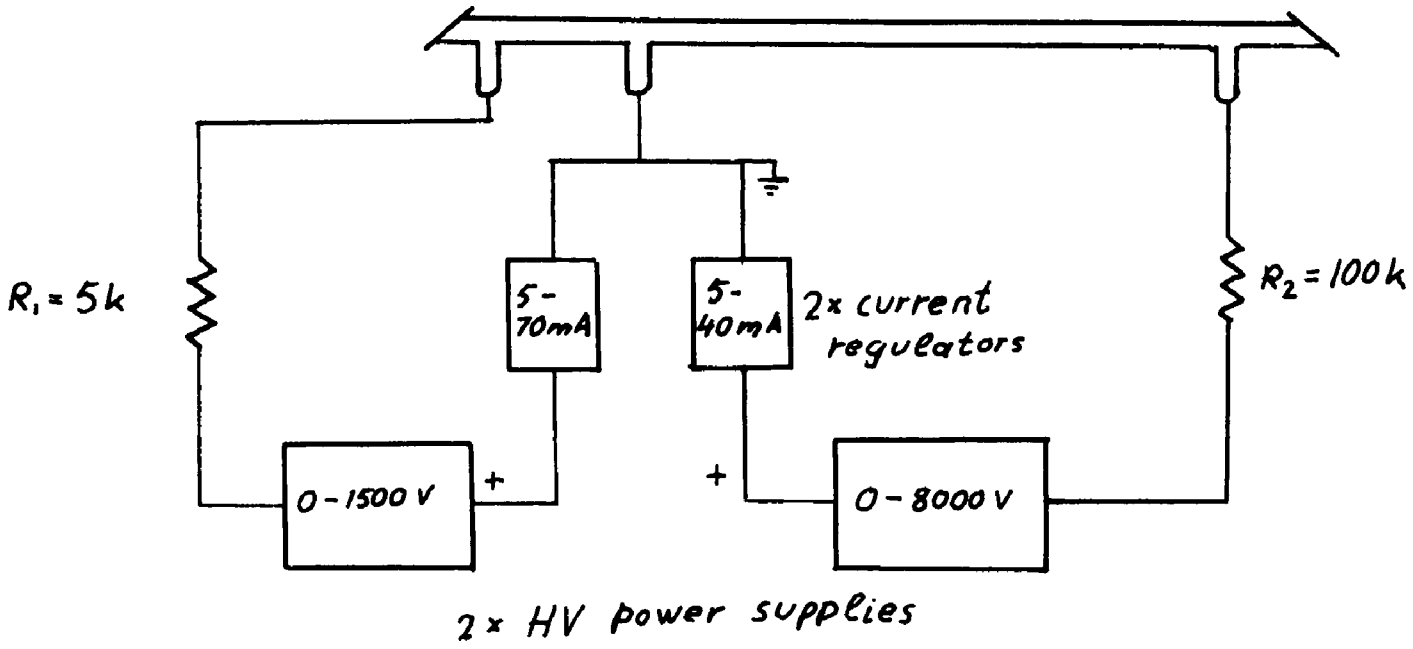

Figure III.13 - Electrical Supplies for Plasma Discharge

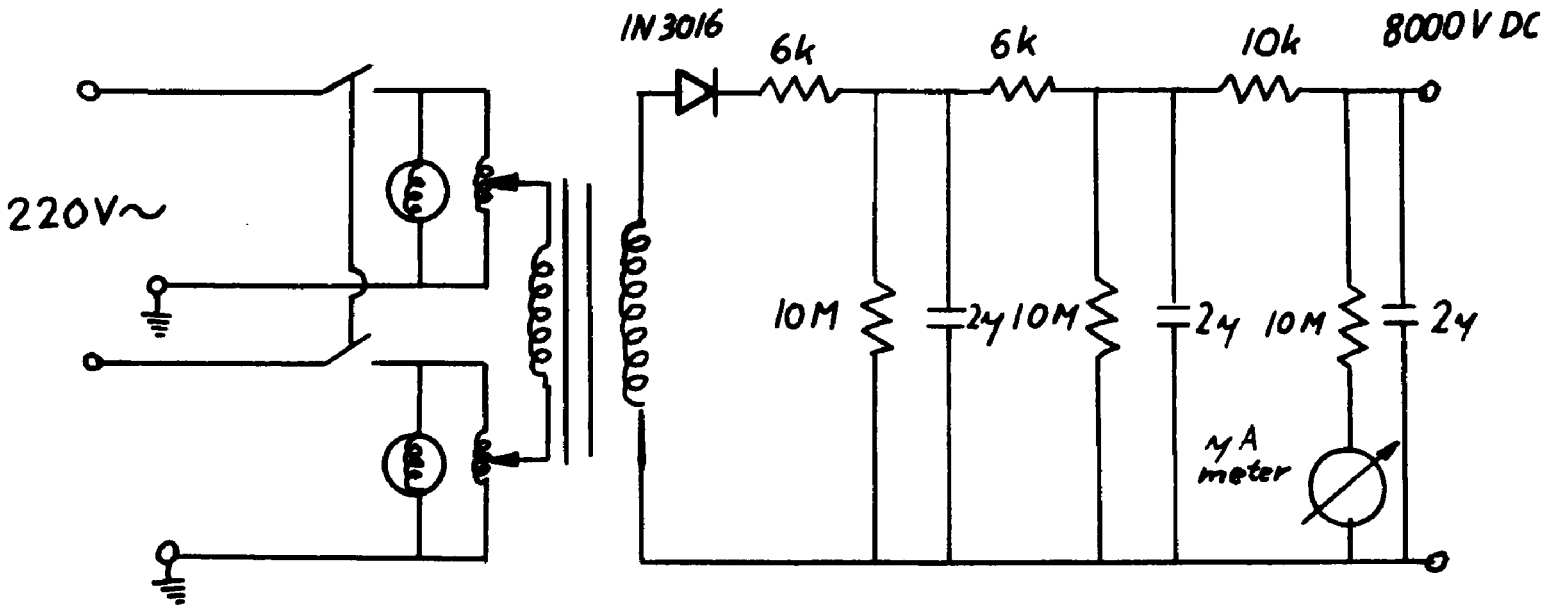

Figure III.14 - High Voltage Power Supply

The current in each section of the laser tube was controlled by a current regulator. The circuits of these current regulators are shown in Figure (III.15) and Figure (III.16). In Figure (III.15), the filaments of the single 6SN7 triodes can be switched on and off, increasing or decreasing the current by roughly 20 mA. In Figure (III.16), the filaments of the 6SN7 triodes closest to ground are controlled by switches. The fine adjustment of the current in both circuits can be accomplished by varying the potentiometer in the cathode circuit of one of the 6SN7 triodes. The current is measured by an ammeter between the cathode resistors and ground.

In order to monitor the output power of the laser, we designed a simple power meter. The circuit is shown in Figure (III.17).

The current of a solar cell was amplified by a μA741 Fairchild operational amplifier and monitored with a micro meter. The gain was controlled by 5 resistors, the values of which are shown in Figure (III.16). This meter was only used for measuring the relative output power, i.e., it was not calibrated. To obtain absolute power measurements, a Spectra Physics Model 401C power meter was used.

In order to derive the reference signal from the chopping wheel, we let the chopper change the electric field between to capacitor plates. The circuit is given in Figure (III.18).

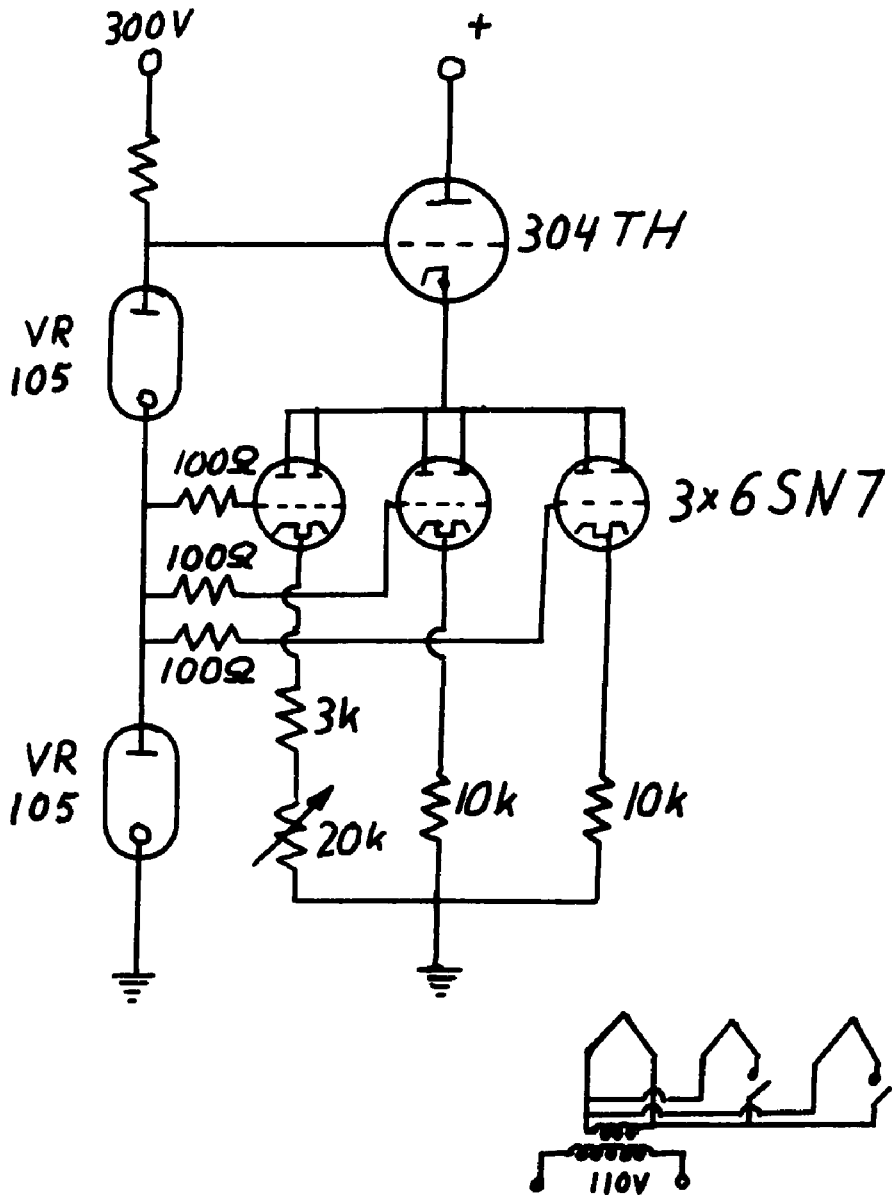

Figure III.15 - Series Current/Regulator for Small Section of Laser Discharge Tube

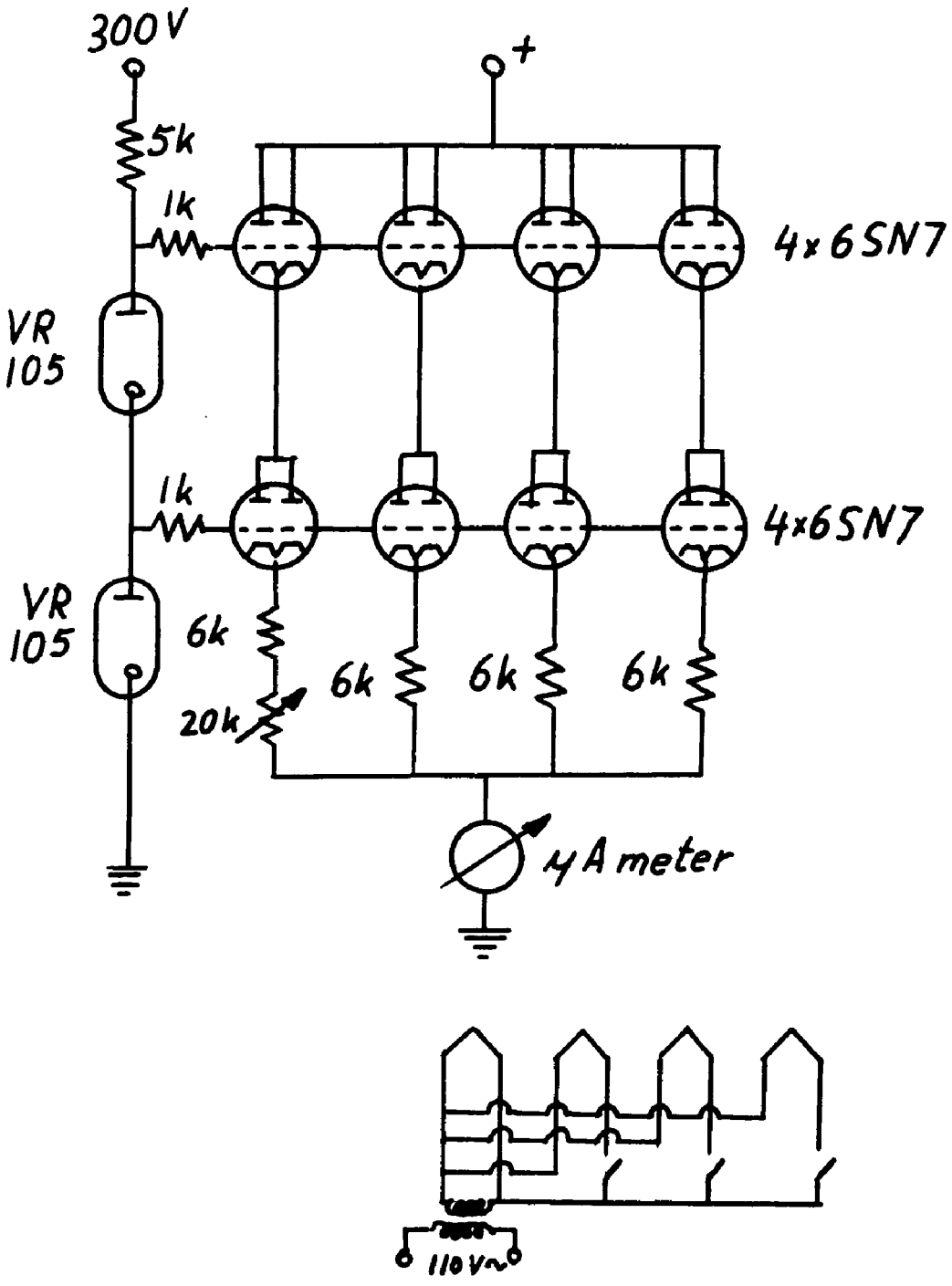

Figure III.16 - Series Current Regulator for Small Section of Laser Discharge Tube

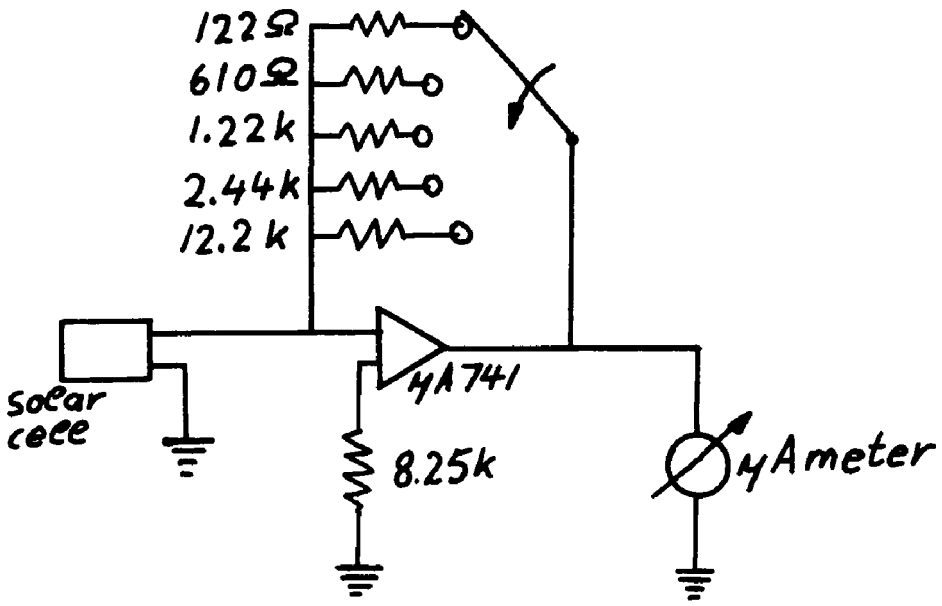

Figure III.17 - Circuit for Power Meter

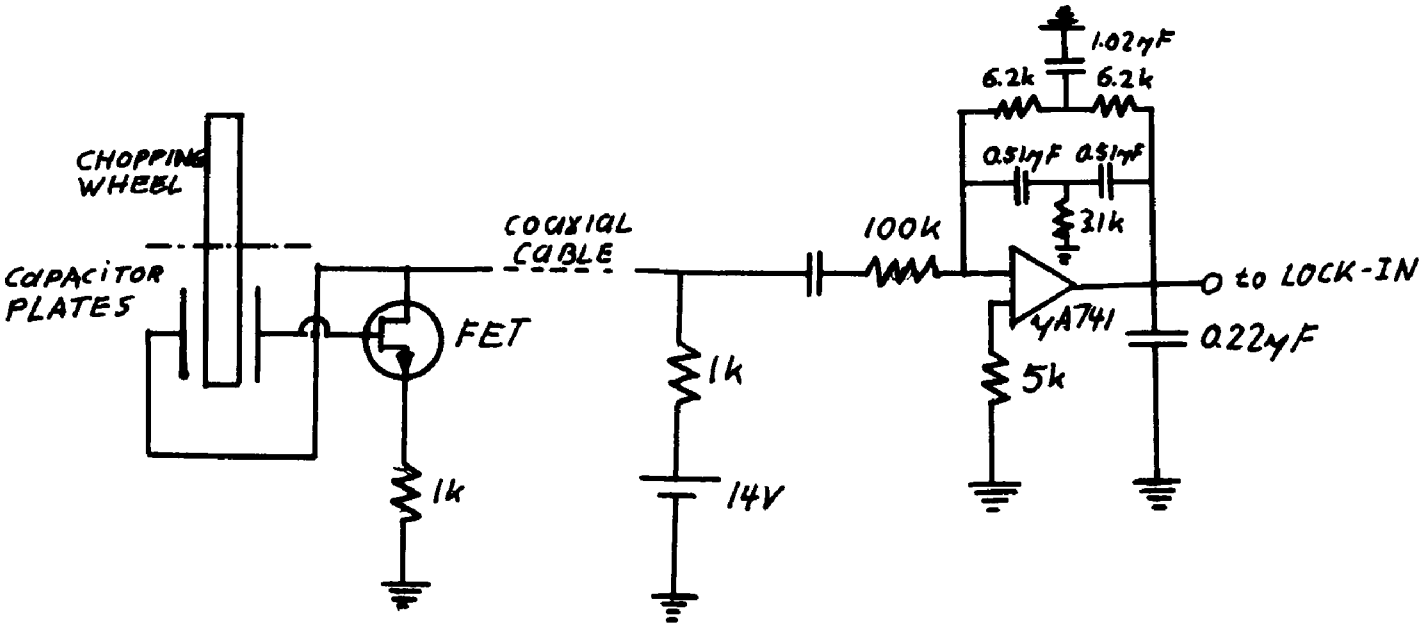

Figure III.18 - Reference Signal Generation

The reference signal picked up was provided by a high input impedance field-effect transistor. Signal and bias voltage were both transmitted on a common coaxial cable since the power supply could not be built into the chopping wheel. Over a small blocking capacitor and a twin T tuned amplifier the signal was then fed into the reference channel of the lock-in amplifier.

As a sidelight detector we used a RCA IP28 photomultiplier. This phototube has a S5 response, and its bias circuit is described in the RCA handbook for phototubes.[20]

It remains to be mentioned that our phase sensitive detector was a PAR lock-in amplifier, model HR8, and that the dc current from the photomultiplier was detected by a battery operated Keithly electrometer.

III.7 Calibration of the Optical Detection System

In order to compare intensities of light of various wavelengths, we had to take into account the spectral response of our measurement, i.e., the glass of the discharge tube, the focusing lens, the monochromator and the photomultiplier. As a standard radiant source we used a calibrated 200 Watt GE tungsten iodine lamp*. The spectral irradiance of this lamp was known for a distance of 50 cm if operated at 6.50 amperes. Since we were only interested in a relative calibration of our system, the exact distance was of minor importance. During our calibration we encountered some difficulties. First, we had to keep the current through the lamp constant at 6.5 A. A 1% change in current produces a 10% in the intensity of the lamp. The circuit used in our calibration is shown in Figure (III.19).

The supply voltage was obtained from a set of automotive 6V lead storage batteries. The crude adjustment of the current was done with the 8Ω rheostat, while the fine adjustment was accomplished with the 780Ω parallel rheostat. In order to monitor the current, we put a shunt of 1/1000Ω in series with the lamp. The voltage across the shunt was indi-

*Calibration at 2500Å, 3500Å, 7500Å, 15000Å and 25000Å was provided by the Eppley Laboratory, Inc., Newport, Rhode Island.

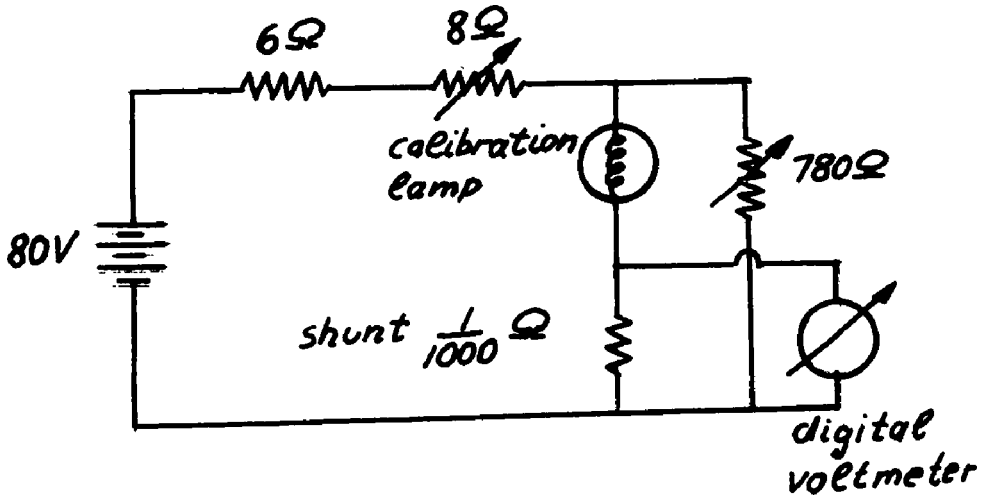

Figure III.19 - Control Circuit for Calibration Lamp

cated by a digital voltmeter* with estimated accuracy ±1μV. From our reading we had to subtract the voltage across the shunt which was indicated by the voltmeter when no current was flowing through the lamp. This voltage is due to thermal EMFS. We were able to keep the current constant to less than 0.3%. Therefore the error in our calibration was probably less than 4%.

The second difficulty occurred in avoiding light from second order diffraction in the monochromator. For wavelengths larger than 6000Å we observed an increase of the photomultiplier current caused by spurious light at 3000Å. This effect could be eliminated by putting a wratten filter #15** which has a strong cutoff region around 5000Å, in front of the monochromator. The calibration arrangement is shown in Figure (III.20), and the calibrated response curve of our system is given in Graph (III.2).

---

* Model Keithley 171 Digital Multimeter.

** Color correction filter, Tiffen Optical Company, Roslyn Heights, New York.

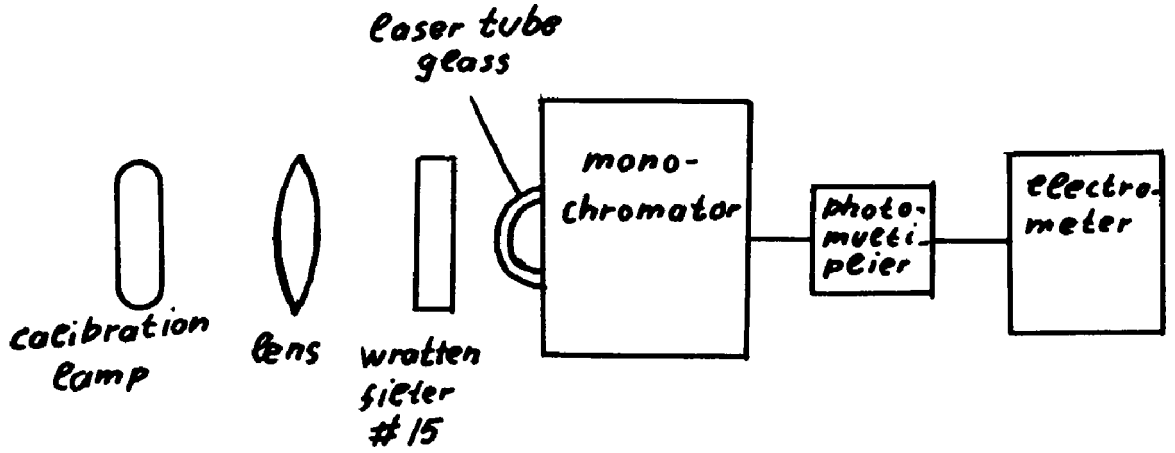

Figure III.20 - Optical Calibration Setup

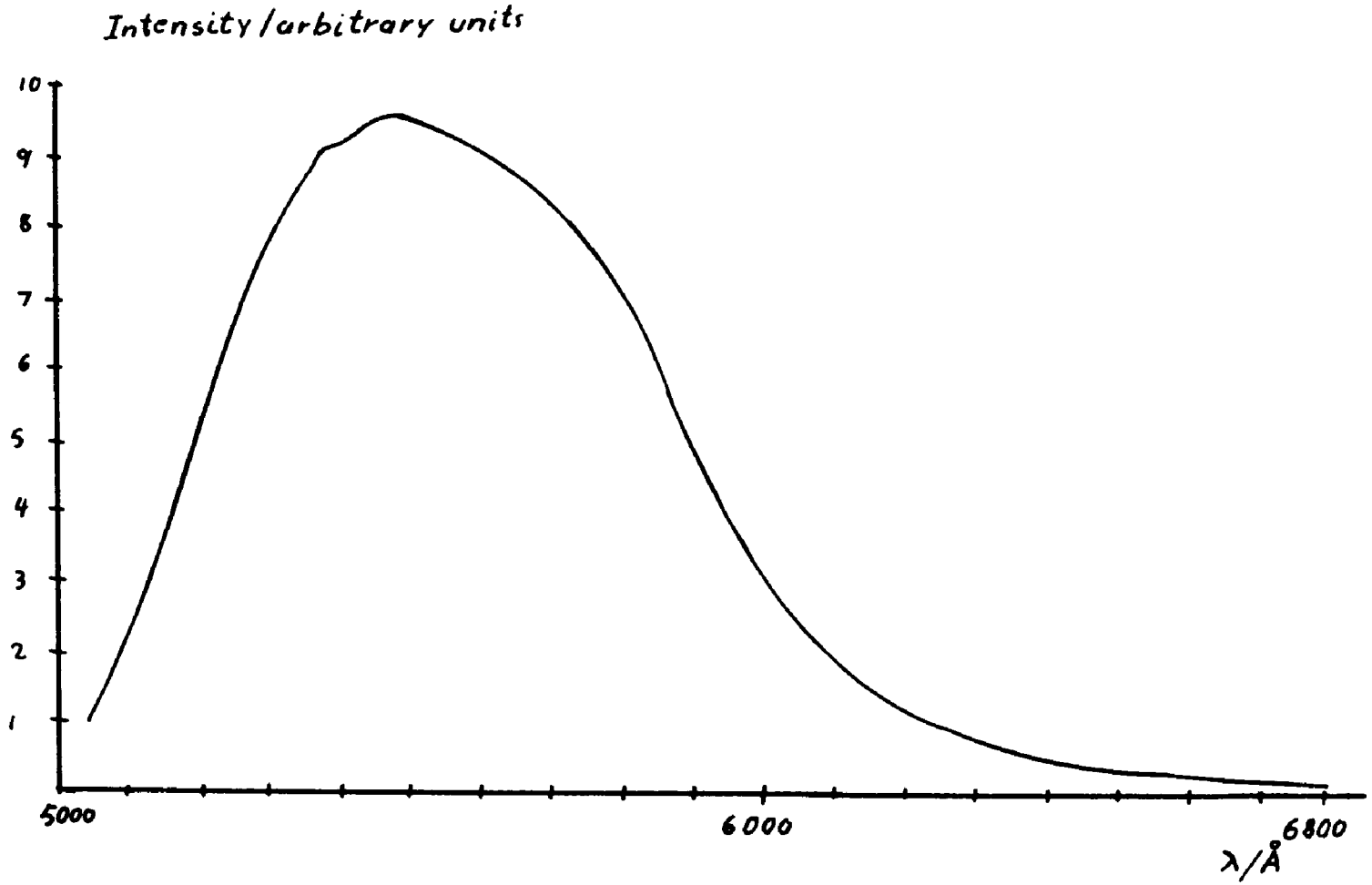

Graph III.2 - Optical Calibration Curve

III.8 Performance of the Experiment

Out of the whole set of lines of Neon, we were only able to resolve a few lines with our instruments without ambiguity. This drastically limited the number of measurements we could make. In our experiment we proceeded in the following way: The laser tube was filled with the He-Ne gas mixture at a selected pressure. After a warm-up period of about 10 minutes, the current in the long section of the tube was adjusted for maximum output power of the laser. For the pressures considered in our experiment, the current range for optimum output was between 10 and 20 mA.

In the next step, we selected the line under investigation by carefully peaking up the dc photomultiplier current. We then fed the ac signal into the PAR HR-8 lock-in amplifier (which had previously been calibrated uisng the procedure outlined in the manual). Using the phase control of the lock-in amplifier, we carefully zeroed the reading on the panel meter and then shifted the phase by 90° to obtain our reading. For each reading the gain of the lock-in amplifier was chosen for the largest possible deflection on the panel meter. The current was measured with a Simpson meter*, choosing always a range for maximum possible deflection on the meter.

*Model 260, Series 5P.

III.9 Care of Optical Surfaces

The output power of the He-Ne laser is very sensitive to losses, and a major source of losses is introduced by imperfect optical surfaces of the mirrors, the windows and the prism. While the quality of these surfaces are determined by the manufacturer and are naturally beyond our control, we could control the surface contamination. After experimenting for a while, we found out that the following cleaning procedures worked best. The mirrors were cleaned by putting a few drops (2-3) of 99% MOL pure acetone on the surface. By tilting the mirrors to all sides, the acetone was distributed over the whole surface and then carefully blown off the mirror with dry air (OMIT DUST REMOVER)*, starting from the center of the mirror. The glass surfaces of the prism and the windows were cleaned with a solution of Alconox detergent before put into our system. After being treated with this solution, they were washed with distilled water and blown dry with dry air. This procedure eventually had to be repeated several times until we were satisfied with the surface. We checked the surfaces by holding them against a strong incadescent light and looking from different angles against a dark background.

While in the system, the glass surfaces were cleaned with KODAK lens cleaning paper which was wrapped around a Q tip and soaked in acetone or absolute ethyl alcohol. Each

*Manufactured by Century Laboratories, Chicago, Illinois.

lens tissue could only be used for one wipe and then had to be replaced.

It may be mentioned here that the biggest improvement for the protection of the optical surfaces was to construct airtight plexiglass cells around each end of the laser tube.

IV. RESULTS AND THEIR DISCUSSION

IV.1 Preliminary Considerations

IV.1a. Proportionality of Intensity Changes of Lines Originating from Upper and Lower Laser Levels

Though we were very careful in suppressing all infrared oscillations by using permanent magnets and a methane cell, we had to prove that no other oscillations were affecting our laser levels, either by ending on them or by producing excessive cascade transitions into them. In order to do this, we had to show that the intensity changes of lines originating from the upper and lower laser levels, ΔI_2 and ΔI_1, are proportional to each other, independent of the intensity of the laser radiation field.[4,5,6] For a fixed current and a fixed pressure, we varied the output power of the laser by detuning the cavity from its optimum alignment. The result is shown in Graph (IV.1) and proves, within an experimental error, the proportionality of ΔI_1 and ΔI_2. Thus the changes of the ratio $\Delta I_2/\Delta I_1$ in dependence of current and pressure can clearly be interpreted as the effect of collision transfer.

IV.1b. Radiation Trapping

A gas emitting photons on a transition which has substantial absorption, tends to self-absorb or entrap these photons. If this "trapping" is significant enough, a photon

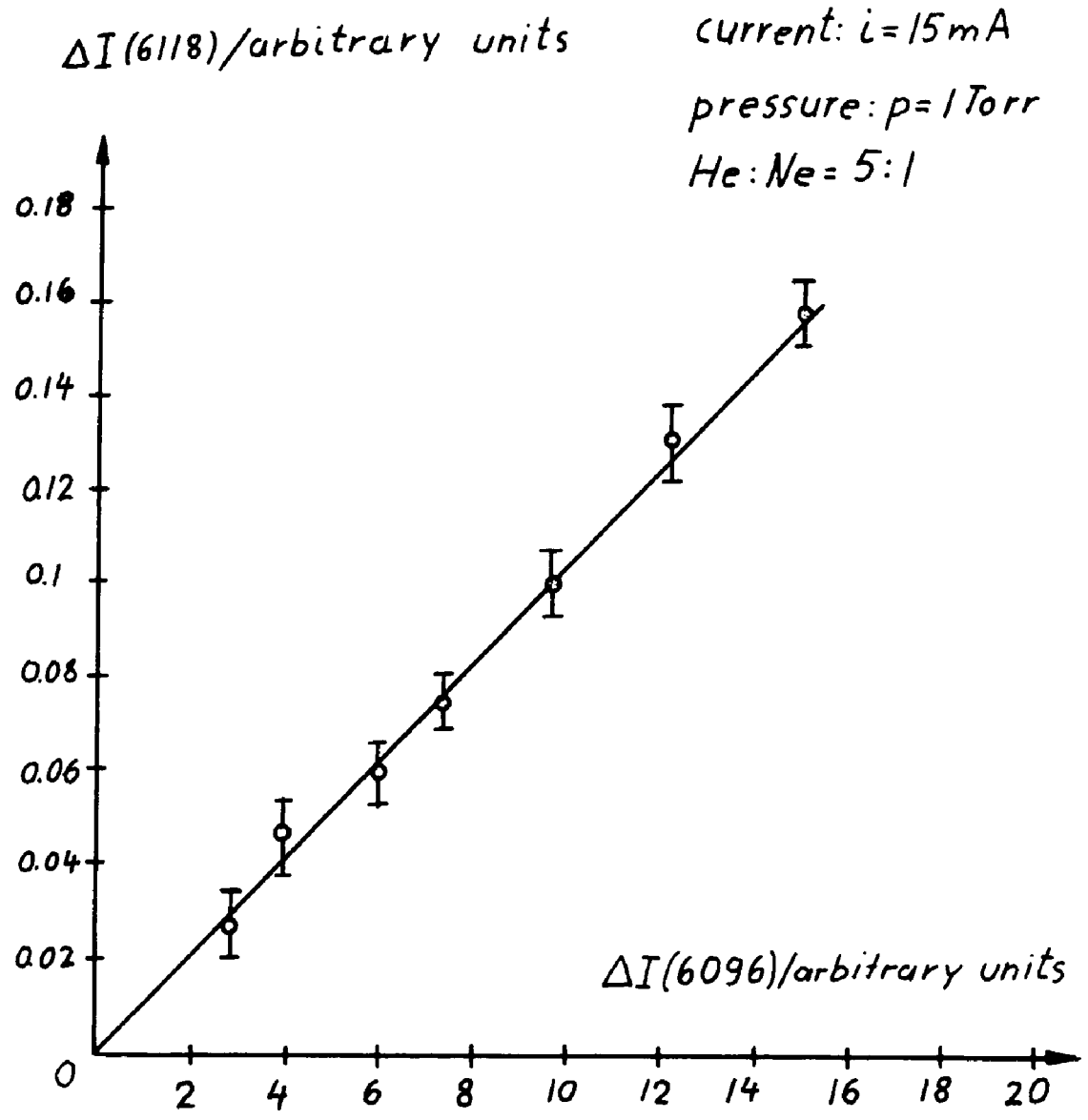

Graph IV.1 - Intensity Change ΔI(6118) versus Intensity Change ΔI(6096). Pressure and Current were kept Constant. Laser Power was Changed by Detuning Cavity

may be emitted and reabsorbed many times before escaping the gas-filled enclosure. This results in an increase of the lifetime of the particular transition. In contrast to transition between excited states, transitions to the ground state are greatly affected by radiation, owing to the presence of a large steady state population in the ground state.

No theory is available which accurately describes the radiation trapping in a He-Ne laser. However, in order to estimate the size of the effect, we can use a formula derived by T. Holstein.[10] This expression is derived for an infinite cylinder in which a Doppler broadened line is emitted by a set of atoms and is given by

$$\frac{\tau_{sp}}{\tau'} = \frac{1.6}{k_o R\sqrt{\pi \ell n k_o R}} \qquad \text{(IV.1)}$$

τ_{sp} is the radiative lifetime of an isolated atom, τ' is the effective lifetime, i.e., the lifetime increased through the effect of radiation trapping, R is the radius of the cylinder and k_o is the absorption coefficient of the gas.

As an example, we want to estimate the effect of radiation trapping on the vacuum UV transition from the $5s'(1/2)_1^0$ Ne level ($3s_2$ level in Paschen notation) to the ground state. The absorption coefficient for this transition is given by

$$k_o = \frac{1}{4\pi} \sqrt{\frac{\ell n 2}{\pi}} \frac{\lambda^2}{\Delta\nu_o \tau_{sp}} \times \frac{g_m}{g_n} \times N_v \qquad \text{(IV.2)}$$

$\Delta\nu_o$ is the Doppler width of the transition, λ is the wavelength of the transition, g_m, g_n are the statistical weights of the $5s'(1/2)^0_1$ level and the ground level, respectively, and N_v is the atom density.

The Doppler width $\Delta\nu_o$ can be calculated from the expression

$$\Delta\nu_o = \frac{1}{\lambda} \sqrt{\frac{8RT\ell n2}{M}} \qquad \text{(IV.3)}$$

R is the universal gas constant, M is the molecular mass of the gas, T is the temperature of the gas with $R_1 = 8.31 \times 10^3 \times \text{Mol}^{-1} \times {}^\circ\text{K}$, M = 20.19 for Ne, T = 350°k and $\lambda \approx .067$m, our Doppler width is found to be

$$\Delta\nu_o = 1.5 \times 10^{10} \text{ Hz} = 15 \text{ GHz} \qquad \text{(IV.4)}$$

At 0.2 Torr partial pressure of Ne, the density of the Ne atoms in our He-Ne laser of 1 Torr total pressure can be calculated from the equation

$$N_v \text{ (atoms/m}^3\text{)} = 9.65 \times 10^{24} \frac{p/\text{Torr}}{T/{}^\circ\text{K}} \qquad \text{(IV.5)}$$

The density of Ne atoms, under the given conditions, is

$$N_v = 5.5 \times 10^{21} \text{ atoms/m}^3 \qquad \text{(IV.6)}$$

The lifetime τ_{sp} for the $5s'(1/2)^0_1$ level, concerning its transition to the ground state, is about 1×10^{-9}s.

Substituting all these values into equation (IV.2), we obtain for the absorption coefficient:

$$k_o = 1.5 \times 10^5 \text{ m}^{-1} \tag{IV.7}$$

The laser tube we chose in our experiment had a radius of R = 0.002 m. Using equation (IV.1), the radiation trapping factor is found to have the value

$$\frac{\tau_{sp}}{\tau'} = 1.27 \times 10^{-3} \tag{IV.8}$$

or, if we solve for the increased lifetime

$$\tau' = 7.9 \times 10^{-7} \text{ sec} \tag{IV.9}$$

We can now write the total probability of transitions from the $5s'(1/2)^0_1$ level as the sum of probabilities of transitions to the ground state, the 2p-states and the 3p-states.

$$A_{5s'(\frac{1}{2})^0_1 \text{ total}} = \sum_{3p} A_{5s'(\frac{1}{2})^0_1 - 3p} + \sum_{2p} A_{5s'(\frac{1}{2})^0_1 - 2p} + A_{5s'(\frac{1}{2})^0_1 - \text{ground state}} \tag{IV.10}$$

The sum of the first two terms was observed to be 1.8×10^7 sec^{-1}.[5] Comparing this value to the effective transition probability which is $A_{eff} = \frac{1}{\tau'} = 1.27 \times 10^6$ sec^{-1}, we see that in equation (IV.10) the first two terms on the right hand side contribute most to the total probability of transitions from level $5s'(1/2)_1^0$. Thus we are justified to neglect, at least in a first approximation, the effect of radiation trapping on the lifetime of our levels.

The applicability of equation (IV.1) is, however, limited by the fact that we do not have a single Doppler broadened line emitted by a group of atoms. Natural neon consists mainly of two Ne isotopes, Ne^{20} (90.5%) and Ne^{22} (9.21%).[12] The frequencies of the transition in the two isotopes differ by several hundred MHz, less than the Doppler width of either. Therefore, the line shape is a superposition of two displaced lines of unequal strength rather than a single Doppler broadened line, a fact not taken into account in Holstein's theory. Therefore, our calculated value for τ_{sp}/τ' can only be looked upon as an estimation.

IV.1c. Remarks on the Racah Notation

For Ne, a $j\ell$ coupling notation proposed by Racah[13] is used. In the $j\ell$ coupling system, the total electron orbital angular momentum and the total electron spin angular momentum of the ion core, couple to form a resultant core angular momentum vector

$$\vec{J}_c = \vec{\ell}_c + \vec{s}_c \qquad \text{(IV.11)}$$

The total core angular momentum couples to the orbital angular momentum of the excited electron to form the vector

$$\vec{K} = \vec{\ell}_e + \vec{J}_c \qquad \text{(IV.12)}$$

This vector then couples with the spin of the excited electron to give the total angular momentum

$$\vec{J} = \vec{K} + \vec{s}_e \qquad \text{(IV.13)}$$

Terms are described by the notation: $n\ell_e[K]^0_J$ or $n\ell'_e[K]^0_J$; n is the total electron quantum number of the excited electron outside the ion core, and ℓ_e or ℓ'_e is the azimuthal quantum number of the excited electron. Unprimed values of ℓ indicate the ion core is in a $2P^o_{3/2}$ ground state; if ℓ_e is primed, the ion core is in a $2P^o_{1/2}$ ground state (Russell-Saunders notation). Values of ℓ_e or ℓ'_e are given by s, p, d, f .. as in the LS coupling notation. K is the quantum number associated with $\vec{K}$, and J is the quantum number associated with the total angular momentum vector $\vec{J}$. The superscript o indicates odd parity; absence of the superscript indicates even parity.

Another notation widely used is the Paschen notation.[1] Below we will list some levels in the Racah notation and in the Paschen notation.

TABLE IV.1 - SOME Ne LEVELS IN RACAH AND PASCHEN NOTATION

Racah Notation	Paschen Notation
$2p^6 1s$	-
$3s'[1/2]^0_1$	$1s_2$
$3p'[1/2]_0$	$2p_2$
$3p'[1\ 1/2]_1$	$2p_5$
$5s'[1/2]^0_1$	$3s_2$
$5s'[1/2]^0_0$	$3s_3$
$5s[1\ 1/2]^0_1$	$3s_5$
$4d'[2\ 1/2]^0_2$	$4s''''_1$
$4d'[2\ 1/2]^0_3$	$4s'''_1$
$4d[1/2]^0_0$	$4d_6$
$4d[1/2]^0_1$	$4d_5$

IV.2 Calculation of the Electron Density and the Average Electron Velocity

In order to calculate the effective cross section of a collision between an atom and an electron, it is necessary to know the electron density and average electron velocity. From Chapter (II.a) we know the relationship between the excitation or de-excitation rate per second through electronic collisions and the electron density, the effective cross section and the average electron velocity

$$\gamma_{ik}^{e} = n_e \cdot \bar{\sigma}_{ik}^{e} \cdot \bar{v}_e \qquad \text{(IV.11)}$$

Labuda and Gordon[15] have shown through microwave measurements that in a normal He-Ne laser plasma, the electron energy is independent of the discharge current. In equation (IV.11), the electron density n_e is proportional to $i/r^2.v$. i is the current through the discharge tube, r is the radius and v is the drift velocity of the electrons in the electric field. $\bar{v}_e$, the average velocity of thermal motion of the electrons, is proportional to $\sqrt{T_e}$, where T_e is the electron temperature. Further it is known in a gas discharge that both, the drift velocity v and the temperature T_e of the electron, are proportional to $\sqrt{E/p}$, where E is the electric field and p is the pressure. Since the electric field E is proportional to $\frac{1}{r}$, v and T_e are proportional to $\frac{1}{\sqrt{rp}}$.

From the measurement of Labuda and Gordon[14] are known the electron density in a He-Ne gas plasma of a partial pressure ratio of He:Ne = 5:1 under the following discharge conditions: i = 40 mA, p.2r = 0.36, d = 0.25 cm. We define

$$i_o = i/40 \text{ mA} \tag{IV.12}$$

$$r_o = r/0.25 \text{ cm} \tag{IV.13}$$

$$p_o = p/0.72 \text{ torr} \tag{IV.14}$$

For γ^e_{ik} we obtain the following expression, substituting the proportionalities into equation (IV.11)

$$\gamma^e_{ik} \sim \frac{i}{r^2 v}\,\sigma^e_{ik}\,\sqrt{T_e} = \frac{i}{r^2 v}\,\sigma^e_{ik}\,\frac{1}{(r\cdot p)^{1/4}}$$

$$= \frac{i}{r^2}\,\sigma^e_{ik}\,\frac{\sqrt{rp}}{(r\cdot p)^{1/4}} \tag{IV.15}$$

$$\gamma^e_{ik} \sim \frac{i}{r^2}\,\sigma^e_{ik}\,(r\cdot p)^{1/4}$$

For the conditions given above, i.e., $i_o = 1$, $r_o = 1$, $p_o = 1$, we know the electron density and therefore can write for the γ^e_{1k}

$$\gamma^e_{1k} = n_{eo}\, v_{eo}\, (r_o p_o)^{1/4}\, \frac{i_o}{r_o^2}\, \sigma_{ik} \tag{IV.16}$$

This can be rewritten in the following way:

$$\gamma^{e}_{ik} = \frac{\bar{v}_{eo}}{(r_o p_o)^{1/4}} n_{eo} i_o \frac{(r_o p_o)^{1/2}}{r_o} \sigma_{ik} \qquad \text{(IV.17)}$$

The electron density and the average electron velocity are given by

$$n_e = n_{eo} \left(\frac{r_o p_o}{r_o^2}\right)^{1/2} i_o \qquad \text{(IV.18)}$$

$$\bar{v}_e = \bar{v}_{eo} \frac{1}{(r_o p_o)^{1/4}} \qquad \text{(IV.19)}$$

From equations (IV.18) and equations (IV.19) we can calculate the n'_{eo} and v'_{eo} for our laser, which has d different diameter. With r = 0.2095 cm, i = 40 mA, p = 0.86 Torr ($p \cdot 2r = 0.36$) and obtain

$$n'_{eo} = n_{eo} \times 1.424 \qquad \text{(IV.20)}$$

or

$$n'_{eo} = 14.24 \times 10^{10}\ \text{cm}^{-3} \qquad \text{(IV.20a)}$$

and

$$\bar{v}'_{eo} = \bar{v}_{eo} \times 1.046 \qquad \text{(IV.21)}$$

with $T_e = 89 \times 10^3$ °K and the relationship

$$\bar{v}_e^2 = \frac{3kT_e}{m} \qquad \text{(IV.22)}$$

we obtain for $\bar{v}'_{eo}$

$$\bar{v}_{eo} = 2.1 \times 10^8 \frac{cm}{sec} \qquad \text{(IV.21a)}$$

Thus we can write for the excitation rate γ^e_{1k}

$$\gamma^e_{1k} = \sigma_{1k} \times 1.424 \times 10'' \times 2.1 \times 10^8 \left(\frac{1}{0.72}\right)^{1/4} \times$$

$$\times \left(\frac{p}{Torr}\right)^{1/4} \times \frac{1}{40} \frac{i}{mA} \qquad \text{(IV.23)}$$

or

$$\gamma^e_{ik} = \sigma_{ik} \quad 8.116 \times 10^{17} \sqrt[4]{\frac{p}{Torr}} \times \frac{i}{mA} \qquad \text{(IV.23a)}$$

Thus, if we know the excitation or de-excitation rate γ^e_{1k}, we can, for a given pressure and a given current, calculate the effective collision cross section for the electron atom collision.

IV.3 Relation between Transition Rates and Atom-Atom Collision Cross Sections in the He-Ne Plasma

In this section we will consider the collision rates among the atoms in the He-Ne gas discharge as a function of pressure, temperature and collision cross sections of the atoms.

From the kinetic theory of gases it is possible to derive expressions for the rates at which collisions will occur in a volume of gas due to the thermal motion of the gas atoms or molecules. In a gas containing a mixture of two different kinds of molecules or atoms - in our case He and Ne atoms (of densities N_{He} and N_{Ne}) the average number of collisions per unit volume per unit time between He atoms and Ne atoms, Z_{He-Ne}, is given by[16]

$$Z_{He-Ne} = N_{He} \cdot N_{Ne} \cdot \sigma_{He-Ne} \sqrt{\frac{8kT}{\pi} \left(\frac{1}{M_{He}} + \frac{1}{M_{Ne}}\right)} \qquad \text{(IV.24)}$$

σ_{He-Ne} is the effective cross section for the collision between He and Ne atoms. T is the temperature of the gas, and M_{He} and M_{Ne} are the molecular masses of He and Ne, respectively. The average number of collisions per second of a Ne atom with a He atom will be the total rate Z_{He-Ne} divided by the total number of Ne atoms

$$\frac{1}{T_{Ne-He}} = N_{He} \cdot \sigma_{He-Ne} \sqrt{\frac{8kT}{\pi} \left(\frac{1}{M_{He}} + \frac{1}{M_{Ne}}\right)} \qquad \text{(IV.25)}$$

The average number of collisions per second of Ne atom with other Ne atoms can be derived from equation (IV.24), for the case that the molecular masses are equal.

$$\frac{1}{T^{*}_{Ne-Ne}} = N_{Ne} \cdot \sigma_{Ne-Ne} \sqrt{\frac{16kT}{\pi} \frac{1}{M_{Ne}}} \qquad \text{(IV.26)}$$

Thus, for the total collision rate of a Ne-atom with other Ne atoms and He atoms we can write

$$\gamma_{Ne} = \frac{1}{T_{Ne-He}} + \frac{1}{T_{Ne-Ne}} = N_{He} \cdot \sigma_{HeNe} \sqrt{\frac{8kT}{\pi} \left(\frac{1}{M_{He}} + \frac{1}{M_{Ne}}\right)}$$

$$+ N_{Ne} \sigma_{Ne-Ne} \sqrt{\frac{16kT}{\pi M_{Ne}}} \qquad \text{(IV.27)}$$

The concentration of atoms in a gas may be related to the partial pressure and temperature of each particular species by[11]

$$N\left(\frac{\text{atoms}}{m^3}\right) = 9.65 \times 10^{24} \frac{p(\text{Torr})}{t(^{\circ}K)} \qquad \text{(IV.28)}$$

Substituting equation (IV.28) into equation (IV.27) we obtain for the total collision rate for Ne:

$$\gamma_{Ne} = 9.65 \times 10^{24} \frac{P_{He/Torr}}{T/^{\circ}K} \sigma_{Ne\,He} \sqrt{\frac{8kT}{\pi} \left(\frac{1}{M_{Ne}} + \frac{1}{M_{He}}\right)}$$

$$+ 9.65 \times 10^{24} \frac{P_{Ne/Torr}}{T/^{\circ}K} \sigma_{NeNe} \sqrt{\frac{16k}{\pi M_{Ne}}} \qquad \text{(IV.29)}$$

For a partial pressure ratio of $P_{He}:P_{Ne} = 5:1$, equation (IV.29) becomes

$$\gamma_{Ne} = \frac{9.65\times10^{24}}{T} P\left[\frac{4}{5} \sigma_{Ne\,He} \sqrt{\frac{8kT}{\pi} \left(\frac{1}{M_{Ne}} + \frac{1}{M_{He}}\right)}\right.$$

$$\left. + \frac{1}{5} \sigma_{Ne\,Ne} \sqrt{\frac{16kT}{\pi M_{Ne}}}\right] \qquad \text{(IV.30)}$$

This is, in general, the collision transfer rate in which He and Ne atoms participate.

IV.4 Measurement Errors

We will now discuss the sources of errors which will enter into our measurements. The three quantities measured in our experiment are the intensity changes, the pressure and the current, and all these quantities can be measured only with a limited accuracy. Furthermore, the calibration of the detection system's optical sensitivity bears its own inaccuracy since it is impossible to keep the current through the calibration light source constant. Thus, all our measured values will have to be reported with an estimated uncertainty.

The intensity changes were measured three times, on different days. For most lines, the signals detected by the lock-in amplifier were strong enough that superimposed noise hardly affected the reading. In these cases we used a time-constant of 3 seconds to obtain an average reading. In some cases, however, the signal to noise ratio was not as favorable, and we had to use a longer time constant to obtain a consistent average reading. For those measurements time constants of 10 seconds and 30 seconds were chosen. It was shown in Chapter (IV.1a) that the ratio of the intensity changes does not depend on the intensity of the laser radiation field present in the gas discharge. Thus we were not forced to keep the laser intensity constant for our measurements performed on different days.

The laser intensity could easily change due to the effects of dust or of slight detuning of the mirrors. Our intensity change ratios, however, were not affected by this, and we could reproduce our measurements within 4%, each time in spite of the daily changes of the laser field intensity in the plasma. Of the three measured values, average values were chozen to fit the expected curves with the method of the least squares.

While the measurement of the intensity changes could be done with fairly high accuracy, the determination of the absolute pressure in the gas discharge tube constituted a more serious problem. First, a correction has to be introduced to our calibration due to the different temperatures existing in the hot part (discharge tube, electrodes) and the cold part (ballast volume, arm to vacuum system, volume near windows) of our discharge arrangement. Since we can only estimate the temperature T in the discharge, we are only able to estimate an upper limit for the correction factor which has to be introduced to compensate for the different temperatures. In the following derivation we assume to have an ideal gas:

Imagine two partial volumes, V_1 and V_2, are filled with the same gas and are at temperatures T_1 and T_2 (Figure IV.1). In the case the temperatures are equal ($T_1 = T_0$), we can write

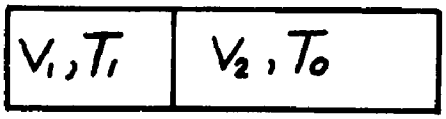

Figure IV.1 - Correction for Different Temperatures in Laser

$$p_o(V_1+V_2) = (n_{01}+n_{02})kT_o \qquad \text{(IV.31)}$$

where p_o is the pressure at the temperature T_o, and n_{01} and n_{02} are the number of gas particles in volume V_1 and V_2, respectively. k is the Boltzmann constant.

If now the temperature of the gas in volume V_1 is increased to T_1, while the gas in volume V_2 remains on the temperature T_0, we can write for the two partial volumes:

$$pV_1 = n_1.k.T_1 \qquad \text{(IV.32)}$$

$$pV_2 = n_2.k.T_0 \qquad \text{(IV.33)}$$

p is the pressure, and n_1 and n_2 are the number of gas particles in V_1 and V_2 under the new conditions.

Since our system is closed, the total number of gas particles remains constant.

$$n_{01} + n_{02} = n_1 + n_2 = n_0 \qquad \text{(IV.34)}$$

Solving equation (IV.32) and equation (IV.33) for n_1 and n_2 and substituting these two expressions into equation (IV.34) and equation (IV.31), we obtain for the correction of the pressure due to the rise of temperature in the partial volume V_1:

$$\frac{p}{p_o} = \frac{1 + \frac{V_1}{V_2}}{1 + \frac{V_1}{V_2}\frac{T_0}{T_1}} \qquad \text{(IV.35)}$$

For our system we estimated the ratio of the volumes V_1/V_2 to be approximately 1/40. Assuming that the gas in the discharge tube is at 400°k while the rest of the gas remains at room temperature, (T_o = 300°k), we obtain for the correction

$$p = 1.006 \times p_o \qquad \text{(IV.36)}$$

This means that the total pressure in our system changed by 0.6% due to the rise of temperature in the discharge portion.

We further have to investigate which correction we have to introduce into calibration procedure. We recall equation (III.5) which gave us the pressure in our laser after the nth "squirt".

$$p_n = p_o(1-\Delta)^n \qquad \text{(III.5)}$$

This equation was derived for the case that the whole system is at room temperature. In the case the temperature is changed in V_1, the pressure after the nth squirt will be

$$p'_n = p_o\ (1+0.006)(1 - (\Delta+0.0006))^n \qquad \text{(IV.37)}$$

Δ was found in Chapter (III) to be 3.47%. Thus, for the ratio of the two pressures after the nth squirt we find:

$$\frac{p'_n}{p_n} = 1.006\ \left(\frac{1-\Delta-0.006}{1-\Delta}\right)^n \qquad \text{(IV.38)}$$

or, with $\Delta = 3.47\%$

$$\frac{p'_n}{p_n} = 1.006 \times 0.99365^n \qquad \text{(IV.39)}$$

We used equation (IV.39) to correct our pressure measurements. For a reduction of the pressure by eight squirts the correction was ≈4%, for a reduction by 17 squirts it was ≈9%, and for a reduction by 29 squirts the correction was ≈17%.

A further uncertainty is introduced by the inaccuracy of the McLeod gauge reading. Its scale is very crude, and we could not reliably read the pressure with more than ±5% accuracy. Thus we assumed our pressure readings accurate to 5% in the analysis of our data.

Measuring the current through the gas discharge introduced another uncertainty. We measured the current with the aid of a Simpson meter, Model 260, Series 5p. The full scale accuracy of this meter is given to be 2%. Thus, using readings larger than 1/5 of full scale, the error is smaller than 10%. In our data analysis we allowed a maximum current variation of 10%.

The calibration of the optical system gives rise to another uncertainty. It is essential to keep the current constant through the tungsten iodine lamp. As a power source we used a bank of lead storage batteries and measured the voltage across a shunt with a digital voltmeter reliable to three decimal places. A current of 6.50A was required, and we were able to keep the current constant than 0.3%. Since a 1% change in the current produces a 10% change in the emitted intensity, we see that in our case the accuracy of the measured intensity is in the order of 3%. This was substantiated by the fact that the fluctuations of the meter reading the photomultiplier current were around 3%.

The errors mentioned above were all taken into account in our analysis in order to estimate the uncertainties of experimentally derived values.

IV.5 De-excitation Rates of the Upper and Lower Laser Levels

In this experiment, we measured the intensity changes of spontaneously emitted sidelight originating from the upper and lower laser levels, $5s'(1/2)^0_1$ and $3p'(1\ 1/2)_2$, in dependence of the current i for four different choices of pressures. The lines chosen were $\lambda = 6118\text{Å}_1$ having its origin on the upper level, and $\lambda = 6096\text{Å}_1$ a line starting from the lower level. Since the laser was lasing in the 6328Å line, we had to chose a line other than $\lambda = 6328\text{Å}$ starting from the $5s'(1/2)^0_1$ level, for our measurement of the intensity change. The reason is that light of the laser radiation field scattered from the glass walls of our laser tube, would have entered our measurements. Thus we chose the $\lambda = 6118\text{Å}$ line, originating from the upper laser level.

An expression for the population change ratio $\Delta n_1/\Delta n_2$ was derived in Chapter (II.c, equation (II.20)). The relation between the population change ratio and the intensity change ratio is given by equation (II.11). In our case this expression becomes:

$$\frac{\Delta n_1}{\Delta n_2} = \frac{\lambda(6096)}{\lambda(6118)} \cdot \frac{A(6118)}{A(6096)} \cdot \frac{\Delta I_1}{\Delta I_2} \times k \qquad \text{(IV.40)}$$

where A(6118) and A(6096) are the Einstein coefficients for the radiative transitions of these particular lines and k is the calibration constant. A(6118) and A(6096) are found in literature[17] and have the values 0.608×10^6 sec^{-1} and 1.79×10^7 sec^{-1}.

Using equation (IV.40), equation (II.20) can be rewritten.

$$\frac{\Delta I_1}{\Delta I_2} = - \text{ const } \frac{A_2 - A_{21} + \gamma_2'^{a} + \sqrt[4]{p}i \times \gamma_2'^{e}}{\gamma_1'^{a} + A_2 + \gamma_1'^{e} \cdot \sqrt[4]{p}i} \qquad \text{(IV.41)}$$

where the const can be derived from equation (IV.40)

$$\text{const} = \frac{\lambda(6118)}{\lambda(6096)} \times \frac{A(6096)}{A(6118)} \frac{1}{k} \qquad \text{(IV.42)}$$

The results of our measurements are shown in Graph (IV.2). For all four pressures, the intensity change ratio ($\Delta I_1/\Delta I_2$) shows a linear dependence on the current. We therefore neglect the third term of the denominator in equation (IV.40) and obtain the expression

$$\frac{\Delta I_1}{\Delta I_2} \times \text{const}^{-1} = - \frac{\frac{A_2 - A_{21}}{A_1} + \frac{\gamma_2'^{a}}{A_1} p + \sqrt[4]{p}i \frac{\gamma_2'^{e}}{A_1}}{1 + \frac{\gamma_1'^{a}}{A_1}} \qquad \text{(IV.41a)}$$

In equation (IV.41a), only the radiative transition probabilities A_2, A_1 and A_{21} are known.[18] Their respective

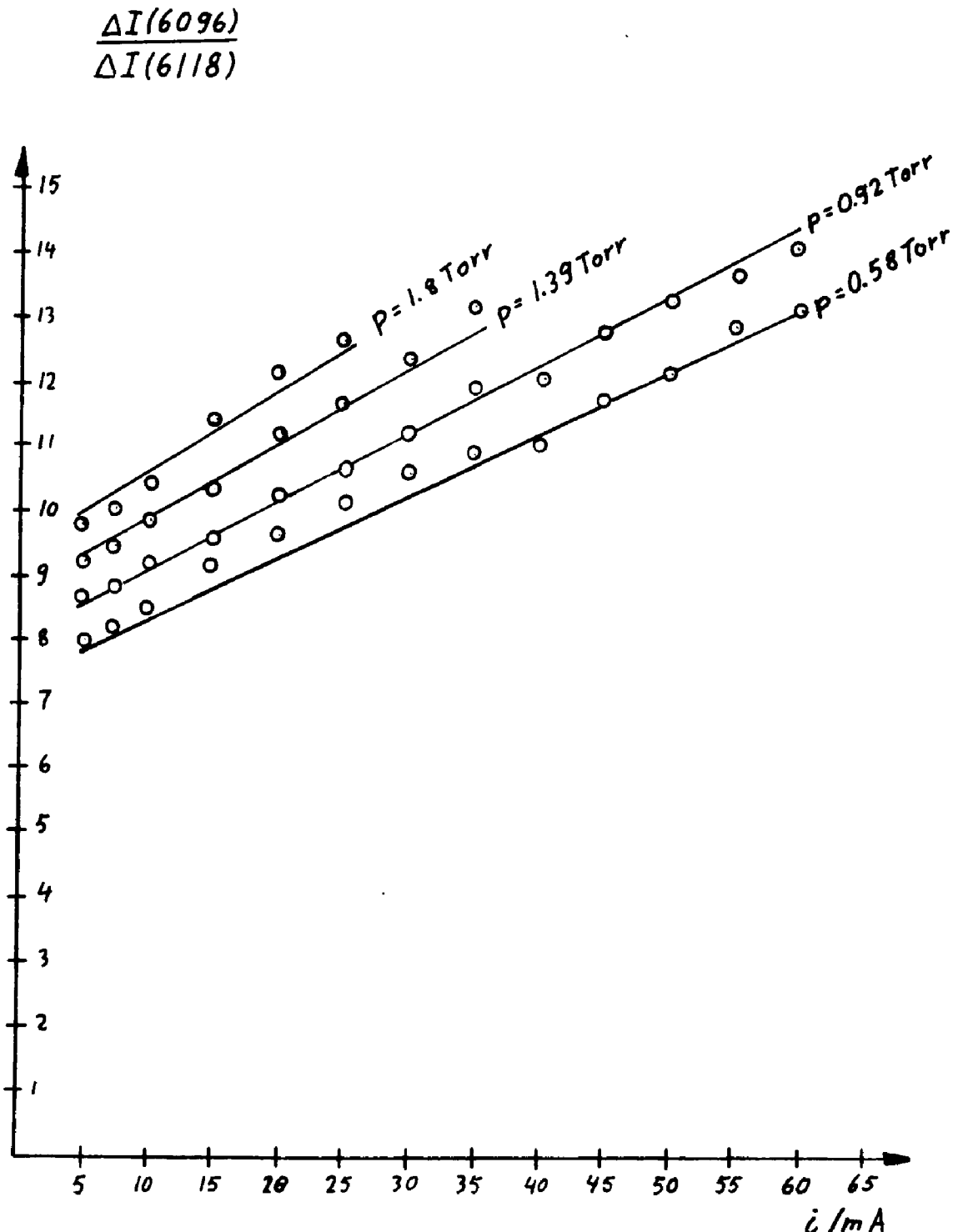

Graph IV.2 - ΔI(6096)/ΔI(6118) versus Current, with Pressure as Parameter

values are 1.42×10^7 sec^{-1}, 5.23×10^7 sec^{-1} and 5.1×10^6 sec^{-1}. Using these values, we fitted equation (IV.41a) to the measured values in Graph (IV.2).

We took into account a 10% uncertainty in the current, a 10% uncertainty in the pressure, a 5% uncertainty in the measured values of the intensity change ratios, and a 5% uncertainty in the calibration factor. For these extremes, we obtained the following values for the transition rates:

$$\gamma_1'^a = (6.80 \begin{smallmatrix} + 0.84 \\ - 1.57 \end{smallmatrix}) \times 10^6 \text{ sec}^{-1} \text{ Torr}^{-1} \qquad \text{(IV.42)}$$

$$\gamma_2'^a = (4.81 \begin{smallmatrix} + 0.73 \\ - 0.84 \end{smallmatrix}) \times 10^6 \text{ sec}^{-1} \text{ Torr}^{-1} \qquad \text{(IV.43)}$$

$$\gamma_2'^e = (2.04 \begin{smallmatrix} + 0.26 \\ - 0.34 \end{smallmatrix}) \times 10^5 \text{ sec}^{-1} \text{ Milliampere}^{-1} \qquad \text{(IV.44)}$$

In the de-excitation of the upper and lower laser level due to atom-atom collisions, He atoms as well as Ne atoms take part, according to equation (IV.29). Thus, it is not possible in our measurement to separate exactly the contributions of He-Ne collisions and Ne-Ne collisions. This is especially true for the upper laser level, since it is less than 1kT apart from the 2^1S_0 He metastable state. For the lower laser level, $3p'[1\ 1/2]_2$, de-excitation due to Ne-Ne collisions is most likely to occur, since no He level is close enough for collisional energy transfer to happen. Thus we can estimate an upper limit for the collision cross section between the

Ne atoms of the lower laser level and the other 3p' levels of Ne. Using equation (IV.29), we can write

$$\sigma_{Ne-Ne} \leq \frac{\gamma_1' a_{5T}}{9.65\times10^{24}} \sqrt{\frac{\pi M_{Ne}}{16kT}} \qquad (IV.45)$$

For a temperature of 350°k, we obtain for σ_{Ne-Ne}

$$\sigma_{Ne-Ne} \leq 1.6 \times 10^{-14} \text{ cm}^2 \qquad (IV.46)$$

At this point we have to mention, however, that energy transfer between atoms in the lower laser level and He atoms is possible in the following way. Atoms in the 2^1P or to 2^3P He metastable states can collide with Ne atoms at the lower laser level, de-exciting them to one of the 3s states, while the He atoms is excited to one of its higher states. This energy transfer mechanism can be written:

$$Ne(3p'(1\ 1/2)_2) + He(2^1P, 2^3P) \rightleftarrows Ne(3s_i) + He(3^1P_1, 3^3P_1, 3^1D, 3^3D) \qquad (IV.47)$$

We confirmed that this kind of energy transfer does occur; we observed modulation of high lying He-levels, having the same phase as the lower laser level. A detailed study of this phenomena, however, is beyond this work.

The relationship between the electronic de-excitation rate and the collision cross section between atoms of the upper laser level and electrons is given by equation (IV.22a). For one Torr pressure, for instance, we obtain

$$\sigma_2^e = (2.51 \begin{smallmatrix} + 0.32 \\ - 0.42 \end{smallmatrix}) \times 10^{-13} \text{ cm}^2 \qquad \text{(IV.48)}$$

We also see that, with $\gamma_2'^e \approx 2 \times 10^5 \text{ sec}^{-1}$, the electronic collision de-excitation of the upper laser level will reach the same importance as the pure radiative de-excitation at currents around 70mA.

The value for σ_2^e varies from the value obtained by T. Sakurai and T. Ohta[18] who obtained a value of $\sigma_2^e = (6.8 \pm 1.2) \times 10^{-13}$ cm^2 in a similar measurement. This can be possibly explained in the following way. First, these authors measured the ratio $\Delta I(6096)/\Delta I(6328)$ of a laser oscillating in the 6328Å transition. Therefore a contribution from the scattered light of the laser radiation field might have entered their measurements. Secondly, they assumed values for $\gamma_1'^a$ and $\gamma_2'^a$ and performed their measurements for only one pressure, namely at 1 Torr. We checked the source of this assumption[21] and could not extract the same information from it.

IV.6 Energy Transfer Between the Ne $5s'(1/2)^0_1$ and $5s'(1/2)^0_0$ Levels

In Chapter (II.d) the modulation of atomic levels other than those directly involved in the lasing action was described, and an equation for the energy transfer from the upper laser level, $5s'(1/2)^0_1$, to the adjacent $5s'(1/2)^0_0$ level was derived (equation (II.28)). We measured the intensity change ratio for the two lines, $\lambda = 6118\text{Å}$ originating from the upper laser level, and $\lambda = 5448\text{Å}$ originating from the lower, adjacent $5s'(1/2)^0_1$ level, as a function of the current i for four pressure points. The results are shown in Graph (IV.3). Using equation (II.29), the variation of the intensity change ratio as a function of current and pressure can be written:

$$\text{const} \times \frac{\Delta I_1}{\Delta I_2} = \frac{\gamma'^{a}_{21} + \gamma'^{e}_{21} \sqrt[4]{pi}}{\gamma'^{a}_{1} p + \gamma^{e}_{1} \sqrt[4]{pi}} \qquad \text{(IV.49)}$$

where $\Delta I_1/\Delta I_2$ is related to the population change ratio by

$$k \cdot \frac{\Delta I_1}{\Delta I_2} \times \frac{\lambda(5448)}{\lambda(6118)} \times \frac{A(6118)}{A(5448)} = \frac{\Delta n_1}{\Delta n_2} \qquad \text{(IV.50)}$$

The subscripts 2 and 1 refer to the $5s'(1/2)^0_1$ and the $5s'(1/2)^0_0$ level, respectively.

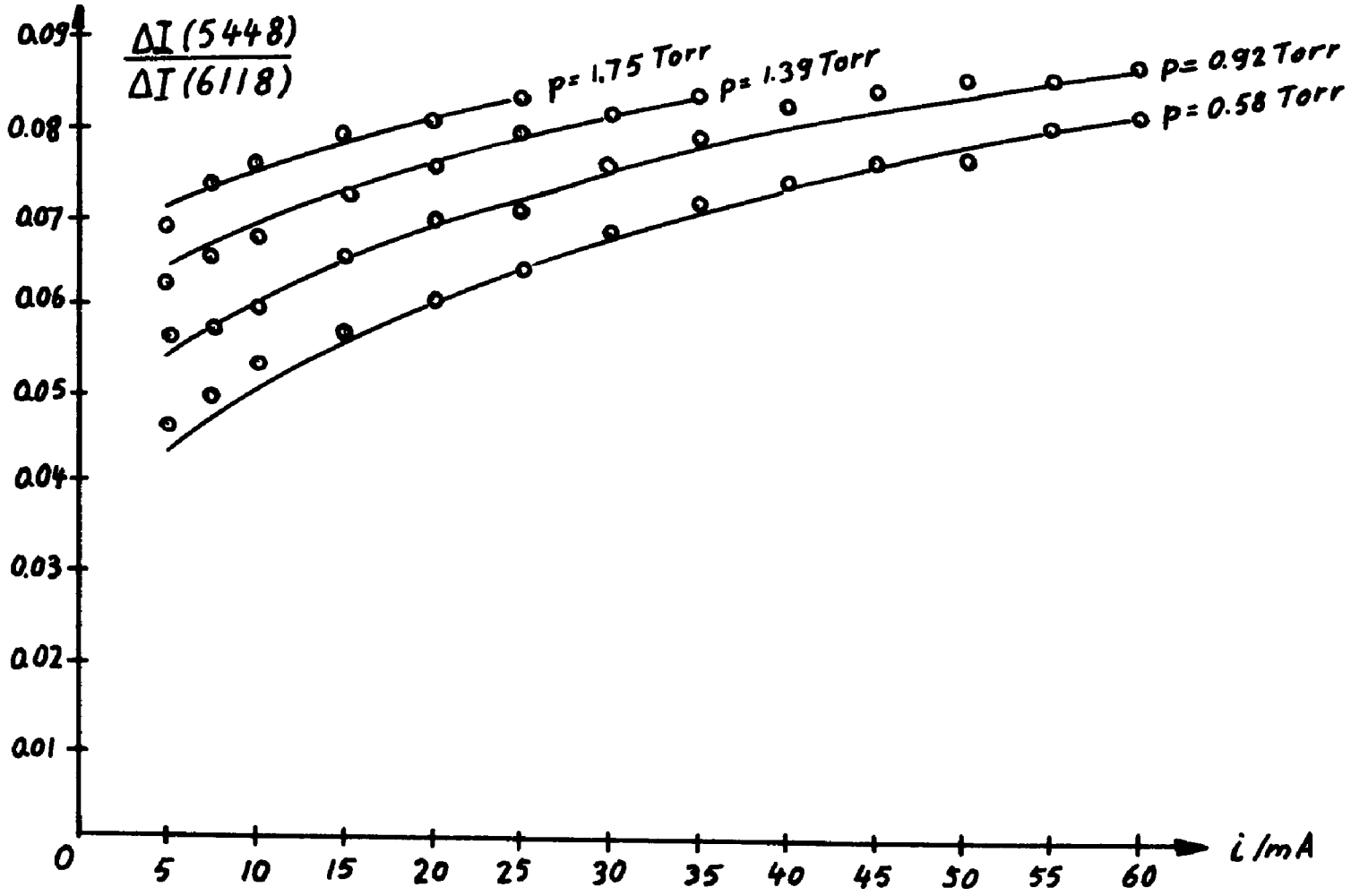

Graph IV.3 - ΔI(5448)/ΔI(6118) versus Current, with Pressure as Parameter

The value for A(6118), the Einstein coefficient for this particular transition, is 0.603×10^6 sec^{-1}.[17] A(5448) was found by Lilly and Holmes[5] to be 0.1×10^6 sec^{-1}, and k is our calibration constant.

Equation (IV.49) was fit to our measured values in Graph (IV.3). The solid line represents the theoretically calculated curve, while the circles represent our measured values. Taking again into account a 10% uncertainty in the current, a 10% uncertainty in the pressure, a 5% uncertainty in the measured values and a 5% uncertainty in the calibration, the least square fit program yielded the following results:

$$\frac{\gamma'^{a}_{1}}{A_1} = (6.51 \begin{smallmatrix} + 0.35 \\ - 0.30 \end{smallmatrix}) \times 10^{-1} \text{ Torr}^{-1} \qquad \text{(IV.51)}$$

$$\frac{\gamma'^{a}_{12}}{A_1} = (8.45 \begin{smallmatrix} + 1.00 \\ - 0.75 \end{smallmatrix}) \times 10^{-2} \text{ Torr}^{-1} \qquad \text{(IV.52)}$$

$$\frac{\gamma'^{e}_{1}}{A_1} = (3.37 \begin{smallmatrix} + 0.22 \\ - 0.20 \end{smallmatrix}) \times 10^{-2} \text{ Milliampere}^{-1} \qquad \text{(IV.53)}$$

$$\frac{\gamma'^{e}_{12}}{A_1} = (4.30 \begin{smallmatrix} + 0.50 \\ - 0.49 \end{smallmatrix}) \times 10^{-3} \text{ Milliampere}^{-1} \qquad \text{(IV.54)}$$

Unfortunately, the lifetime of the $5s'(1/2)^0_0$ level, $\tau_1 = 1/A_1$, is not known. At pressures around 1 Torr, however, we see that the de-excitation of the $5s'(1/2)^0_0$ level due to electron atom collisions becomes comparable to the radiative lifetime of this level at currents around 30mA. We also see

that the collision transfer of atoms from the $5s'(1/2)_0^0$ level to the $5s'(1/2)_1^0$ level through electron atom collisions is about 1/8 of the electron collision transfer to all other levels. Almost the same ratio is obtained for the atom-atom collisional transfer between these two levels and the total atomic collisional de-excitation of the $5s'(1/2)_0^0$ level. Again, we have to emphasize that we cannot separate the contributions to the energy transfer of He-Ne atom collisions from Ne-Ne atom collisions.

IV.7 Energy Transfer to Higher Lying Ne Levels

In this experiment we investigated the excitation of the 4d', 5d' and 6s' levels through electron impact from the upper laser level, $5s'(1/2)^1_0$. Electron impact excitation is the most likely energy transfer mechanism between these levels since their energy difference is larger than 1kT which excludes energy exchange through atom-atom collisions. We observed a strong current dependence of the intensity change ratio $\Delta I_2/\Delta I_1$, where ΔI_2 represents the intensity change of a spontaneously emitted line originating from one of the mentioned upper levels, while ΔI_1 is the intensity change of the $\lambda = 6118\mathring{A}$ line starting from the upper laser level. The excitation process can be written:

$$Ne(5s'(1/2)^0_1) + e \rightleftarrows Ne(4d',5d',6s') + e \qquad (IV.55)$$

The equation which describes this situation is derived in Chapter (II.d) equation (II.39)

$$\frac{\Delta n_2}{\Delta n_1} = \frac{\frac{\gamma'^e_{12}}{A_2}.i}{1 + \frac{\gamma'^e_2}{A_2}i} \qquad (II.39)$$

However, before we evaluate our data, we have to give some consideration to the interpretation of the radiative, atomic and electronic parameters occurring in equation

(II.39). Unlike in the cases described in the preceding chapters, we were not able to separate single lines in this experiment. As an example we may refer to the measurement of the $\lambda = 5902\text{Å}$ lines. There are four lines, each originating from one of the 4d' levels and terminating on the $3p'(1\ 1/2)_2$ level, that have a wavelength of approximately 5902Å. Of course, our monochromator was not able to resolve these lines. Instead, we were measuring the sum of the intensities of all four lines. Hence, we have to give a different meaning to the excitation and de-excitation parameters. The Einstein coefficient A(5902) has to be written

$$A(5902) = \sum_{4d'} W_{4d'}\, A_{4d'-3p'(1\ 1/2)_2} \qquad \text{(IV.56)}$$

where $W_{4d'}$ is a statistical factor. The total radiative de-excitation rate of the 4d' levels has the explicit form

$$A_2 \equiv \sum_{4d'} W_{4d'}\left(A_{4d'-\text{ground}} + \sum_{3p} A_{4d'-3p} + \sum_{4p} A_{4d'-4p}\right) \qquad \text{(IV.57)}$$

Also, the electronic collision rates have to get a new interpretation. The excitation rate, γ^e_{12}, is the sum of the electronic excitation rates of atoms from the $5s'(1/2)^0_1$ (the upper laser level) to the individual 4d' levels

$$\gamma_{12}^{'e} \equiv \sum_{4d'} W_{4d'}\, \gamma_{12}^{'e}{}_{(5s'(1/2)_1^0 - 4d')} \qquad \text{(IV.58)}$$

Similarly, we can write for the total de-excitation rate of the 4d' level due to electron-atom collisions:

$$\gamma_{2}^{'e} \equiv \sum_{4d'} W_{4d'}\, \gamma_{2}^{'e}\,(4d' - \text{other levels}) \qquad \text{(IV.59)}$$

The results of our measurements for the excitation of the 4d' levels due to electron impact is shown in Graph (IV.3). We measured the current dependence of the ratio $\Delta I(5902)/\Delta I(6118)$ for 4 pressure points. Though equation (II.30) does not include pressure dependent terms, we obtain different curves for different pressures. A possible explanation for this effect is illustrated in Figure (IV.2).

Besides the 4d' levels, the 5p' levels are also excited through electron impact from the $5s'(1/2)_1^0$ upper laser level. The 5p' levels, however, can exchange energy with the 4d' levels through atom-atom collisions since their energy spacing is smaller than 1kT. Therefore, in order to obtain the purely electronic effect, we have to extrapolate our measured values to zero pressure.

The results for the excitation of the 4d' levels are shown in Graph (IV.3). We measured the intensity change ratio $\Delta I(5902)/\Delta I(6118)$ as a function of current for four

pressure points and extrapolated to zero pressure. The error bars on the extrapolated curve take into account a 10% uncertainty in pressure, a 5% uncertainty in the calibration and a 5% uncertainty in the measured values of the intensity change ratio $\Delta I(5902)/\Delta I(6118)$. The extrapolated curve then was fit to equation (II.39), and the following results were obtained

$$\frac{\gamma_2'^e}{A_2} = (9.32 \begin{smallmatrix} + 0.47 \\ - 0.48 \end{smallmatrix}) \times 10^{-4} \text{ Milliampere}^{-1} \qquad \text{(IV.60)}$$

and

$$\frac{\gamma_{12}'^e}{A_2} \times A(5902) = (3.96 \begin{smallmatrix} + 0.40 \\ - 0.73 \end{smallmatrix}) \times 10^{3} \text{ Milliampere}^{-1} \times \text{sec}^{-1} \qquad \text{(IV.61)}$$

A_2 is the radiative transition probability of the 4d' levels and is given by equation (IV.57). A(5902) is the transition probability for the particular transition from the 4d' levels to the $3p'(1\ 1/2)_2$ level and is given by equation (IV.56). $\gamma_{12}'^e$ and $\gamma_2'^e$ are given by the expressions (IV.58) and (IV.59), respectively.

We see that the de-excitation $\gamma_2'^e$ of the 4d' levels due to electron-atom collisions is very small compared to the radiative transition probability A_2 of these levels. Unfortunately, we do not know the radiative transition proba-

bilities A_2 and A(5902). However, we can estimate a lower limit for γ'^{e}_{12} in the following way: In equation (IV.57), the first term, i.e., the transition rates to the ground state can be neglected because of radiation trapping as was shown in Chapter (IV.a2). The ratio of the second term to the transition probability A(5902) was calculated by Minaeva[19] and found to be 6.5. With this value, γ'^{e}_{12} can be estimated from equation (IV.61):

$$\gamma'^{e}_{12} \geq 2.6 \times 10^{4} \text{ Milliampere}^{-1} \qquad \text{(IV.62)}$$

This corresponds to a cross section of

$$\sigma^{e}_{12} \geq 3.2 \times 10^{-14} \text{ cm}^2 \qquad \text{(IV.63)}$$

In the same way we determined the excitation and deexcitation parameters of the 5d' levels. We measured the ratio $\Delta I(5145)/\Delta I(6118)$ for four pressures, and the results are shown in Graph (IV.4). The extrapolated curve was fit to equation (II.38), and we obtained the following results:

$$\frac{\gamma'^{e}_{2}}{A_2} = (5.23 \pm 0.3) \times 10^{-3} \text{ Milliampere}^{-1} \qquad \text{(IV.64)}$$

and

$$\frac{\gamma'^{e}_{12}}{A_2} \cdot A(5145) = (6.99 \pm 0.71) \times 10^{2} \text{ Milliampere}^{-1} \times \text{sec}^{-1} \qquad \text{(IV.65)}$$

where

$$A(5145) \equiv \sum_{5d'} W_{5d'} A_{5d'} - 3p'(1\ 1/2)_2 \qquad \text{(IV.66)}$$

$$A_2 \equiv \sum_{5d'} W_{5d'} \left(A_{5d'\text{-ground}} + \sum_{3p} A_{5d'-3p} + \sum_{4p} A_{5d'-4p}\right) \qquad \text{(IV.67)}$$

$$\gamma'^{e}_{12} \equiv \sum_{5d'} W_{5d'} \gamma^{e}_{12\ 5s'(1/2)^0_1 - 5d'} \qquad \text{(IV.68)}$$

$$\gamma'^{e}_{2} \equiv \sum_{5d'} \gamma'^{e}_{2\ 5d' - \text{all other levels}} \qquad \text{(IV.69)}$$

We see from equation (IV.64) that the de-excitation of the 5d' levels due to electron-atom collisions is quite small compared to the radiative transition probability A_{21}; however, it has more importance than for the 4d' levels. Again, a lower limit for γ'^{e}_{12} can be estimated, neglecting the first and the last terms on the right hand side of equation (IV.67). The term $\sum_{5d'} \sum_{3p} A_{5d'-3p}/A(5145)$ was calculated by Minaeva[19] to be 12. Thus, for our lower limit we obtain

$$\gamma'^{e}_{12} \geq 8.4 \times 10^3 \text{ Milliampere}^{-1} \qquad \text{(IV.70)}$$

which corresponds to a cross section of

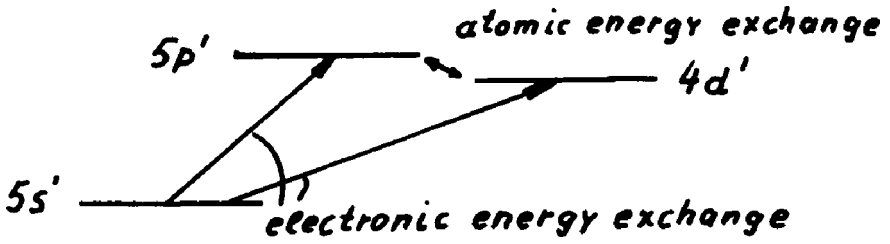

Figure IV.2 - Explanation for Pressure Dependence of the Ratio $\Delta I(5902)/\Delta I(6118)$

Figure (IV.2)

$$\sigma_{12}^{e} \geq 1.0 \times 10^{-14} \text{ cm}^2 \qquad \text{(IV.71)}$$

The last two measurements agree within an order of magnitude with those of Khaikin[6] under the same experimental conditions. Khaikin obtained the following results:

$$\gamma_{12}^{'e}(4d') = 4 \times 10^{4} \text{ sec}^{-1} \text{ Milliampere}^{-1}$$

$$\gamma_{2}^{'e}/A_2 = 7.9 \times 10^{-3} \text{ Milliampere}^{-1}$$

$$\gamma_{12}^{'e}(5d') = 4 \times 10^{3} \text{ sec}^{-1} \text{ Milliampere}^{-1}$$

$$\gamma_{2}^{'e}/A_2 = 1.3 \times 10^{-2} \text{ Milliampere}^{-1}$$

The difference between his results and our results, however, can be easily explained. Khaikin confined his measurements to one pressure and did not extrapolate to zero pressure. Thus we feel our values are more reliable. For comparison, we took our curves for the lowest pressure value and fit it to equation (II.58). Our results were almost identical with those obtained by Khaikin.

While in the two preceding cases we determined the excitation and de-excitation parameters of a group of levels, we were able in one case to measure the excitation and de-excitation rates of a single higher level, namely the $6s'(1/2)_0^0$ level. We measured the intensity change ratio $\Delta I(5280)/\Delta I(6118)$ as a function of the current for four pressures. The $\lambda = 5280$ line originates from the $6s'(1/2)_0^0$ and could be resolved by our monochromator. The results are shown in Graph (IV.5), and the least square fit programs yielded the following results:

$$\frac{\gamma_2'^e}{A_2} = (7.98 \begin{smallmatrix} + 0.41 \\ - 0.40 \end{smallmatrix}) \times 10^{-3} \text{ Milliampere}^{-1} \qquad \text{(IV.72)}$$

$$\frac{\gamma_{12}'^e}{A_2} \cdot A(5280) = (1.05 \begin{smallmatrix} + 0.2 \\ - 0.16 \end{smallmatrix}) \times 10^2 \text{ Milliampere}^{-1} \times \text{sec}^{-1} \qquad \text{(IV.73)}$$

A_2 is the transition probability of the $6s'(1/2)_0^0$ level, and A(5280) is the Einstein coefficient for this particular

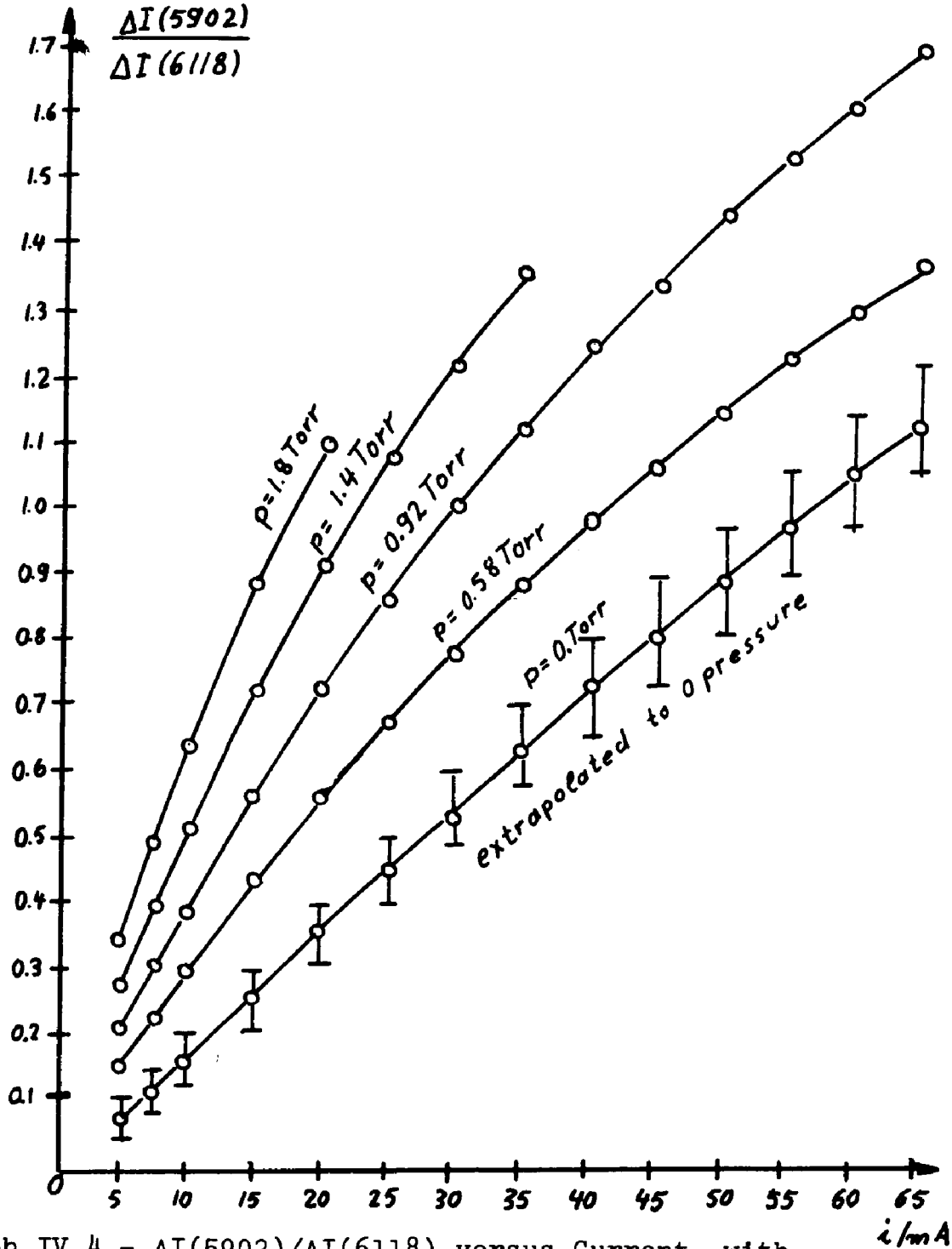

Graph IV.4 - ΔI(5902)/ΔI(6118) versus Current, with Pressure as Parameter

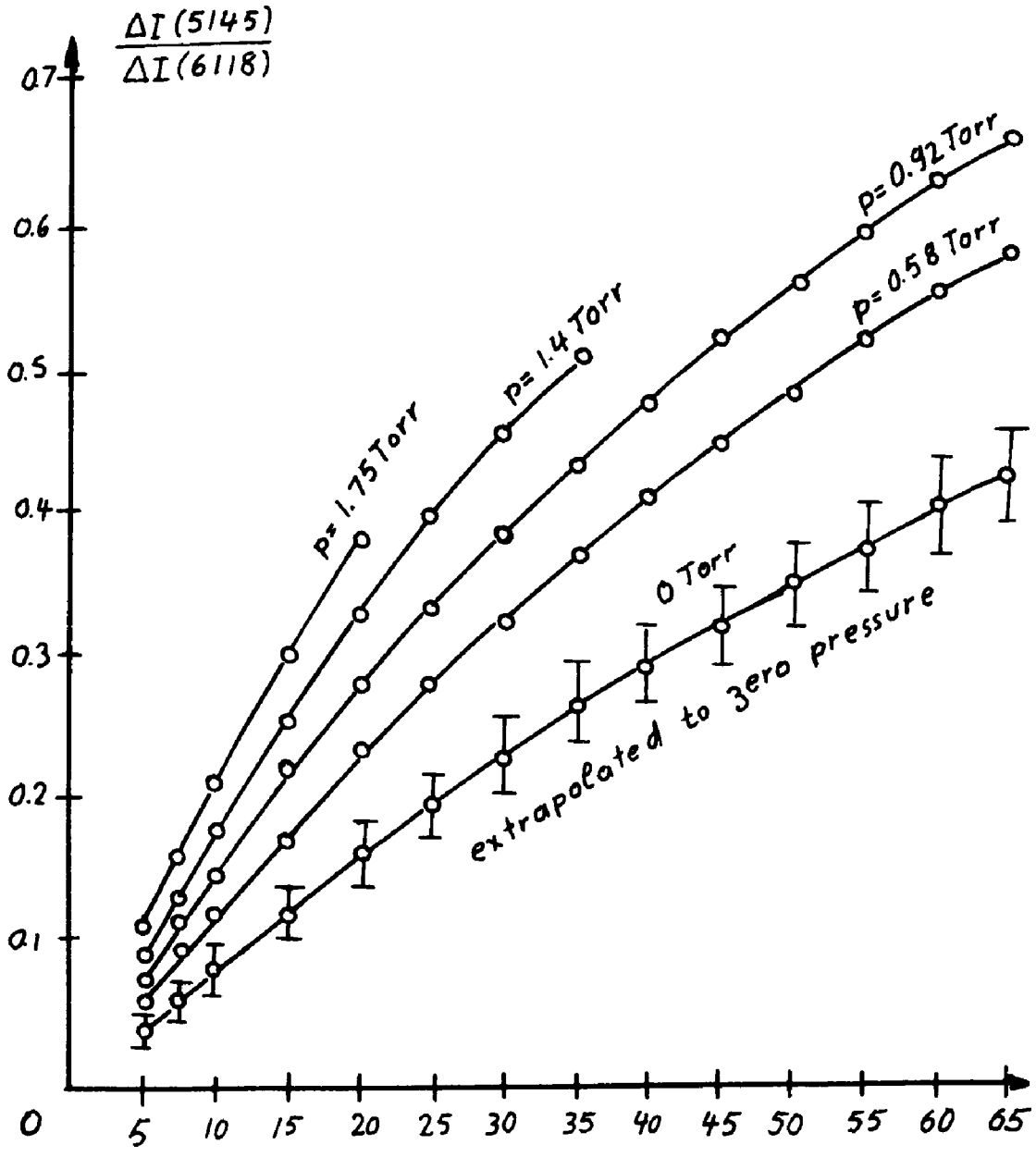

Graph IV.5 - ΔI(5145)/ΔI(6118) versus Current, with Pressure as Parameter

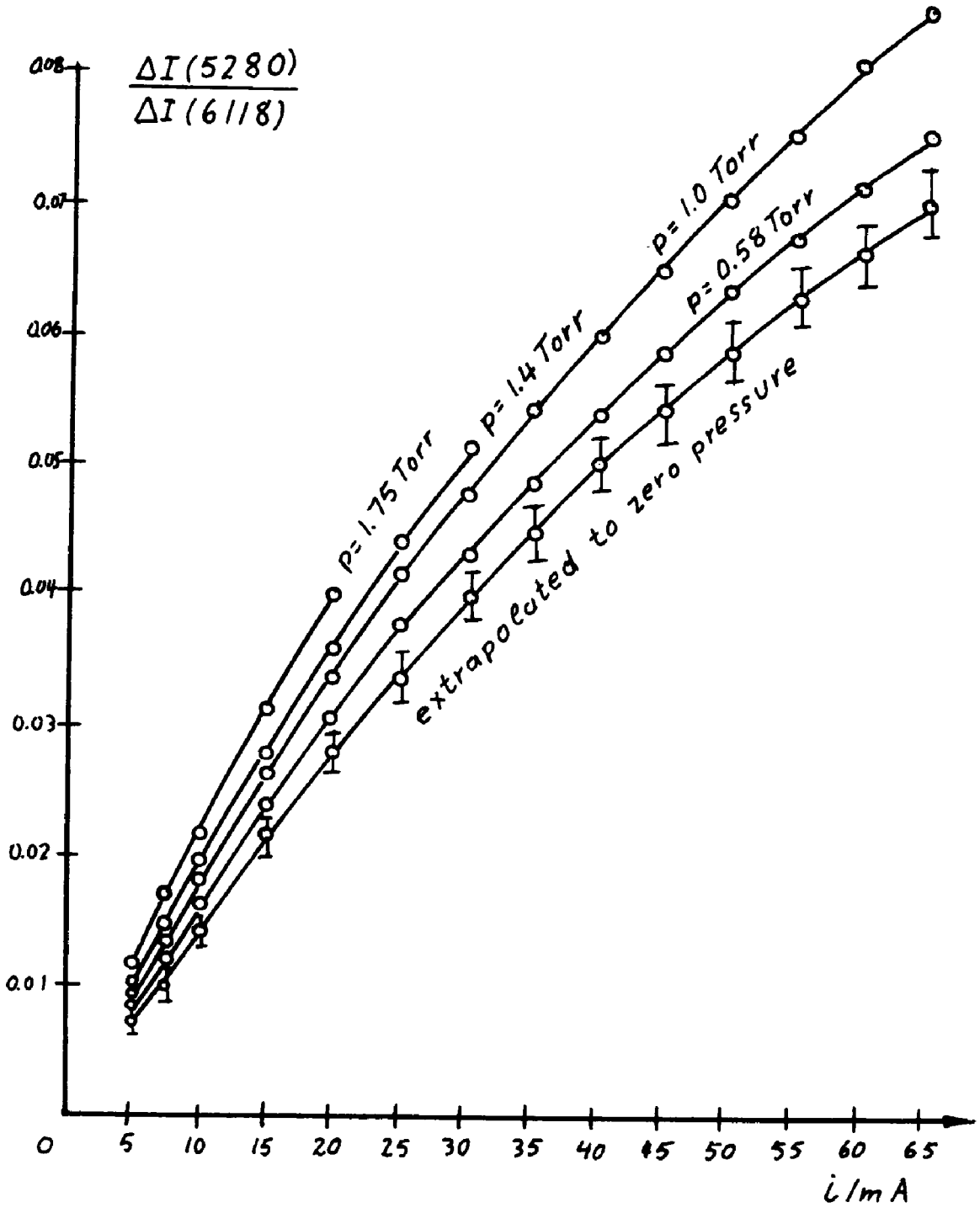

Graph IV.6 - ΔI(5280)/ΔI(6118) versus Current, with Pressure as Parameter

single transition. We see again that the electronic de-excitation rate is small compared to the radiative transition rate A_2. Unfortunately, A(5280) and A_2 are not known, so that we cannot estimate the size of $\gamma_{12}^{'e}$.

IV.8 Energy Transfer Between States of Different Azimuthal Quantum Numbers

In all our experiments described in the preceding chapter, we considered collisions in which atoms were excited and de-excited between states of the same azimuthal quantum number ℓ_e'. We are also interested in the possibility of energy transfer through electron-atom collisions between the states with different azimuthal quantum numbers, ℓ_e and ℓ_e'. Khaikin[6] reported that this energy transfer does not occur. The fact that the ℓ_e states are modulated shows that some kind of energy transfer is present between the ℓ_e' and ℓ_e states. Three mechanisms can possibly cause the modulation of the ℓ_e states: First, higher ℓ_e' states can be excited through electron impact from the upper laser level and then cascade into the ℓ_e states. A second possibility is that the ℓ_e levels are excited through atom-atom collisions between ℓ_e atoms and ℓ_e' atoms. A third possibility can be electron excitation from a ℓ_e' state.

At first we investigated the energy transfer from the upper laser level to the 4d levels. The energy spacing between these levels and the upper laser level is in the order of 1kT, so that both electronic and atomic collisions are responsible for the modulation of the 4d levels. In contrast to the measurement made for the 4d' levels, we were able to resolve one single line originating from the

$4d(3\ 1/2)_3^0$ level, namely the 5820Å line. The curves for the intensity change ratio $\Delta I(5820)/\Delta I(6118)$ for four different pressure points are shown in Graph (IV.6). These curves were fit to an expression similar to equation (IV.49) with the method of the least squares. Again, we took into account a 10% uncertainty in the pressure, a 10% uncertainty in the current, a 5% uncertainty in the measured intensity change ratio, and a 5% uncertainty in the calibration. The analysis yields the following results:

$$\frac{\gamma_2'^a}{A_2} = (4.76 \pm \begin{matrix} 0.25 \\ 0.23 \end{matrix}) \times 10^{-2}\ \text{Torr}^{-1} \qquad \text{(IV.74)}$$

$$\frac{\gamma_2'^e}{A_2} = (6.98 \pm \begin{matrix} 0.46 \\ 0.42 \end{matrix}) \times 10^{-3}\ \text{Milliampere}^{-1} \qquad \text{(IV.75)}$$

$$\frac{\gamma_{12}'^a}{A_2} \cdot A(5820) = (5.81 \pm \begin{matrix} 0.67 \\ 0.42 \end{matrix}) \times 10^{4}\ \text{Torr}^{-1} \times \text{sec}^{-1} \qquad \text{(IV.76)}$$

$$\frac{\gamma_{12}'^e}{A_2} \cdot A(5820) = (6.49 \pm \begin{matrix} 0.84 \\ 0.55 \end{matrix}) \times 10^{2}\ \text{Milliampere}^{-1} \times \text{sec}^{-1} \qquad \text{(IV.77)}$$

The subscript 2 designates the $4d(3\ 1/2)_3^0$ level, and the subscript 1 designates the upper laser level.

Again, we do not know the radiative transition probabilities A_1 and A(5689). We see, however, that the de-excitation due to electron-atom collisions becomes very im-

portant for the $5s(1\ 1/2)_2^0$ level for fairly low currents compared to the total radiative transition probability.

It is also possible to study the energy transfer through electron-atom collisions between two unprimed states. For this purpose, we measured the intensity change ratio $\Delta I(5820)/\Delta I(5689)$, where the $\lambda = 5689\text{Å}$ line originates from the $5s(1\ 1/2)_2^0$ level. The results are shown in Graph (IV.7). We observe a strong current dependence of this ratio. However, it is impossible for us to analyze these curves, since we do not know the explicit pressure dependence of these curves. The energy exchange between all 5s levels has to be studied in detail. Due to the limitation of our instruments we could not resolve a line starting from the $5s(1\ 1/2)_1^0$ level, thus we do not have enough information to analyze our curves.

In another case we were interested in the energy transfer due to electron-atom collisions between the primed and unprimed 5s states of Ne, i.e., states with different azimuthal quantum numbers. We were however only able to resolve a line originating from the $5s(1\ 1/2)_2^0$ level, the lowest of the 5s states. We measured the ratio $\Delta I(5689)/\Delta I(6118)$, and the results are shown in Graph (IV.8). The pressure dependence of this ratio would have to be described by a complicated set of equations described in Chapter (II), equations (II.30) to (II.35). In order to obtain the pure

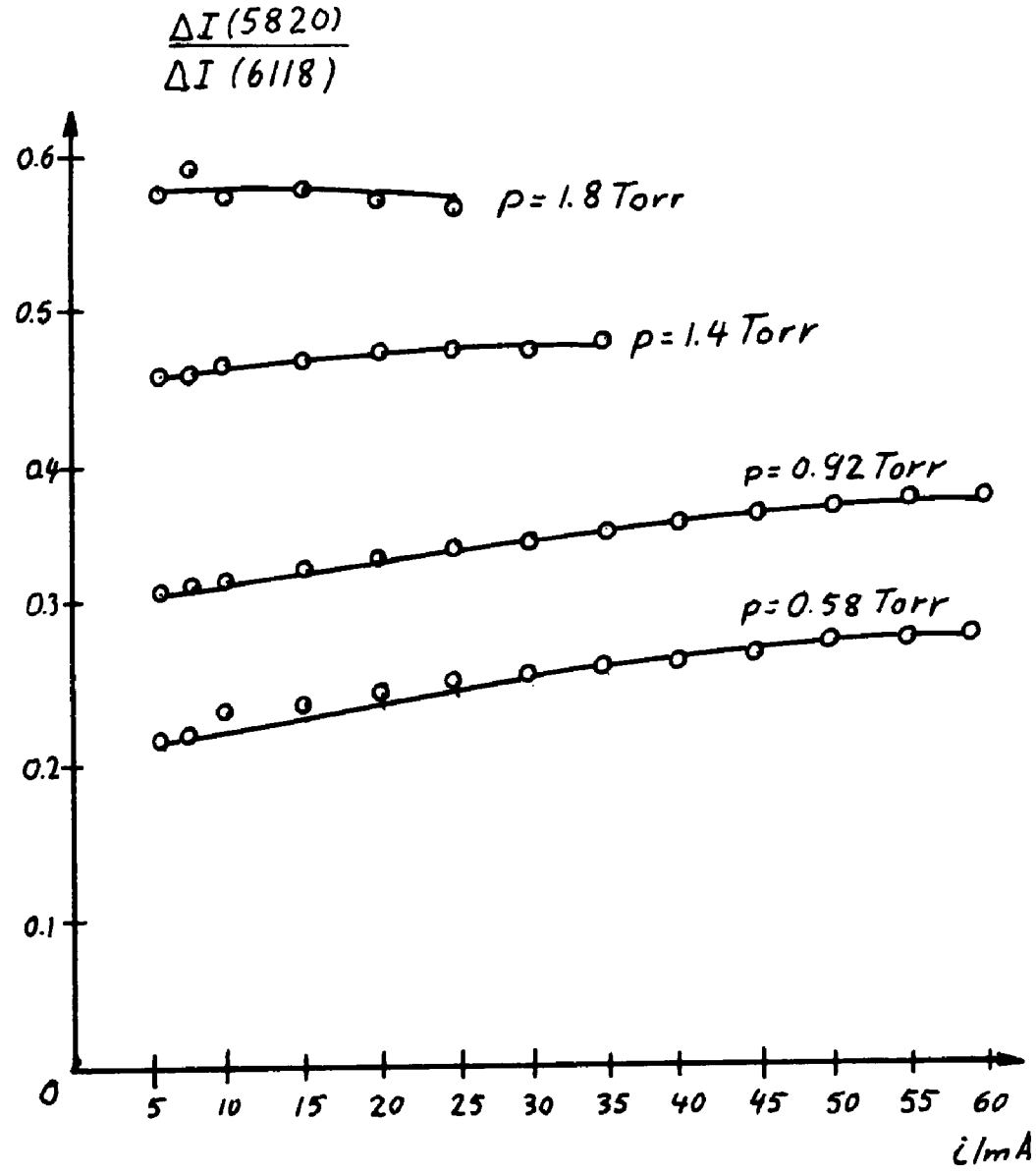

Graph IV.7 - ΔI(5820)/ΔI(6118) versus Current, with Pressure as Parameter

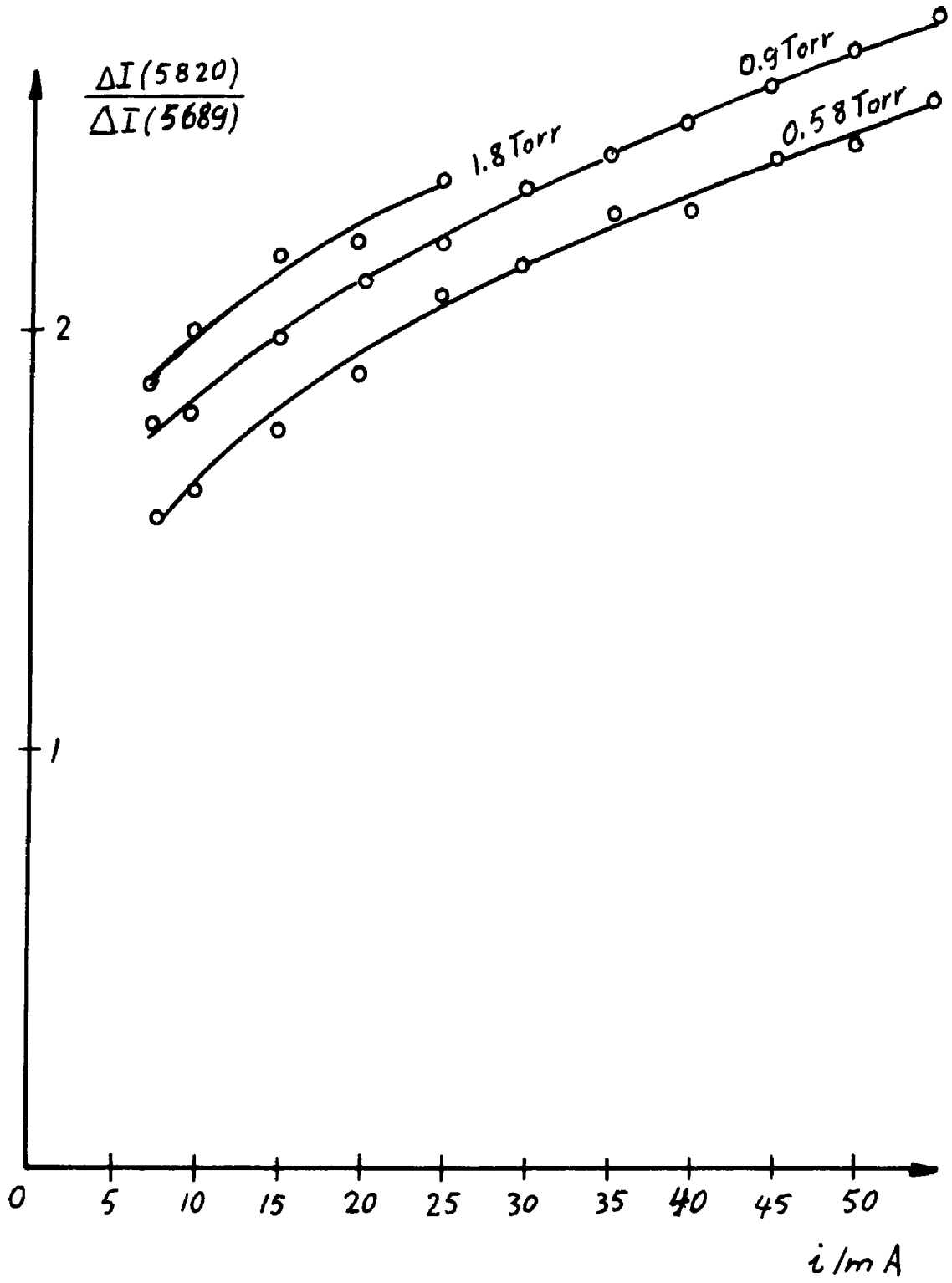

Graph IV.8 - ΔI(5820)/ΔI(5689) versus Current, with Pressure as Parameter

electron impact effect, we extrapolated to zero pressure, and with the already described uncertainties, we obtained the following parameters:

$$\frac{\gamma_1'^e}{A_1} = (8.76 \pm^{0.45}_{0.5}) \times 10^{-2} \text{ Milliampere}^{-1} \qquad \text{(IV.78)}$$

$$\frac{\gamma_{21}'^e}{A_1} \times A(5689) = (1.25 \pm^{0.24}_{0.227}) \times 10^{3} \text{ Milliampere}^{-1} \times \text{sec}^{-1} \qquad \text{(IV.79)}$$

where the subscript 1 designates the $5s(1\ 1/2)^0_2$ level and the subscript 2 designates the upper laser level.

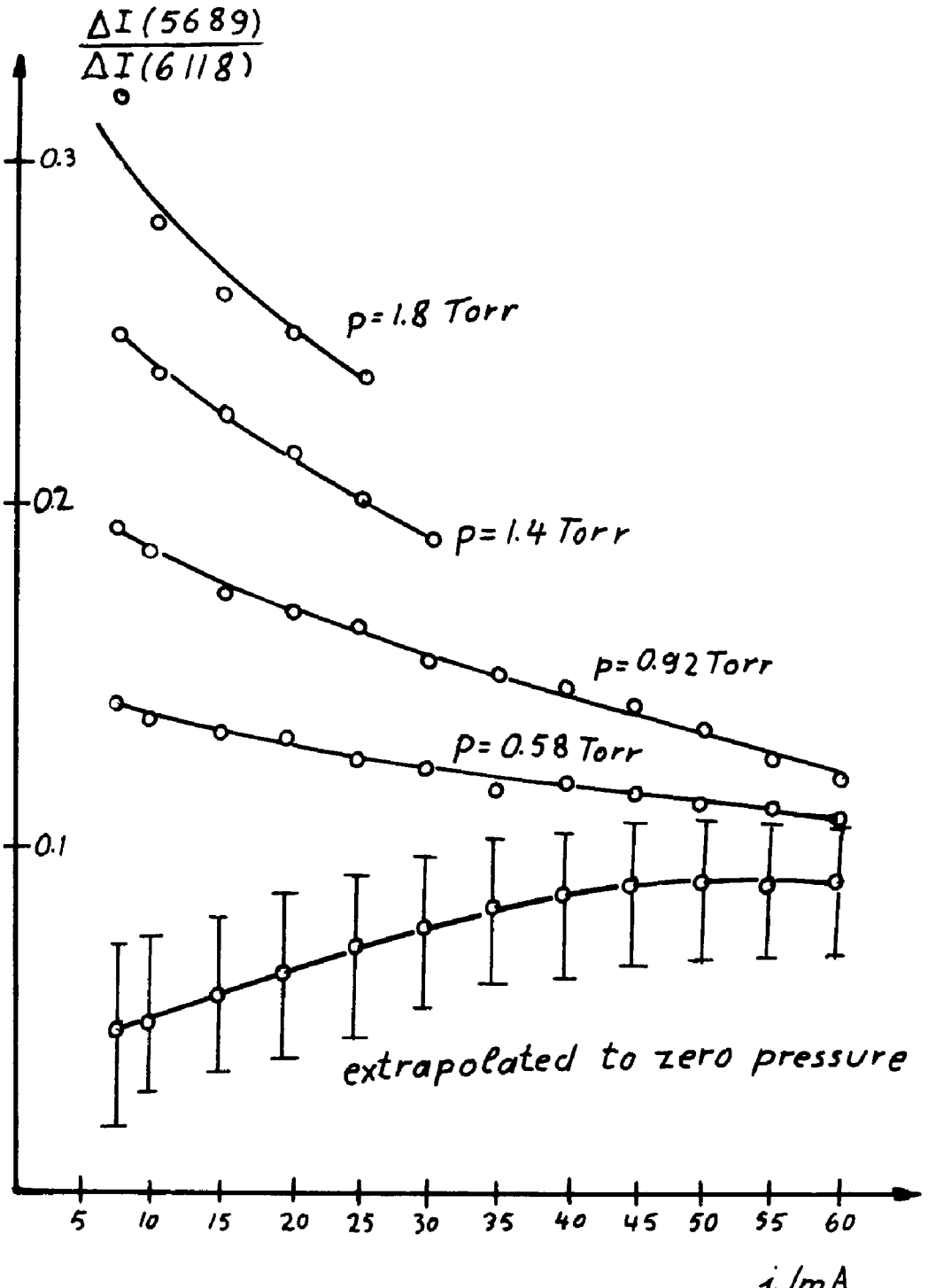

Graph IV.9 - ΔI(5689)/ΔI(6118) versus Current, with Pressure as Parameter

V. CONCLUDING REMARKS

The experiment described in the preceding chapters gives us information about the energy transfer processes between some excited levels in Ne due to atom-atom and electron-atom collisions, and the results are shown in Table (V.1). It was found that in a He-Ne laser under normal operating conditions ($p \approx 1$ Torr, $10mA \leq i \leq 60mA$) the de-excitation rates of the $5s'(1/2)_1^0$ upper laser level due to electron-atom and atom-atom collisions have an importance comparable to the radiative transition rate. While the atomic collisional energy transfer occurs only between the upper laser level (the $5s'(1/2)_1^0$ level) and the neighbouring 5s levels, the 4d levels, and the He 2'S level, states lying well above the upper laser level are populated through electron impact from the upper laser level.

The approximate selection rule for electronic collisions that each atom preserves its azimuthal quantum number appears valid. Some exceptions have been observed, but the effective cross sections for collisions that change the azimuthal quantum number are apparently much smaller than for collisions that do not change the quantum number.

Sidelight modulation measurements represent a successful technique to determine the rate constants to model laser kinetics. In this experiment, the technique was applied to a He-Ne laser system, but the same technique can

also be employed to obtain rate constants for other laser systems.

TABLE V.1a

De-excitation Rates		
Level	atomic	electronic
$3p(1/2)_1$	$\gamma'^{a} = (6.80^{+0.84}_{-1.57}) \times 10^{6}\ Torr^{-1}\ sec^{-1}$	———
$5s'(1/2)^{o}_{1}$	$\gamma'^{a} = (4.81^{+0.73}_{-0.84}) \times 10^{6}\ Torr^{-1}\ sec^{-1}$	$\gamma'^{e} = (2.04^{+0.26}_{-0.34}) \times 10^{5}\ (mA)^{-1}\ sec^{-1}$
$5s'(1/2)^{o}_{0}$	$\gamma'^{a}/A_{5s'(1/2)^{o}_{0}} = (6.51^{+0.31}_{-0.30}) \times 10^{-1}\ Torr^{-1}$	$\gamma'^{e}/A_{5s'(1/2)^{o}_{0}} = (3.37^{+0.22}_{-0.20}) \times 10^{-2}\ (mA)^{-1}$
$4d'$	———	$\gamma'^{e}/A_{4d'} = (9.32^{+0.47}_{-0.48}) \times 10^{-4}\ (mA)^{-1}$
$5d'$	———	$\gamma'^{e}/A_{5d'} = (5.23^{+0.30}_{-0.30}) \times 10^{-3}\ (mA)^{-1}$
$6s'(1/2)^{o}_{0}$	———	$\gamma'^{e}/A_{6s'(1/2)^{o}_{0}} = (7.98^{+0.41}_{-0.40}) \times 10^{-3}\ (mA)^{-1}$
$4d(3\frac{1}{2})^{o}_{3}$	$\gamma'^{a}/A_{4d(3\frac{1}{2})^{o}_{3}} = (4.76^{+0.25}_{-0.23}) \times 10^{-2}\ Torr^{-1}$	$\gamma'^{e}/A_{4d(3\frac{1}{2})^{o}_{3}} = (6.98^{+0.46}_{-0.42}) \times 10^{-3}\ (mA)^{-1}$
$5s(1\frac{1}{2})^{o}_{2}$	———	$\gamma'^{b}/A_{5s(1\frac{1}{2})^{o}_{2}} = (8.76^{+0.45}_{-0.50}) \times 10^{-2}\ (mA)^{-1}$

TABLE V.1b

Excitation from $5s'(1/2)_1^0$ level		
to	atomic	electronic
$5s'(1/2)_0^0$	$\gamma'^a_{12}/A_{5s'(1/2)_1^0} = (8.45^{+1.00}_{-0.75}) \times 10^{-2}\ Torr^{-1}$	$\gamma'^e_{12}/A_{5s'(1/2)_1^0} = (4.31^{+0.50}_{-0.49}) \times 10^{-3}\ (mA)^{-1}$
$4d'$	———	$(\gamma'^e_{12}/A_{4d'})A(5902) = (3.96^{+0.40}_{-0.30}) \times 10^{+3}\ (mA)^{-1}\ sec^{-1}$
$5d'$	———	$(\gamma'^e_{12}/A_{5d})A(5145) = (6.99^{+0.71}_{-1.30}) \times 10^{+2}\ (mA)^{-1}\ sec^{-1}$
$6s'(1/2)_0^0$	———	$(\gamma'^e_{12}/A_{6s'(1/2)_0^0})A(5280) = (1.05^{+0.20}_{-0.16}) \times 10^{2}\ (mA)^{-1}\ sec^{-1}$
$4d(3\,1/2)_3^0$	$(\gamma'^a_{12}/A_{4d(3\,1/2)_3^0})A(5820) = (5.81^{+0.67}_{-0.42}) \times 10^{4}\ Torr^{-1}\ sec^{-1}$	$(\gamma'^e_{12}/A_{4d(3\,1/2)_3^0})A(5820) = (5.81^{+0.67}_{-0.42}) \times 10^{4}\ (mA)^{-1}\ sec^{-1}$
$5s(1\,1/2)_2^0$	———	$(\gamma'^e_{12}/A_{5s(1\,1/2)_2^0})A(5689) = (1.25^{+0.24}_{-0.23}) \times 10^{3}\ (mA)^{-1}\ sec^{-1}$

LIST OF REFERENCES

1. C. E. Moore, Atomic Energy Levels, Vol. 1, Natl. Bur. Std. (U.W.) Circ. 467, 1949.

2. H. S. W. Massey and E. H. S. Burhop, Electronic and Ionic Impact Phenomena, Vol. 1, Oxford at the Clarendon Press, 1969, Chapter 1.1.

3. E. U. Condon and G. H. Shortley, Theory of Atomic Spectra (Cambridge University Press, New York, 1952), p. 133.

4. J. H. Parks and A. Javan, Phys. Rev. 139, (1965), A1352.

5. R. A. Lilly and J. R. Holmes, J. Opt. Soc. 58 (1968), 1406.

6. A. S. Khaikin, Soviet Phys. JEPT 24 (1967), 25.

7. A. L. Bloom, Appl. Phys. Letters 2 (1963), 101.

8. C. B. Moore, Appl. Opt. 4 (1965) 252 A. B. White and J. D. Ridgen, Appl. Phys. Letters 2 (1963) 211.

9. See for example: Uleen, and Muller, Laser, Springer Verlag Berlin, Heidelberg, New York 1969, p. 250.

10. T. Holstein, Phys. Rev. 72 (1947) 1212; ibid. 83 (1951) 1159.

11. A. E. Siegman, Introd. to Lasers and Masers, McGraw Hill, New York 1971, p. 121.

12. C. G. B. Garrett, Gas Lasers, McGraw Hill, New York, 1967, p. 9, 4.

13. G. Racha, Phys. Rev. 61 (1942) 537 (1).

14. E. F. Labuda and E. I. Gordon, J. Appl. Phys. 35 (1964) 1647.

15. Compare: T. Sakurai, T. Ohta, and T. Ogawa, IEEE J. Quantum Electronics QE-4 (1968) 65.

16. A. C. G. Mitchell and M.W. Zemansky, Resonance Radiation and Excited Atoms, Cambridge University Press, New York, 1961, Chapter 4.

17. W. R. Bennett and P. J. Kindlmann, Phys. Rev. 149 (1966) No. 1, 38, S. Inatsugu and J. R. Holmes, Phys. Rev. A 8 (1973) 1678.

18. T. Sakurai and T. Ohta, Jap. J. Appl. Phys. 10, No. 2 (1971) 234.

19. L. A. Minaeva, FIAN (Phys. Inst. Acad. Sci.) No. 23, 1967.

20. RCA Handbook of Phototubes, Vol. No. 3.4.

21. A Szoke and A. Javan, Phys. Rev. Letters 10 (1963) 521.

VITA

Heinrich-Joachim Siebeneck, second son of Franz and Hedwig M. Siebeneck, was born in Landsberg, West Germany, on September 30, 1943. He attended 'Volksschule' from 1949 to 1953 and graduated from the 'Hitforf-Gymnasium' in Recklinghausen in 1962. From 1963 to 1969 he studied Electrical Engineering at the Technische Hochschule Karlstuhe from where he received the degree of a Dipl. Ing. In the Fall of 1969 he entered the graduate school at Lehigh University. He worked as a teaching assistant in electrical engineering, and at the same time he did his doctoral work under Professor E. E. Bergmann.

He is a member of the Institute of Electrical and Electronics Engineers.